

# **A Study into the Electronic and Photophysical Properties of Polycarbazoles**

Mathew James Stevenson

Submitted for the degree of Doctor of Philosophy

Department of Physics and Astronomy

July 2009



The  
University  
Of  
Sheffield.

# Abstract

This thesis details an investigation into the electronic and photophysical properties of a series of 2,7-linked polycarbazoles. This class of conjugated polymer has recently attracted interest as a potential blue-emitting material in electroluminescent devices.

Polymer light-emitting diodes were fabricated using a variety of device structures. The most promising devices incorporated a triarylamine-substituted carbazole-oxadiazole alternating copolymer (**P7**). Time-of-flight photocurrent measurements suggested that this material may favour electron transport. By including a thin layer of TFB (that functioned as a complimentary hole transport layer) an EL turn on voltage of 2.8 V, maximum luminance of 2,240 cd/m<sup>2</sup> and efficiency of 1.12 cd/A was achieved.

The thermal stability of the polymers was investigated by monitoring changes in their photoluminescence spectra after a variety heat treatments. All of the polymers that were studied exhibited reduced emission after being annealed in air at 150 °C. However, polymer **P6** (a triarylamine-substituted carbazole homopolymer) exhibited good colour stability over a two hour treatment. The absence of degradation under an inert N<sub>2</sub> atmosphere suggested that these polymers may oxidise to form an emission quenching defect.

Solution photoluminescence spectra that were obtained from polymer **P6** revealed a strong solvatochromic effect. This was attributed to the presence of a charge transfer (CT) state between the carbazole backbone and triarylamine pendant group. By changing the polarity of the solvent, the relative intensities of the intrinsic 'locally-excited' (LE) state and low-energy CT state could be controlled. Time-resolved photoluminescence decay measurements also revealed a significant increase in the PL lifetime with solvent polarity.

# Acknowledgements

First of all, I should like to express my gratitude to Professor David Lidzey for the support and assistance that he has given me. His knowledge and advice has been invaluable throughout this project. Many thanks also go to Dr. Ahmed Iraqi and his research group for providing me with the polymers upon which this work was based.

Thank you to Dr. Theo Kreouzis for giving me the opportunity to visit Queen Mary University of London and participate in the TOF measurements.

Thank you to the many members of staff that have helped me over the years. I would especially like to thank Ashley for his assistance in obtaining TCSPC data. Thank you to Iain, Ali, Liam and Farhad for showing me the ropes when I started. Special thanks go to Iain for helping me with LaTeX. Thank you to Al and David P. for keeping the Lesker up and running. A big thank you goes to David M. for his boundless enthusiasm, motivational talks, and not least for providing me with accommodation in a time of need. Thank you to Chung for the polyfluorene spectra. I should also like to thank Claire and Matt for helping to relieve some of the workload.

Of the many positives that I have taken from my time at Sheffield, I am most grateful to have met such great friends. In this regard I would especially like to mention Iain, Jon and David.

Last, but certainly not least I would like to express my sincerest gratitude to my family. Thank you Nat for the computer and the expert photography, but most importantly thank you for your encouragement and support. Finally, my deepest thanks must go to my parents for both putting me up, and putting up with me over the past year.

# Contents

## 1 Introduction

1.1	Introduction . . . . .	1
1.2	Electronic Conjugation in Organic Materials . . . . .	2
1.2.1	Hybridisation . . . . .	2
1.2.2	Molecular Orbital Theory . . . . .	3
1.3	Optical Transitions . . . . .	5
1.3.1	Vibrational Energy Levels . . . . .	7
1.3.2	Interchain Excitations . . . . .	9
1.4	Polymeric Light-Emitting Diodes . . . . .	10
1.4.1	Current-Voltage Characteristics of PLEDs . . . . .	13
1.5	Device Efficiency . . . . .	16
1.6	Summary . . . . .	18
	References . . . . .	22

## 2 Experimental Methods

2.1	Introduction . . . . .	25
2.2	The Polymers Under Investigation . . . . .	26
2.2.1	Arylene-Based Polymers . . . . .	26
2.2.2	Carbazole-Based Polymers . . . . .	27
2.2.3	2,7-Linked Polycarbazoles . . . . .	29
2.3	Sample Preparation . . . . .	33
2.3.1	Polymer Solutions . . . . .	33
2.3.2	Thin-Film Deposition . . . . .	34
2.4	Steady-State Spectroscopy . . . . .	34
2.4.1	UV/Vis Spectroscopy . . . . .	34
2.4.2	Fluorescence Spectroscopy . . . . .	35
2.4.3	Photoluminescence Quantum Yield . . . . .	35
2.5	Time-Resolved Photoluminescence Decay . . . . .	41
2.6	Device Fabrication and Characterisation . . . . .	41
2.6.1	Substrate Preconditioning . . . . .	43
2.6.2	Device Fabrication . . . . .	43
2.6.3	LED Characterisation . . . . .	45
2.6.4	LED Performance Metrics . . . . .	47
2.7	Time-of-Flight Photocurrent . . . . .	48
	References . . . . .	51

### 3 Thermal Stability of Polycarbazoles

3.1	Introduction . . . . .	54
3.2	Degradation in Arylene-Type Polymers . . . . .	55
3.2.1	Degradation Studies on Carbazole-Based Materials . . . . .	59
3.3	Sample Preparation . . . . .	60
3.4	Photoluminescence Measurements . . . . .	60
3.5	Thermal Stability of PFO . . . . .	61
3.6	Thermal Stability of Poly(alkyl-carbazole)s . . . . .	64
3.7	Thermal Stability of Poly(aryl-carbazole)s . . . . .	68
3.8	Comparison of Emission Intensities . . . . .	70
3.9	Conclusions . . . . .	71
	References . . . . .	72

### 4 Charge Transport in Triarylamine-Substituted Polycarbazoles

4.1	Introduction . . . . .	74
4.2	Transient Photocurrents . . . . .	75
4.3	Results . . . . .	78
4.3.1	Time-of-Flight Photocurrents . . . . .	79
4.3.2	Field-Dependent Mobility . . . . .	82
4.4	Conclusion . . . . .	84
	References . . . . .	86

### 5 Optoelectronic Characterisation of 'Single-Component' LEDs

5.1	Introduction . . . . .	87
5.2	Device Structure . . . . .	88
5.2.1	The Conducting Polymeric Anode . . . . .	88
5.2.2	Active Layer Thickness . . . . .	90
5.2.3	Cathode . . . . .	92
5.3	Electrochemical Characterisation . . . . .	93
5.4	Results . . . . .	94
5.4.1	Alkyl-Substituted Polymers . . . . .	94
5.4.2	Aryl-Substituted Polymers . . . . .	105
5.4.3	Triarylamine-Substituted Polymers . . . . .	112
5.5	Conclusions . . . . .	119
	References . . . . .	121

### 6 Optoelectronic Characterisation of Heterojunction LEDs

6.1	Introduction . . . . .	124
6.2	Butyl-PBD Heterojunction Devices . . . . .	125
6.2.1	Distributed Heterojunction LEDs . . . . .	128
6.2.2	Bilayer Heterojunction Devices . . . . .	137
6.2.3	Spectral Stabilisation in Heterojunction Devices . . . . .	140
6.3	TFB Interlayer . . . . .	144

6.4 Conclusions . . . . .	152
References . . . . .	154

**7 Solvatochromism in Triarylamine-Substituted Polycarbazoles**

7.1 Introduction . . . . .	157
7.2 Results . . . . .	158
7.2.1 Solvent Dependant Spectra . . . . .	158
7.2.2 Solution Concentration . . . . .	162
7.2.3 Time-Resolved PL Decay . . . . .	165
7.3 Discussion . . . . .	167
7.4 Conclusions . . . . .	172
References . . . . .	173

**8 Conclusions and Suggestions for Further Work**

8.1 Conclusions . . . . .	175
8.2 Further Work . . . . .	181
References . . . . .	185

# Chapter 1

## Introduction

### 1.1 Introduction

In 1987, Tang and Van Slyke of the Eastman Kodak Company reported upon the fabrication of a novel thin-film organic electroluminescent diode.<sup>1</sup> This bilayer device represented the first practical demonstration of a technology that could be viable for commercial use. The discovery of efficient electroluminescence from the conjugated polymer poly(*p*-phenylenevinylene) (PPV) followed soon after,<sup>2</sup> tapping into the potential benefits of solution-processable manufacturing techniques. Almost two decades of research has recently culminated in the release of the world's first full-colour organic LED television, the Sony XEL-1.<sup>3</sup>

## 1.2 Electronic Conjugation in Organic Materials

In organic chemistry, a conjugated molecule is said to comprise an arrangement of alternating single and double, or single and triple covalent bonds. Here, the term 'conjugation' refers to the coupling of electron wave functions across multiple atoms, resulting in the formation of new orbitals that are delocalised over an extended region of the molecule. It is the transitions that occur within these molecular orbitals that govern the electronic and optical properties of organic semiconductors.

### 1.2.1 Hybridisation

In its ground-state, the electronic configuration of carbon is  $1s^2 2s^2 2p_x 2p_y$ . Valence bond theory would therefore predict that carbon should form two covalent bonds, each incorporating one of the unpaired p-electrons. This however, is inconsistent with the known structures of many organic compounds. For instance, methane ( $\text{CH}_4$ ) incorporates four  $\sigma$ -bonds of equivalent length and energy.

To explain the existence of various carbon-based molecules, the concept of orbital-hybridisation is used. The formation of these hybrid orbitals first requires that the carbon atom adopts an excited state electronic configuration. This occurs via the promotion of a single electron from the 2s orbital to the remaining unoccupied p orbital. The new excited state configuration is then  $1s^2 2s^1 2p_x 2p_y 2p_z$ , providing the four unpaired valence electrons that are necessary for tetravalent bonding. It is the wave functions of these electrons that combine to form hybrid orbitals.

In the aforementioned case of methane, hybridisation of the 2s electron with all three 2p electrons results in the formation of four equivalent  $sp^3$  orbitals. This molecule thus adopts a tetrahedron structure with an angle  $109.5^\circ$  subtended by any two bonds.<sup>4</sup> In conjugated molecules that incorporate an arrangement



of alternating single and double bonds, it is the  $sp^2$  hybrid structure of carbon that is present. Here, the 2s orbital combines with two of the 2p orbitals to form three equivalent  $sp^2$  orbitals, adopting a trigonal structure with planar geometry. The remaining p orbital is oriented such that its axis is orthogonal to the plane of the hybrid orbitals.

## 1.2.2 Molecular Orbital Theory

The spatial distribution of electrons within an organic molecule is determined by the formation of molecular orbitals. These orbitals can be considered to result from a linear combination of atomic orbitals (LCAO). This concept is illustrated for the ethene molecule in figure 1.1. Here, two  $sp^2$  hybrid orbitals that are associated with adjacent carbon atoms interact when their electronic wave functions overlap. When the wave functions are in-phase, a bonding orbital is formed whereby the interaction results in an increase of the electron density between the two nuclei. This molecular orbital is stabilised relative to the isolated  $sp^2$  hybrid orbitals. Conversely, an anti-bonding orbital is formed when the interaction of the two electronic wave functions is out-of-phase. This destructive interaction results in a decrease of the electron density between the two nuclei and forms a molecular orbital that is destabilised relative to the isolated atomic orbitals.

When the two hybrid orbitals interact,  $\sigma$  (bonding) and  $\sigma^*$  (anti-bonding) molecular orbitals are formed. These orbitals exhibit circular symmetry about the internuclear axis. Due to the extensive overlap of electron wave functions, the orbitals have a large interaction energy. In the ground state, the  $\sigma$  bonding orbital is fully occupied by two electrons of opposing spin and the  $\sigma^*$  anti-bonding orbital is vacant.

As illustrated in figure 1.1, the ethene molecule also contains an additional  $\pi$  bond. This results from the interaction of p orbitals that are aligned along a

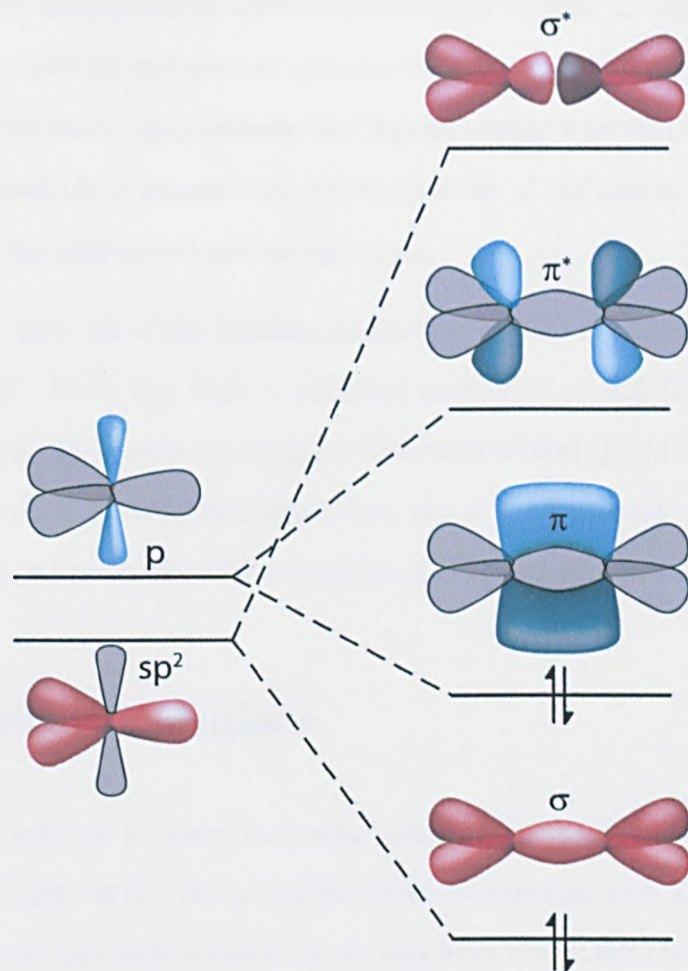


**Fig. 1.1:** An illustration of  $\sigma$  and  $\pi$  bond formation in ethene. The relative energy levels of the bonding and anti-bonding molecular orbitals is also shown, along with the ground state electronic configuration.

common axis. Consequently, this molecule possesses a rigid planar structure. Again, the electronic wave functions can interact constructively or destructively to form  $\pi$  bonding or  $\pi^*$  anti-bonding orbitals respectively. These orbitals are located above and below the plane of the molecule, with a node that is situated along the internuclear axis. Their interaction energy is smaller than that of the  $\sigma$  orbitals owing to a lesser degree of orbital overlap. The relative energies of the four orbitals that make up a carbon-carbon double bond is illustrated in the figure.

In conjugated materials,  $\pi$  electrons delocalise over extended regions of the

molecule. The interaction of additional electrons results in the formation of new molecular orbitals and further splitting of the energy levels. This results in a decrease in the energy gap between the highest energy  $\pi$  orbital and the lowest energy  $\pi^*$  orbital. As a general rule, the magnitude of the energy gap decreases as the size of the conjugated system increases.

In its ground state, all of the bonding molecular orbitals of ethene are electronically occupied. Here, the highest occupied molecular orbital (HOMO) is a  $\pi$  bonding orbital. The lowest unoccupied molecular orbital (LUMO) is a  $\pi^*$  antibonding orbital. It is these two states that are of most interest with regard to the electronic and photophysical properties of conjugated molecules.

### 1.3 Optical Transitions

Electronic transitions between molecular orbitals can be induced through the absorption of light. When the conjugated system interacts with a photon of appropriate energy, an electron can be promoted from the HOMO into the LUMO. The region of a molecule over which this occurs is called a chromophore. This process leaves an electronic vacancy (hole) in the HOMO which is now singularly occupied by an unpaired electron. The promoted electron and resultant hole are coulombically bound to each other, forming a neutrally charged quasiparticle termed an exciton. In the absence of external influences, this exciton will decay back to the ground state. Recombination may occur radiatively, with the wavelength of emission being dependent upon the HOMO-LUMO energy gap. The region of a molecule that is involved in emission is called a fluorophore.

As mentioned, the size of the HOMO-LUMO energy gap is dependent upon the degree of conjugation in the molecule. It is important to note that electronic conjugation may not necessarily extend throughout an entire molecule, even if bond alternation is maintained. This is particularly true of large polymeric molecules in which intrinsic defects (such as kinks and twists) and extrinsic defects (such

as the presence of impurities and structural anomalies) can disrupt electronic delocalisation. Furthermore, the study of well-defined oligomeric materials has shown that there is a fundamental limit to the degree of conjugation, even in highly rigid molecules.<sup>5</sup> Beyond this 'effective conjugation length' further extension of the oligomer produces no notable change in the properties of its absorption and emission spectra. Consequently, a single large molecule (some conjugated polymers can have a number-averaged molecular weight that is equivalent to several hundred repeat units) can host numerous conjugated segments which behave as individual chromophores.

Many conjugated materials have a low dielectric constant. As a result, the coulombic interaction between electron and hole is typically much larger than in conventional inorganic semiconductors. With a high binding energy (of around 0.1-1.0 eV) these excitons (termed Frenkel excitons) are usually localised to a single molecule and are relatively stable at room temperature.<sup>6</sup> The redistribution of electronic charge that accompanies the formation of an exciton can cause the molecular lattice to adopt a new configuration. To reflect this fact, these excitations are often referred to as polaron-excitons.<sup>7</sup> The relaxation process further stabilises the exciton against dissociation.

Excitons can be defined by their spin multiplicity. In its ground state, the HOMO of a conjugated molecule is occupied by two electrons of antiparallel spin. The net spin quantum number of this state is  $S=0$ , making it of singlet multiplicity. When one of these electrons is optically excited into the LUMO, a singlet excited state is generated. Such a transition is labeled using the notation  $S_0 \rightarrow S_1$ . Transitions to higher lying singlet states are also possible. However, the  $S_0 \rightarrow S_1$  transition is of the most practical relevance when discussing the optical and electroluminescent processes of a conjugated polymer. In the reverse process, a singlet exciton may decay back to the ground state via the emission of a photon. Typically, singlet excitons have a relatively short lifetime of the order of  $10^{-9}$  s.<sup>8,9</sup> The process of their radiative decay is termed fluorescence.

Triplet excitons have a spin quantum number of  $S=1$ . Such a state cannot be directly generated from, nor can it directly decay to the singlet ground state. The triplet state can however be formed from a singlet exciton in a process known as intersystem crossing (ISC). As will be discussed later, the triplet state can also be generated electronically. The lowest lying excited triplet state  $T_1$  is lower in energy than the  $S_1$  state. In large conjugated polymers, the exchange energy between the two states is relatively large (around 0.7 eV).<sup>10</sup> This will inhibit a thermally induced reverse transition back to the singlet state. Triplet excitons are relatively long-lived with the typical lifetime ranging from from  $10^{-6}$  s to 1 s.<sup>8,9</sup>

### 1.3.1 Vibrational Energy Levels

In addition to inducing electronic excitations, the process of light absorption can also impart vibrational energy to a molecule. A transition that involves both electronic and vibrational energy is termed 'vibronic'. Such transitions can be illustrated using the potential energy diagram shown in figure 1.2. Here, the Morse potential of the ground and excited states of a simple diatomic molecule are represented as a function of the internuclear separation  $r$ . In more complex polyatomic molecules, the term  $r$  is replaced by the nuclear configuration coordinate  $Q$ .

In figure 1.2, the vibrational states of the molecule are represented by horizontal lines that are bounded by the two morse curves. At room temperature, it is highly likely that the molecule will occupy the lowest vibronic level level  $\nu_0$  of the ground state  $U$ . In general, the absorption of light will cause a transition to some excited vibronic state  $\nu'_n$ . The lowest energy transition (often denoted as the 0-0 transition) is to the  $\nu'_0$  vibronic level of the excited state  $U'$ . Excitation to a higher vibronic level requires more energy and will thus absorb light at a shorter wavelength. During its typical lifetime, an excited molecule will relax to the  $\nu'_0$  vibronic level prior to de-excitation to the ground state. During this

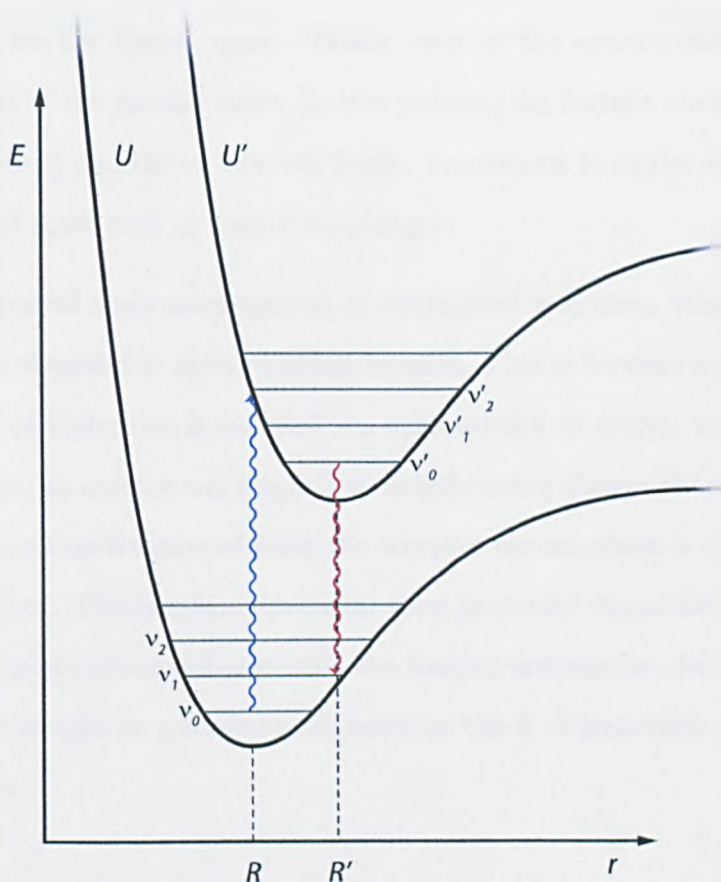


**Fig. 1.2:** Schematic configuration coordinate diagram illustrating the potential energy curves of the ground state  $U$  and excited state  $U'$  of a simple diatomic molecule. Horizontal lines represent vibrational states  $\nu$ , and vertical lines represent optical transitions (blue for absorption and red for emission).

non-radiative process, thermal energy is dissipated to the surrounding medium.

In some organic materials, these vibronic transitions are manifest by a series of narrow absorption bands. However, such features are generally absent from the absorption spectra of conjugated polymers. Due to the disordered nature of these materials, the ensemble of chromophores that are sampled during the process of absorption are subject to a distribution of energies. This causes the vibronic peaks to broaden and merge. Consequently, the  $\pi - \pi^*$  transition is typically characterised by a single featureless absorption band.

The process of emission is also depicted in figure 1.2. Here, a radiative transition occurs between the lowest lying vibronic level of the excited state and some vibronic level of the ground state. In this process, the highest energy transition is between the  $\nu'_0$  and the  $\nu_0$  vibronic levels. Transitions to higher vibronic levels in the ground state emit at longer wavelengths.

Unlike the typical absorption spectra of conjugated polymers, vibronic features can often be observed in their emission spectra. This is because a much smaller distribution of molecules is sampled - a consequence of energy transfer. After its generation, an exciton can migrate to neighbouring chromophores prior to its decay. This process is favoured when the acceptor chromophore is of lower energy than the donor. The emission spectrum then generally represents a fraction of the lowest energy chromophores with the longest conjugation lengths. Energy transfer also results in a Stokes shift between the 0-0 transition of absorption and emission.

### 1.3.2 Interchain Excitations

When two or more conjugated molecules are brought into close proximity, their  $\pi$ -electrons can interact. Depending upon the nature of the interaction, a variety of intermolecular states can be formed.

If the interaction occurs between two molecules of the same species when they are both in the ground state, the resulting intermolecular state is termed an aggregate. In the formalism described by Schwartz *et al.*,<sup>11</sup> the term aggregate strictly refers to the conjoining of electronic systems on adjacent molecules. This should be distinguished from agglomeration which describes the process of molecular coalescence without any significant modification of the individual electronic systems. The aggregate state is characterised by a new absorption band that is red-shifted relative to the intramolecular transitions of isolated chromophores.<sup>12</sup> Emission from the aggregate is usually broad and featureless and is also red-

shifted relative to the emission of the intrachain state. Aggregate formation is often identified by significant variations in a material's thin-film and solution spectra.

An intermolecular state can also result from the interaction between an excited chromophore and a ground-state chromophore. When the two interacting chromophores are of the same species, the new state is called an 'excimer' (contracted from the term 'excited-dimer'). Like aggregates, excimers are also characterised by a broad and featureless emission band that is red-shifted relative to the intrachain emission. However, as these are generated by an intramolecular transition, excimers exhibit no distinguishable absorption features. When the two interacting chromophores are of different species, the resulting excitation is called an exciplex (contracted from the term 'excited-complex'). Generally, exciplexes involve some degree of charge transfer between an electron donor and electron acceptor. Both excimers and exciplexes are dissociative in the ground state.<sup>13</sup>

The above discussion considers only the interactions that occur between neighbouring molecules. However, given that a single polymer chain can consist of multiple chromophores, it is also possible for these 'interchain' states to form between two conjugated segments on the same molecule.

## 1.4 Polymeric Light-Emitting Diodes

In its simplest format, the polymer light-emitting diode consists of a single layer of electroluminescent material that has been deposited between two unlike electrical contacts. When an appropriate driving bias is applied to this structure, charge carriers of opposing polarity (electrons and holes) are injected from the two electrodes. These will then drift towards each other under the influence of the electric field. A percentage of the carriers will approach closely enough such that their mutual Coulombic interaction becomes significant. At a critical distance  $r_c = e^2/4\pi\epsilon k_B T$  (where  $\epsilon$  is the electric permittivity of the polymer,  $T$



is the temperature and  $k_B$  is the Boltzmann constant), the Coulombic binding energy of the electron and hole exceeds the thermal energy of the individual carriers, and bimolecular recombination becomes inevitable.<sup>14</sup> Light is then generated when the resultant exciton undergoes radiative relaxation to the ground state.

The principles of operation of a polymer light-emitting diode can be understood by considering the energy level diagram shown in figure 1.3. For charge injection to occur at the respective polymer-electrode interfaces, a potential barrier must be overcome. The magnitude of the barrier to electron injection ( $\Delta E_e$ ) is determined by the difference in energy between the electron affinity of the polymer (EA) and the work function of the cathode ( $\phi_c$ ). Likewise, the injection barrier to holes ( $\Delta E_h$ ) is dependent upon the ionisation potential (IP) of the polymer and the work function of the anode ( $\phi_a$ ). The facile injection of charge carriers is achieved by minimising these barriers.

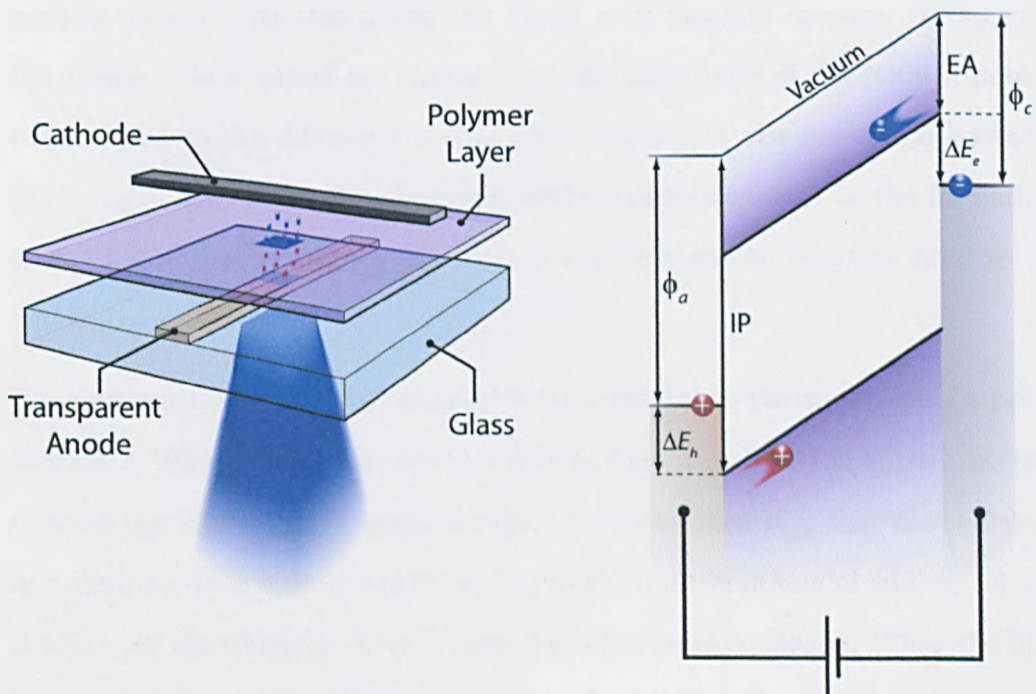


**Fig. 1.3:** (Left) An illustration of the constituent layers of a simple organic light-emitting diode with a bottom-emission structure. (Right) The corresponding energy level diagram when the diode has been biased in the forward direction.

Typically, low work function metals such as barium,<sup>15</sup> calcium<sup>16</sup> and magnesium (alloyed with silver)<sup>17</sup> are used as a cathode material. However, these metals are highly reactive and have been identified as a possible source of instability during device operation.<sup>16,18–20</sup> An alternative cathode structure has been investigated whereby a thin buffer layer of lithium fluoride or cesium fluoride is used to enhance injection from an air stable metal such as aluminium.<sup>21,22</sup>

An alloy of indium and tin oxide (ITO) is commonly used for the anode. Not only does this material have a high work function (4.8 eV) that is well matched to the ionisation potential of many conjugated polymers, but it is also largely transparent over the visual spectrum. In the standard bottom-emitting OLED structure, emission from the device is viewed through an ITO coated glass substrate.

The difference in the work functions of the two electrode metals results in the formation of a built-in potential ( $V_{bi}$ ). During the fabrication of the metal-semiconductor-metal structure, electronic redistribution will occur until equilibrium is reached. At this point, the Fermi level remains constant throughout the device. These principles suggest that the magnitude of the built-in potential is equal to the difference in the work function of the two metal contacts ( $V_{bi} = \phi_a - \phi_c$ ). In practice however, additional factors such as the formation of dipoles or the occurrence of chemical reactions at the interface need to be considered.

The presence of the built-in potential is fundamental to the operation of a polymer LED. When there is no external driving bias, the direction of built-in field opposes the injection of charge carriers. A driving bias  $V_{app}$  that is equivalent in magnitude (but opposite in direction) to the built-in potential will cancel out the internal electric field. This is termed the flat band condition. When the bias is increased beyond  $V_{bi}$ , a bipolar drift current is induced.

### 1.4.1 Current-Voltage Characteristics of PLEDs

The flow of current through a polymer light-emitting diode is ultimately determined by the rate of charge injection from the electrodes, and the subsequent drift of carriers under an applied field. The relative influence that these processes have on the electronic response of the diode is dependent upon the mobility of the semiconductor ( $\mu$ ) and the magnitude of the injection barriers ( $\Delta E$ ).<sup>23</sup> The current-voltage (I-V) characteristics of an OLED can thus be identified as being either injection-limited or bulk-limited.

#### Charge Carrier Transport

In the bulk-limited regime, the drift velocity of the charge carriers is insufficient to accommodate the injection current at the polymer/electrode interface. This causes an accumulation of carriers in the vicinity of the contact. The build-up of space charge acts to reduce the electric field across the interface, and inhibits the injection of further carriers. The current that is drawn by the device is then dependent upon the properties of the bulk film and not the contacts, which are said to be ohmic.

Child's law is used to describe the bias dependence of a trap-free space charge limited current (TFSLC) that flows through a dielectric solid.<sup>24,25</sup>

$$J_{TFSLC} = \frac{9}{8} \epsilon_0 \epsilon_r \mu \frac{V^2}{d^3} \quad (1.1)$$

The current density,  $J_{TFSLC}$ , exhibits a quadratic dependence on the net bias,  $V = V_{app} - V_{bi}$ . When expressed in terms of the internal field, the current density is proportional to the reciprocal of the film thickness  $d$ . It should be noted that this formalism does not consider the influence of carrier traps,<sup>26</sup> nor does it account for the field dependent mobility that has been observed in many organic semiconductors.<sup>27,28</sup>

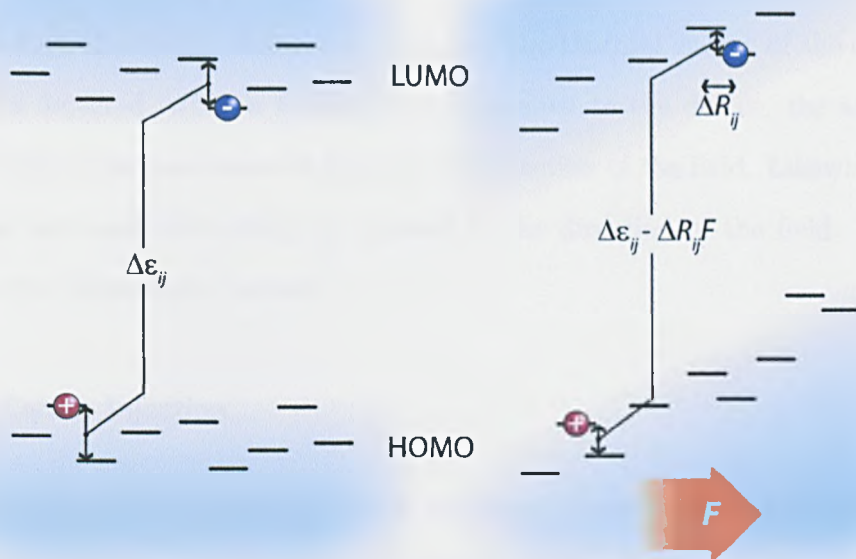


**Fig. 1.4:** A schematic diagram of charge-hopping within a distribution of transport states. Under an applied field  $F$ , the energy barrier to hopping in the forward direction  $\Delta\varepsilon_{ij}$  is reduced by  $\Delta R_{ij}F$ .

The process of charge carrier transport in a disordered organic semiconductor is manifest by a series of hopping events between localised states. This mechanism is depicted in figure 1.4. Electron transport can be considered as a series of oxidation and reduction events as the carrier vacates and occupies neighbouring conjugated segments in sequence. Hole transport can be considered as the reverse of this process. Each site that is vacated undergoes reduction back to its neutral state as the newly occupied site is oxidised.

During its transit across the film, a carrier may undergo multiple hopping events. As illustrated, this process will sample a series of transport states that are subject to both spatial and energetic distributions. The motion of the charge carrier can be modeled using the Miller-Abrahams formalism.<sup>29,30</sup>

$$v_{i \rightarrow j} = v_0 \exp(-2\gamma\Delta R_{ij}) \begin{bmatrix} \exp -[(\varepsilon_j - \varepsilon_i)/k_b T]; & \varepsilon_j > \varepsilon_i \\ 1; & \varepsilon_j < \varepsilon_i \end{bmatrix} \quad (1.2)$$

Here, the probability that a charge carrier will hop from an occupied site  $i$  to a neighbouring vacant site  $j$  is dependent upon the spatial separation of the two states ( $\Delta R_{ij}$ ), the energy barrier ( $\epsilon_j - \epsilon_i$ ), and the thermal energy of the carrier ( $k_b T$ ). As depicted, when a forward bias is applied to the device, the average barrier height is reduced when  $\Delta R_{ij}$  is in the direction of the field. Likewise, the barrier is increased when  $\Delta R_{ij}$  is opposed to the direction of the field. A net drift current is therefore induced.

### Charge Carrier Injection

When the barrier to charge injection is significant, the resulting current flow is considered to be contact limited. The charge carriers have sufficient mobility to drift across the device without the build-up of space charge at the injecting contact. In this scenario, the factor that determines current flow is the rate at which charge can be transferred from the contact into the semiconductor. There are two main processes that are considered to be important with regard to carrier injection; thermal excitation into the transport states and tunneling through the energy barrier. Thermionic emission is described by the Richardson equation

$$J_{TE} = AT^2 \exp \frac{-E_b}{k_b T} \quad (1.3)$$

where  $A$  is Richardson's constant,  $T$  is the temperature and  $E_b$  is the energy barrier at the interface. Here, a reduced barrier term  $E_b$  has been introduced to represent the Schottky effect whereby the presence of an injected charge carrier at the interface induces an image charge at the surface of the contact.<sup>31</sup> The field that is produced by this charge effectively lowers the injection barrier by  $\sqrt{Fq/4\pi\epsilon}$  relative to the zero-field barrier  $\Delta E$ . The thermionic emission current is then dependent upon the electric field ( $F$ ) across the interface.

Thermionic emission has been identified as the dominant injection process for most device structures under standard operating conditions.<sup>14,32</sup> However, at

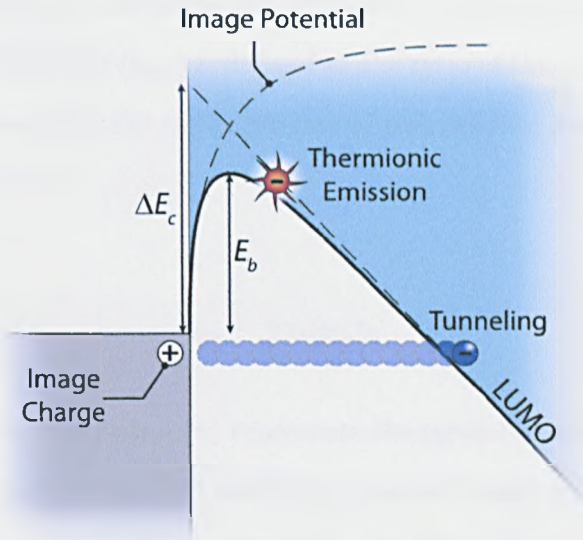


**Fig. 1.5:** Schematic diagram of thermionic and tunneling carrier injection. The effective reduction in barrier height due to the image charge has also been illustrated.

low temperatures and high applied bias, a significant tunneling current can be sustained. This current is described by the Fowler-Nordheim equation for a carrier tunneling through a triangular energy barrier.<sup>33</sup>

$$J_{FE} \propto F^2 \exp\left(\frac{-8\pi\sqrt{2m^*}}{3qh} \frac{\Delta E^{3/2}}{F}\right) \quad (1.4)$$

Here,  $m^*$  is the effective mass of the carrier.

It should be noted that when in the injection-limited regime, the actual current that passes through the device is substantially less than is predicted by either the thermionic or field emission equations. This is accounted for by an interface recombination current that results from the back flow of injected carriers.

## 1.5 Device Efficiency

In an ideal device, each of the injected charge carriers will contribute to the emission of light. In practice however, there are both fundamental limits and

extraneous processes that diminish the efficiency of electroluminescence. The external quantum efficiency ( $\eta_{\text{ext}}$ ) is defined as the ratio of the number of photons that are emitted from the LED to the number of charges that are flowing through the external circuit.<sup>7,34</sup>

$$\eta_{\text{ext}} = \gamma \chi_s \eta_{\text{PL}} \eta_c \quad (1.5)$$

The first term in this expression ( $\gamma$ ) represents the recombination efficiency. Not all of the charges that are injected into the device will come within the coulomb capture radius of an oppositely charged carrier prior to their extraction. These charges contribute to a leakage current that flows through the device without forming excitons. The magnitude of this current is significantly enhanced when there is an imbalance in the flow of holes and electrons. Numerical simulations have shown that an imbalance in the mobility of the two carriers can be compensated for through the manipulation of their respective injection barriers.<sup>35</sup>

In contrast to the process of photoluminescence, electrically generated excitons can be of either singlet or triplet spin multiplicity. As the radiative decay of triplet excitons is a forbidden transition, only the fraction of excitons that are formed in the singlet state ( $\chi_s$ ) will contribute to emission. If it is assumed that the electrical generation of excitons is indiscriminate of spin, a singlet to triplet ratio of 1:3 may be expected. Although this is close to the experimentally determined value for small molecular materials,<sup>36</sup> it has been suggested that higher ratios can be obtained from some polymers.<sup>37</sup> This inherent limit on OLED efficiency can be overcome through the use of phosphorescent dopants. These materials (which contain a high-atomic-weight element such as platinum or iridium) facilitate luminescence from the triplet state. High internal efficiencies approaching 100% have been reported using such materials.<sup>38</sup>

The third term ( $\eta_{\text{PL}}$ ) describes the radiative efficiency of singlet excitons. As these are necessarily generated by the absorption of light, this value can also be

referred to as the photoluminescence quantum efficiency (assuming the process of intersystem crossing followed by phosphorescence to be negligible). Some conjugated dyes such as 9,10-diphenylanthracene<sup>39</sup> and Rhodamine 6G<sup>9</sup> have a PL quantum efficiency close to 100%. Typically however, non-radiative processes will decrease this value to below the ideal. This is especially true of solid samples within which the influence of a low concentration quenching centers can be greatly enhanced via exciton migration. Nonetheless, solid-state PL quantum efficiencies above 50% have been attained from some polymeric materials.<sup>40</sup>

The product of the first three terms in equation 1.5 is known as the internal quantum efficiency ( $\eta_{int}$ ) and is defined as the ratio of the number of photons generated inside the device to the number of electrons injected. Due to the occurrence of internal reflection at the constituent interfaces, only a fraction of these photons escape the device in the forward viewing direction. The internal and external quantum efficiencies are therefore related via the outcoupling efficiency ( $\eta_c$ ).

An estimation of  $\eta_c \approx 1/2n^2$  can be calculated by considering the emission from an isotropic point source within a polymeric layer of refractive index  $n$ . Consequently, an outcoupling efficiency as small as 20% is not unusual from a standard device structure. Various techniques have been investigated in an attempt to improve the extraction efficiency of organic LEDs. This has been achieved through the incorporation of structures such as microlenses<sup>41</sup>, photonic crystals<sup>42</sup> and scattering layers<sup>43</sup>.

## 1.6 Summary

With regard to the development of OLED technologies, several key milestones have already been reached. In 1997, Tohoku Pioneer Corporation incorporated the first commercially available monochrome OLED into a car stereo display.<sup>44,45</sup> This was followed by the development of full-colour active-matrix displays. In a



joint venture between the Eastman Kodak Company and Sanyo, the first of these devices (introduced with the Kodak EASYSHARE LS633 digital camera) was released in 2003.<sup>46,47</sup> More recently, Sony have produced an 11" OLED television, the XEL-1<sup>3</sup> and OQO have incorporated a 5" OLED touch screen into their model 2+ ultra mobile PC.<sup>48</sup>

Although a less mature technology than the small-molecule OLED (SMOLED) devices, polymer-based LEDs have also reached the consumer market. In 2002, Philips released the Norelco Spectra 8894XL electric razor, incorporating a monochrome PLED display.<sup>49</sup> The fabrication of more complex full-colour displays has also been demonstrated. This technology however is in need of further development prior to commercial release. Issues regarding the lifetime, efficiency and colour saturation of PLED devices have been of particular concern. As a consequence, there are ongoing efforts to develop new materials and device architectures.

Of the three primary colours, it is the development of a stable and efficient blue-emitting PLED that has proven the most problematic. Researchers at Cambridge Display Technologies (CDT) have recently reported upon the fabrication of a blue device with an efficiency of 12 cd/A and a lifetime of approximately 18,000 hours.<sup>50</sup> Although a significant achievement, these properties are still inferior to the latest red and green emitting PLEDs with efficiencies of up to 60 cd/A and lifetimes reaching 200,000 hours. It should be noted that the lifetimes quoted here represent the time over which the device's luminance decays to half of its initial value (of 1000 cd/m<sup>2</sup>) when driven with a constant current. This does not necessarily represent the application-dependent lifetime over which the device is useable. For instance, differential aging between the three primary sub-pixels of a full-colour display would result in a notable image artifact over a much shorter period of time.

One of the primary focusses of PLED development is the synthesis and characterisation of new electroluminescent materials. This thesis documents the inves-

tigation into a series of newly synthesised wide energy-gap conjugated polymers - 2,7-linked poly(N-substituted carbazole)s. These materials are intrinsically blue-emitting. However, through the use of appropriate copolymerisation or side-chain attachment, polycarbazoles can be engineered to emit throughout the visible and near IR regions of the electromagnetic spectrum.

Seven different polymers were investigated during this work. In chapter 2, these materials are introduced and broadly categorised by their side-chain substitutions - alkyl, aryl and triarylamine groups. This chapter also details the experimental techniques that have been employed. The fabrication of electroluminescent devices is discussed along with their electronic and optical characterisation.

Chapter 3 details an investigation into the stability of these materials. This study focussed upon a selection of the polymers that were exposed to variety of thermal treatments. The occurrence of degradation was monitored by recording the evolution of each polymer's photoluminescence spectrum at various times throughout the treatment. The role of oxidation was considered by comparing samples that were exposed to air with those that were kept under an inert N<sub>2</sub> atmosphere.

The process of charge-carrier flow under an applied bias is fundamental to the operation of an organic LED. To investigate this phenomenon, a range of analytical techniques have been developed. Among these, the time-of-flight (TOF) photocurrent measurement has been frequently adopted. Chapter 4 reports upon TOF measurements that were carried out using two of the polymers. These measurements were used to relate the mobility of different charge carriers to the chemical composition of the polymer.

Chapters 5 and 6 cover the fabrication and characterisation of light-emitting diodes. In the first of these chapters, LEDs that were fabricated using a simplified 'single-component' device structure are discussed. Multi-component heterojunction devices are the topic of chapter 6. The performance of each device was determined through the measurement of spectroscopic and current-voltage-

luminance (I-V-L) characteristics.

The final results chapter details the solvatochromic behaviour that was observed from one of the polymers. When in solution, the photoluminescence (PL) spectrum of this material exhibited a strong dependence upon the polarity of the solvent. Both steady-state and time-resolved spectroscopies were employed to investigate this phenomenon.

---

**References**

- [1] Tang, C. W. and Vanslyke, S. A. *Appl. Phys. Lett.* **51**(12), 913–915 (1987).
- [2] Burroughes, J. H., Bradley, D. D. C., Brown, A. R., Marks, R. N., Mackay, K., Friend, R. H., Burns, P. L., and Holmes, A. B. *Nature* **347**(6293), 539–541 (1990).
- [3] Sony, *www.sony.com*. Last accessed 19/06/2009.
- [4] Anslyn, E. V. and Dougherty, D. A. *Modern Physical Organic Chemistry*. University Science, (2006).
- [5] Klaerner, G. and Miller, R. D. *Macromolecules* **31**(6), 2007–2009 March (1998).
- [6] Fox, M. A. *Optical Properties of Solids*. Oxford University Press, (2001).
- [7] Friend, R. H., Gymer, R. W., Holmes, A. B., Burroughes, J. H., Marks, R. N., Taliani, C., Bradley, D. D. C., Dos Santos, D. A., Bredas, J. L., Logdlund, M., and Salaneck, W. R. *Nature* **397**(6715), 121–128 (1999).
- [8] Valeur, B. *Molecular Fluorescence*. Wiley-VCH, 1st edition, (2002).
- [9] Lakowicz, J. R. *Principles of Fluorescence Spectroscopy*. New York : Springer, 3rd edition, (2006).
- [10] Köhler, A. and Beljonne, D. *Adv. Funct. Mater.* **14**(1), 11–18 January (2004).
- [11] Schwartz, B. J. *Annu. Rev. Phys. Chem.* **54**, 141–172 (2003).
- [12] Nguyen, T. Q., Doan, V., and Schwartz, B. J. *J. Chem. Phys.* **110**(8), 4068–4078 (1999).
- [13] Birks, j. b. *Rep. Prog. Phys.* **38**(8), 903–974 (1975).
- [14] Scott, J. C., Brock, P. J., Salem, J. R., Ramos, S., Malliaras, G. G., Carter, S. A., and Bozano, L. *Synth. Met.* **111**, 289–293 June (2000).
- [15] Brewer, P. J., Lane, P. A., Huang, J. S., DeMello, A. J., Bradley, D. D. C., and DeMello, J. C. *Phys. Rev. B: Condens. Matter Mater. Phys.* **71**(20), 205209 May (2005).
- [16] Broms, P., Birgersson, J., Johansson, N., Logdlund, M., and Salaneck, W. R. *Synth. Met.* **74**(2), 179–181 (1995).
- [17] Tsutsui, T., Aminaka, E., and Tokuhisa, H. *Synth. Met.* **85**(1-3), 1201–1204 (1997).
- [18] Gong, X. O., Iyer, P. K., Moses, D., Bazan, G. C., Heeger, A. J., and Xiao, S. S. *Adv. Funct. Mater.* **13**(4), 325–330 (2003).
- [19] Luo, S. C., Chung, H. H., Pashuck, E. T., Douglas, E. P., and Holloway, P. H. *Thin Solid Films* **478**(1-2), 326–331 May (2005).

- [20] Chen, Z. Y. and Ma, D. G. *Mater. Sci. Eng. B-Solid State Mater. Adv. Technol.* **141**(1-2), 71–75 June (2007).
- [21] Hung, L. S., Tang, C. W., and Mason, M. G. *Appl. Phys. Lett.* **70**(2), 152–154 (1997).
- [22] Brown, T. M., Friend, R. H., Millard, I. S., Lacey, D. J., Burroughes, J. H., and Cacialli, F. *Appl. Phys. Lett.* **79**(2), 174–176 (2001).
- [23] Wolf, U., Barth, S., and Bassler, H. *Appl. Phys. Lett.* **75**(14), 2035–2037 October (1999).
- [24] Abkowitz, M., Facci, J. S., and Rehm, J. *J. Appl. Phys.* **83**(5), 2670–2676 March (1998).
- [25] Campbell, A. J., Bradley, D. D. C., and Antoniadis, H. *J. Appl. Phys.* **89**(6), 3343–3351 March (2001).
- [26] Campbell, A. J., Bradley, D. D. C., and Lidzey, D. G. *J. Appl. Phys.* **82**(12), 6326–6342 December (1997).
- [27] Murgatroyd, P. N. *J. Phys. D: Appl. Phys.* **3**(2), 151 (1970).
- [28] Malliaras, G. G. and Scott, J. C. *J. Appl. Phys.* **85**(10), 7426–7432 May (1999).
- [29] Miller, A. and Abrahams, E. *Phys. Rev.* **120**(3), 745–755 (1960).
- [30] Bassler, H., Schonherr, G., Abkowitz, M., and Pai, D. M. *Phys Rev B: Condens Matter Mater Phys* **26**(6), 3105–3113 (1982).
- [31] Sze, S. M. *Physics of Semiconductor Devices*. Wiley-Interscience, 3<sup>rd</sup> edition, (2007).
- [32] Davids, P. S., Campbell, I. H., and Smith, D. L. *J. Appl. Phys.* **82**(12), 6319–6325 December (1997).
- [33] Parker, I. D. *J. Appl. Phys.* **75**(3), 1656–1666 (1994).
- [34] Forrest, S. R., Bradley, D. D. C., and Thompson, M. E. *Adv. Mater.* **15**(13), 1043–1048 (2003).
- [35] Crone, B. K., Davids, P. S., Campbell, I. H., and Smith, D. L. *J. Appl. Phys.* **84**(2), 833–842 July (1998).
- [36] Baldo, M. A., O'Brien, D. F., Thompson, M. E., and Forrest, S. R. *Phys. Rev. B: Condens. Matter Mater. Phys.* **60**(20), 14422–14428 November (1999).
- [37] Wilson, J. S., Dhoot, A. S., Seeley, A. J. A. B., Khan, M. S., Kohler, A., and Friend, R. H. *Nature* **413**(6858), 828–831 October (2001).
- [38] Adachi, C., Baldo, M. A., Thompson, M. E., and Forrest, S. R. *J. Appl. Phys.* **90**(10), 5048–5051 November (2001).

- [39] Gore, M. G., editor. *Spectrophotometry and Spectrofluorimetry*. OUP Oxford, 2<sup>nd</sup> edition, (2000).
- [40] Ariu, M., Lidzey, D. G., Sims, M., Cadby, A. J., Lane, P. A., and Bradley, D. D. C. *J. Phys.: Condens. Matter* **14**(42), 9975–9986 (2002).
- [41] Möller, S. and Forrest, S. R. *J. Appl. Phys.* **91**(5), 3324–3327 March (2002).
- [42] Lee, Y. J., Kim, S. H., Huh, J., Kim, G. H., Lee, Y. H., Cho, S. H., Kim, Y. C., and Do, Y. R. *Appl. Phys. Lett.* **82**(21), 3779–3781 May (2003).
- [43] Bathelt, R., Buchhauser, D., Garditz, C., Paetzold, R., and Wellmann, P. *Org. Electron.* **8**(4), 293–299 August (2007).
- [44] Tohoku Pioneer Corporation, <http://pioneer.jp/topec/index-e.html>. Last accessed 19/06/2009.
- [45] Kim, Y. and Ha, C.-S. *Advances in Organic Light-Emitting Devices*. Trans Tech Publications, (2008).
- [46] Kodak, [www.kodak.com](http://www.kodak.com). Last accessed 19/06/2009.
- [47] Kafafi, Z., editor. *Organic Electroluminescence*. CRC Taylor and Francis Group, (2005).
- [48] OQO, [www.oqo.com](http://www.oqo.com). Last accessed 19/06/2009.
- [49] Li, Z. R. and Meng, H., editors. *Organic Light-Emitting Materials and Devices*. CRC Press, (2006).
- [50] Halls, J. ‘Polymer OLED Technology Fundamentals, Status and Prospects’: Presented at SID 2008 - Los Angeles. Available from [www.cdtltd.co.uk](http://www.cdtltd.co.uk). Last accessed 24/03/2009.

## Chapter 2

# Experimental Methods

### 2.1 Introduction

This chapter provides an introduction to the materials that were under investigation. The molecular structure of each polymer is presented, and the motivation behind their synthesis is discussed.

The experimental techniques that have been used during this work are also detailed here. Spectroscopic measurements were carried out on both solutions and thin-films and included linear absorption and photoluminescence spectroscopy, time-resolved photoluminescence and PL quantum yield measurements.

The fabrication and characterisation of polymer light-emitting diodes is described. The preparation of time-of-flight samples is also discussed along with a brief description of the measurement technique as carried out at Queen Mary, University of London.

## 2.2 The Polymers Under Investigation

The synthesis and characterisation of new electroluminescent polymers is motivated by the need to develop more efficient and stable materials. Among the requisites for a promising material are the ability to accommodate mobile charge carriers, efficient luminescence, high stability both under operation and storage, and processability. There exists a number of synthetic strategies that have been adopted to attain these properties.

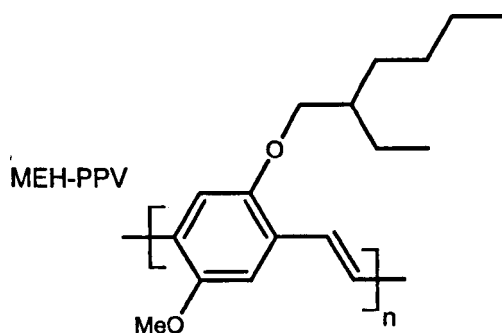
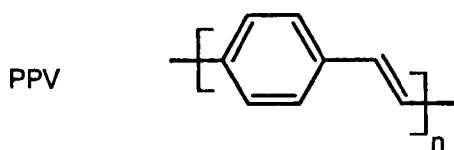
### 2.2.1 Arylene-Based Polymers

To date, there has been a substantial body of work reported on the development of new electroluminescent conjugated polymers. Much of this has been focussed on the synthesis of polyarylene and poly(arylene vinylene) type materials. Being the first conjugated polymer to exhibit electroluminescence, the parent compound of the poly(arylene vinylene)s, poly(*p*-phenylene vinylene) (PPV), and its derivatives are still some of the most widely researched compounds.

PPV itself is a green-yellow emitting polymer that is insoluble in organic solvents. Devices fabricated from PPV relied on the use of a precursor polymer that was soluble in methanol, and could be thermally converted after it had been spin-coated onto the substrate. However, these early devices operated at comparably high voltages (greater than 14V) with a low efficiency of 0.05% *ph/e*.<sup>1</sup> A soluble PPV derivative, poly[2-methoxy-5-(2-ethylhexyloxy)-*p*-phenylenevinylene] (MEH-PPV), was synthesised soon after.<sup>2</sup> Through the incorporation of solubilising alkoxy sidechains, this material could be spun directly from organic solvents such as xylene or tetrahydrofuran, simplifying the fabrication process. In addition, these devices were no longer susceptible to the detrimental affects of incomplete conversion or the formation of carbonyl defects that resulted from the precursor fabrication route of PPV.<sup>3</sup>



## Poly(arylene vinylene)s



## Polyarylenes

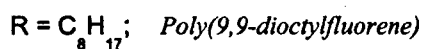
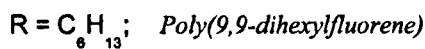
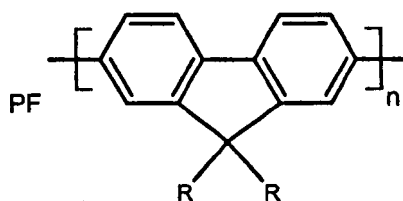
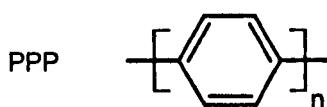


**Fig. 2.1:** The molecular structures of poly(*para*-phenylene vinylene) (PPV), poly(*para*-phenylene) (PPP), poly[2-methoxy-5-(2-ethylhexyloxy)-*p*-phenylenevinylene] (MEH-PPV) and polyfluorene (PF).

The first blue emitting polymer LED was fabricated using poly(9,9-dihexylfluorene).<sup>4</sup> A derivative of the polyarylenes, polyfluorene consists of a repeating biphenyl unit that is bridged at the 9-position (see figure 2.1). The added rigidity afforded by this structure leads to an increase in electronic conjugation along the molecule. Through the incorporation of a variety of functional units, polyfluorene copolymers have been synthesised that emit light throughout the visible spectrum.<sup>5,6</sup> Owing to their high emissive efficiency and excellent electrical properties, these materials have generated a great deal of interest.<sup>7,8</sup>

## 2.2.2 Carbazole-Based Polymers

Carbazole-based materials have been studied for many years. Poly(*N*-vinylcarbazole) (PVK) was first recognised for its photoconductive properties<sup>9</sup> but

has since found application as a hole transport material in organic light-emitting diodes. Unlike the materials discussed above however, PVK is not a fully conjugated molecule as the carbazole units are attached as isolated pendant groups to a saturated polyvinyl backbone. The first devices to incorporate main-chain polycarbazoles were reported by Romero *et al.* in 1996.<sup>10</sup> In poly(*N*-butyl-3,6-carbazolylene) (PBK), neighbouring carbazole units are attached at the 3- and 6-positions such that they are integral to the polymer backbone.

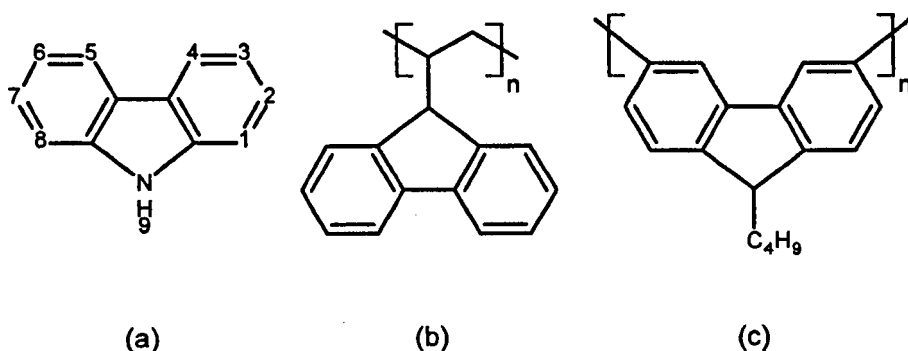


**Fig. 2.2:** Carbazole structures. (a) Diagram showing enumeration of the locants,<sup>11</sup> (b) the molecular structure of poly (*N*-vinylcarbazole) (PVK) and (c) the molecular structure of poly(*N*-butyl-3,6-carbazolylene) (PBK).

More recently, the synthesis of 2,7-linked polycarbazoles has been reported.<sup>12</sup> Like in PBK, these materials incorporate the carbazole unit into the polymer backbone. However, due to the increased electronic coupling afforded by their para linkages, these materials exhibit a higher degree of conjugation than their 3,6-linked analogs. The fabrication of a blue-emitting poly(*N*-alkyl-2,7-carbazole) electroluminescent device has also been published.<sup>13</sup>

Electrochemical analysis suggests that this new class of polymer has an intrinsically low ionisation potential.<sup>14</sup> However, these studies also revealed that the polymers were unstable. It has been postulated that, under oxidation, adjacent polymer chains could form cross-links due to the reactive nature of the

3,6-positions. The formation of these defects under device operation could result in reduced carrier mobilities and quenched emission.

Due to their low ionisation potential, these materials present a much smaller barrier to the injection of holes from an ITO interface than the poly(dialkyl fluorene)s. As the efficient generation of electroluminescence is dependent upon the balance of n- and p-type currents, 2,7-linked polycarbazoles could potentially be used in the fabrication of high-efficiency polymer light-emitting diodes. Before this can be realised however, issues regarding the stability of the material must be addressed.

### 2.2.3 2,7-Linked Polycarbazoles

It is the main-chain polycarbazoles described in this section are the subject of this thesis. The synthesis and preliminary chemical analyses of these materials were carried out by Dr Ahmed Iraqi's group in the Department of Chemistry at the University of Sheffield.

Figure 2.3 shows the molecular structure of three alkyl substituted polymers. As discussed above these molecules possess a high degree of electronic conjugation due to the 2,7-linkage between consecutive carbazole units. Unlike the previously reported materials however, these polymers incorporate protecting methyl substituents at the 3,6-positions. Electrochemical studies have been used to confirm that this strategy was successful in improving the materials electrolytic stability.<sup>15</sup>

Polymer **P1** is the 3,6-protected homopolymer within which every carbazole unit contains the methyl substitutions. The copolymer **P2** incorporates the methyl protection on alternating units. **P1** exhibits a wider band-gap and larger ionisation potential as a consequence of the increased steric interactions between adjacent monomers.<sup>15</sup> The stability of both the homopolymer and copolymer appear to benefit from the presence of the 3,6-protecting groups.

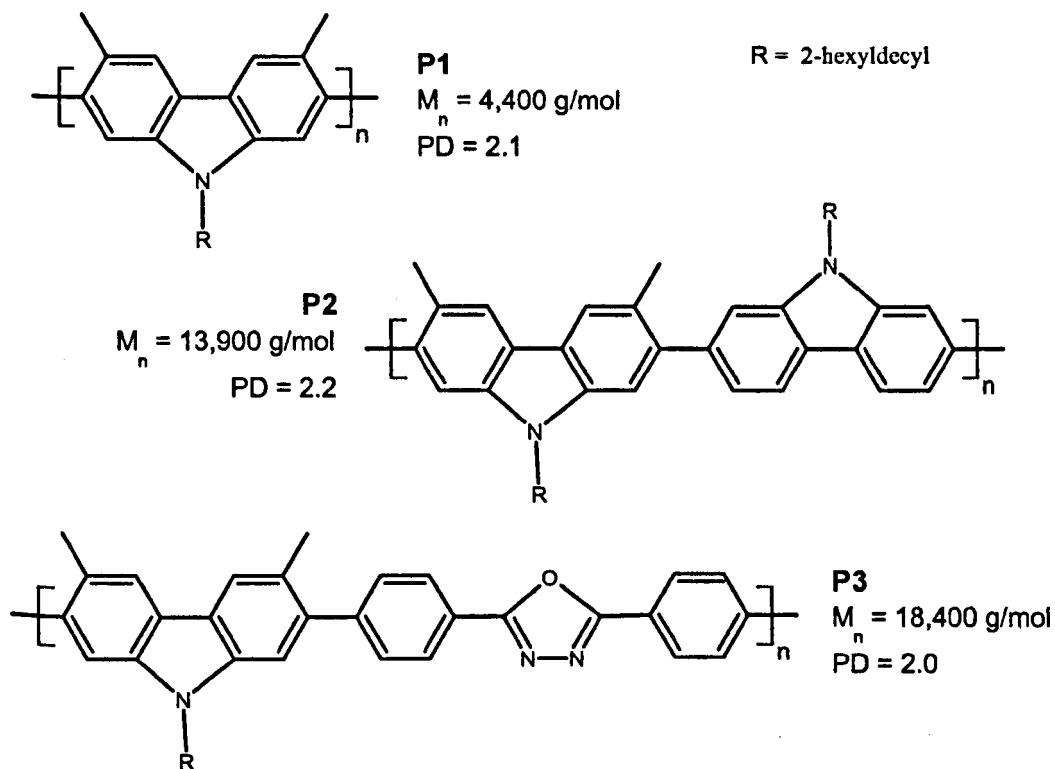


**Fig. 2.3:** The molecular structure of the alkyl-substituted polycarbazoles **P1**, **P2** and **P3**. The number averaged molecular weight ( $M_n$ ) and polydispersity (PD) of the samples are also presented.

Polymer **P3** is an alternating copolymer consisting of a methyl protected carbazole subunit and a biphenyl oxadiazole subunit. Oxadiazole containing compounds such as Bu-PBD have commonly been used as electron transporting and hole blocking materials in organic LEDs. Conventionally, they have been incorporated either as a separate layer deposited beneath the cathode,<sup>16</sup> or have been blended into the active layer.<sup>17,18</sup> An alternative approach is to incorporate the oxadiazole moiety directly into the emitting polymer. This can be done via a side-chain attachment<sup>19</sup> or by introducing it directly into the polymer backbone.<sup>20-22</sup> As carbazole containing polymers are generally efficient at accommodating and transporting hole polarons, the introduction of an oxadiazole moiety into **P3** is expected to improve the balance of charge carriers.

Figure 2.4 shows the molecular structure of two aryl substituted polycarbazoles. As is the case with the PPVs and the PFs, the presence of the side-chain helps to solubilise the molecule. However, when compared against the alkyl-substituted polycarbazoles, the larger steric demand of the phenyl moiety should make these polymers less susceptible to the formation of weakly emissive intermolecular excitations. This synthetic strategy has already been utilised with polyphenylene and poly(phenylene vinylene) type materials.<sup>23,24</sup> In polyindenofluorenes, it was also found that the aryl substituted polymer was less susceptible to the formation of ketone defects than the alkyl substituted molecule.<sup>25</sup>

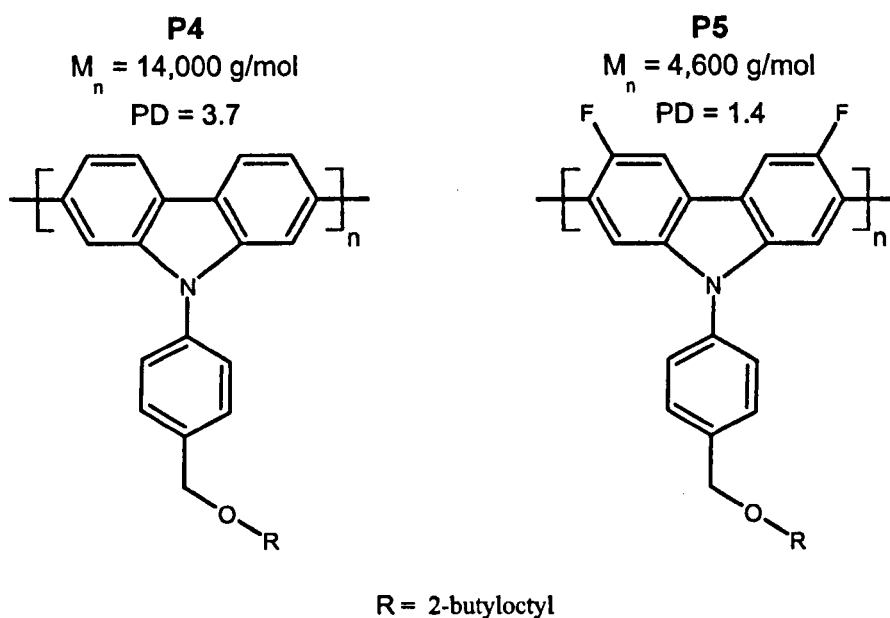


**Fig. 2.4:** The molecular structure of the aryl-substituted polycarbazoles **P4** and **P5**. The number averaged molecular weight ( $M_n$ ) and polydispersity (PD) of the samples are also presented.

Both polymers **P4** and **P5** are aryl-substituted carbazole homopolymers. **P5** differs from **P4** in that it has fluorine substitutions at the 3,6-positions. As discussed above, these substitutions help to stabilise the material during electrochemical analysis. Being highly electronegative however, these fluorine atoms not only protect the 3,6-positions, but also modify the electronic properties of the molecule. The incorporation of fluorine into PPV has been shown to increase its

electron affinity.<sup>26</sup> Improved performance was also reported from light-emitting diodes that contained a fluorinated fluorene-based copolymer when compared to a non-fluorinated analog.<sup>27</sup>

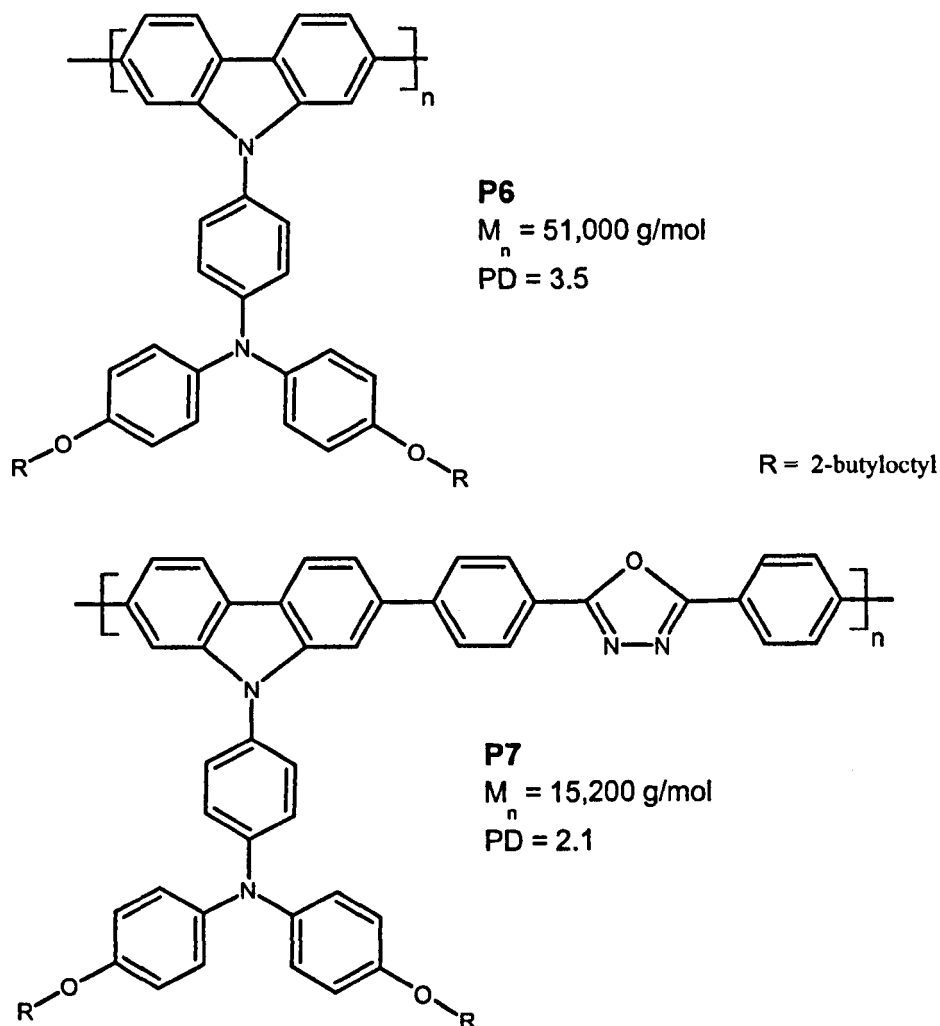


**Fig. 2.5:** The molecular structure of the triarylamine-substituted polycarbazoles **P6** and **P7**. The number averaged molecular weight ( $M_n$ ) and polydispersity (PD) of the samples are also presented.

The final class of polycarbazole to be investigated were the triarylamine substituted materials (see figure 2.5). Conventionally, triarylamine containing compounds such as the small molecule *N,N'*-Bis(3-methyl-phenyl)-*N,N'*-diphenyl-[1,1'-biphenyl]-4,4'-diamine (TPD)<sup>16</sup> and the polymer poly(9,9'-dioctylfluorene-*co-N*-(4-butylphenyl)diphenylamine) (TFB)<sup>28</sup> have been used as hole transport-

ing materials in light-emitting diodes. Due to their low ionisation potential, these materials present a small barrier to the injection of holes from an ITO anode. In addition, their high mobilities suggest that, when under a small driving bias these materials should be capable of sustaining a large hole current.<sup>29</sup>

In polymers **P6** and **P7** the triarylamine moiety is attached as a pendant group to the main-chain. These bulky side-groups should reduce the possibility of close molecular packing and minimise the formation of weakly emissive inter-chain species. Triarylamine substituents have been successfully introduced at the 9-position of a fluorene based polymer.<sup>30</sup> This material showed improved hole injection and stability over the analogous alkyl substituted polyfluorene. In addition, **P7** is copolymerised with the biphenyl oxadiazole unit which, as discussed above, should improve the injection and transport of electrons.

## 2.3 Sample Preparation

### 2.3.1 Polymer Solutions

All of the materials covered in this thesis were readily soluble in common organic solvents. The resulting solutions were primarily used in the fabrication of polymer thin films. Spectroscopic measurements were also carried out on solutions of varying polarity in order to investigate the interactions between the excited state and its local environment.

Solutions were prepared in pre-cleaned vials that had been rinsed with either acetone or IPA and dried under a pressurised stream of air. Typically, a few milligrams of material were weighed out into the vial, and an appropriate volume of solvent was added to it. The concentration of the solutions varied from 0.01 mg/ml to 80 mg/ml. All solutions were prepared using HPLC grade solvents. Whenever possible, the desired volume of solvent would be transferred to the vial using an adjustable-volume digital micropipette. However, when us-

ing highly volatile solvents such as chloroform, leakage within the micropipette necessitated the use of a conventional graduated pipette.

### **2.3.2 Thin-Film Deposition**

A variety of methods exist for the deposition of polymer thin films including dip-casting, drop-casting, soft lithography and ink-jet printing. However, when reproducibility and film uniformity are of importance, spin-casting<sup>31</sup> is the most suitable technique. All thin films discussed in this thesis were fabricated using this method. The films were cast using a Laurell Technologies manual dispense spin processor. Solutions for spin-casting were typically made at concentrations of 10 to 20 mg/ml. To ensure the removal of undissolved material and any particulates, the solutions were filtered using 0.2  $\mu\text{m}$  PTFE syringe mounted filters. Blend solutions were prepared by mixing pure solutions of the individual components at the required volume ratio.

Film thickness was measured using a Dektak 3ST surface profilometer. Part of the film was removed by running the rounded tip of a spatula across the sample whilst applying a small amount of pressure. Care was taken to ensure the surface of the underlying substrate was not scratched in the process. The the depth of the indentation was then measured. A stylus force of 10 mg was light enough to ensure that the surface of the film was not modified during the measurement.

## **2.4 Steady-State Spectroscopy**

### **2.4.1 UV/Vis Spectroscopy**

Absorption spectra were obtained using a Unicam UV 500 spectrometer. All solutions were measured in 1 mm path length quartz cuvettes. The baseline was measured with both the sample and reference cuvette filled with solvent. The



sample cuvette was then filled with the solution and the absorption spectrum obtained. Film samples were spun onto 15 × 15 mm Spectrosil 2000 substrates. A clean substrate was also placed in the reference beam.

## 2.4.2 Fluorescence Spectroscopy

The primary absorption band of all samples occurred in the near UV. Excitation could thus be achieved using the 325 nm line of a HeCd laser or the 351 nm and 364 nm lines of an Ar<sup>+</sup> laser. To minimise sample degradation, the beam was defocussed using a UV transmissive lens. Using a power density of no more than 0.1 mW/cm<sup>2</sup>, stable emission under ambient conditions was observed.

Time-integrated photoluminescence spectra were acquired using an Andor Technology Shamrock SR-303i imaging spectrograph. Light was coupled into the spectrograph through a Lumatec 380 series liquid lightguide and detected using an Andor DV420 CCD. The detector was cooled to -40 °C to improve the signal to noise ratio. All measurements reported in this thesis have been corrected for the spectral response of the system, and have had the background signal removed.

## 2.4.3 Photoluminescence Quantum Yield

Not all singlet excitons decay with the emission of light. There exist a number of non-radiative channels through which the excited molecule can relax to the ground state. It is the ratio of radiative ( $k_r$ ) to non-radiative ( $k_{nr}$ ) decay rates that determines the emissive efficiency of a fluorophore.

$$\eta_{\text{PL}} = \frac{k_r}{k_r + k_{nr}} \quad (2.1)$$

The photoluminescence quantum yield  $\eta_{\text{PL}}$  is the probability of photonic emission once a fluorophore has been optically excited. It can also be expressed as the

ratio of emitted to absorbed photons.

$$\eta_{\text{PL}} = \frac{\# \text{ photons emitted}}{\# \text{ photons absorbed}} \quad (2.2)$$

The measurement of  $\eta_{\text{PL}}$  of a material in solution is simplified by the assumption of isotropic emission. The light that is detected over a given solid angle is proportional to the total emission from the sample. With this requisite, it is possible to measure the emission from a sample relative to that of a well determined standard<sup>32</sup>. If the absorbance of the two samples and the refractive indices of the solutions is known then the quantum yield can be calculated from

$$\eta_{\text{PL}} = \eta_{\text{St}} \frac{I}{I_{\text{St}}} \frac{A_{\text{St}}}{A} \left( \frac{n}{n_{\text{St}}} \right)^2 \quad (2.3)$$

where  $I$  is the integrated intensity of the recorded emission spectrum,  $A$  is the absorbance of the sample and  $n$  is the refractive index of the solution. The subscript St denotes measurements taken of the standard. A commonly used standard is quinine sulphate in 0.1 M sulphuric acid with a known  $\eta_{\text{St}}$  of 0.577.<sup>32</sup>

In contrast, the intensity of emission from a thin film has a strong angular dependence. This makes it very difficult to measure the quantum yield of a sample relative to a standard. An alternative approach is to excite the film inside an integrating sphere. The internal surface of the sphere is made from a highly reflecting and diffusive material. Light that enters, or is produced within the sphere, undergoes multiple reflections before exiting through an aperture or being absorbed. The light flux within the sphere becomes spatially integrated and no longer exhibits an angular dependence. Emission from the sphere, detected from a small aperture or exit port, is then proportional to the net flux within the sphere, regardless of its angular distribution.

Greenham *et al.* reported the quantum efficiency of several poly(arylene vinylene) and polythiophene based thin-films using an integrating sphere.<sup>33</sup> The film

was excited using an Ar<sup>+</sup> laser, and emission from the sphere was detected by a calibrated photodiode. Using this technique, it is necessary to determine the absorption of the sample at the excitation wavelength. This was measured outside of the sphere using an absorption spectrometer. However, during the quantum yield measurement, laser light that is not initially absorbed by the sample is scattered from the rear surface of the sphere and redistributed. A fraction of this light will pass back through the sample and be absorbed. Therefore an additional measurement to determine the extent of this 'secondary' absorption and subsequent emission is required.

Emission from the sphere can also be recorded with a spectrometer.<sup>34</sup> Using this technique, the number of photons absorbed by the sample can be inferred from the spectra, negating the use of an independent absorption measurement. The methodology described here has been previously used to calculate the PL quantum efficiency of pristine<sup>35</sup> and blended<sup>36</sup> PFO films.

The samples were spun onto clean Spectrosil 2000 substrates that were transparent at the excitation and emission wavelengths. Typical film thicknesses were between 50 and 150 nm. All of the films were excited using the 351 and 364 nm lines of an Ar<sup>+</sup> laser that was allowed to stabilise for approximately two hours prior to use. The sample was excited through a small quartz window that was fitted to the entrance port of the sphere. Using a custom-made PTFE mount, the substrate was held at an oblique angle to the excitation beam such that the directly reflected light would not leave the sphere through the entrance port. To minimize the occurrence of photo-oxidation, the laser beam was defocussed to a diameter of approximately 1 cm and a power of no greater than 0.5 mW was used. During excitation, the sphere was continuously flushed with nitrogen. A small baffle was positioned between the sample and the exit port to prevent the direct incidence of emission on to the detector. At the exit port, light was collected by an optical fibre bundle and coupled to a SPEX 270M scanning monochromator with a 500 nm blaze, 1200 ln/mm grating. The output from the monochromator

was detected using a Hamamatsu R928 photomultiplier tube. The monochromator was connected to a DataScan control unit. Via an RS-232 serial link, this was then interfaced to a PC. Data was acquired using the Spectrad software that was supplied with the monochromator.

Calibration of the experimental setup is an important procedure. The sphere, collection fibre, monochromator and photomultiplier tube each have a different spectral response. A correction function for the combined system  $R(\lambda)$  was determined by measuring the emission from a calibrated 1000 W tungsten-halogen lamp. The lamp was placed perpendicular to the entrance port of the sphere, at a distance of 1-2 m. The measured spectrum  $S(\lambda)$  was then used to calculate the correction function using

$$S(\lambda) = E_{lamp}(\lambda) \times R(\lambda) \quad (2.4)$$

where  $E_{lamp}(\lambda)$  is the spectral irradiance of the calibrated lamp. All PL quantum yield measurements were corrected by multiplying the measured signal by  $1/R(\lambda)$  at each wavelength. Figure 2.6 shows the conversion factor from 300 nm to 800 nm.

To relate this data to a flux of detected photons, the corrected signal was then multiplied by the wavelength at which it was measured. Hence, using the notation specified above,

$$\phi(\lambda) \propto S(\lambda) \times \frac{1}{R(\lambda)} \times \lambda \quad (2.5)$$

where  $\phi(\lambda)$  is the total flux of photons being emitted at the exit port of the sphere. Exact determination of the photonic flux was not necessary as the proportionality constant cancels out in the final calculation of the PL quantum yield.

The measurement procedure consisted of two parts. In both cases, the laser was incident upon the sphere. The first measurement was of the spectrum obtained

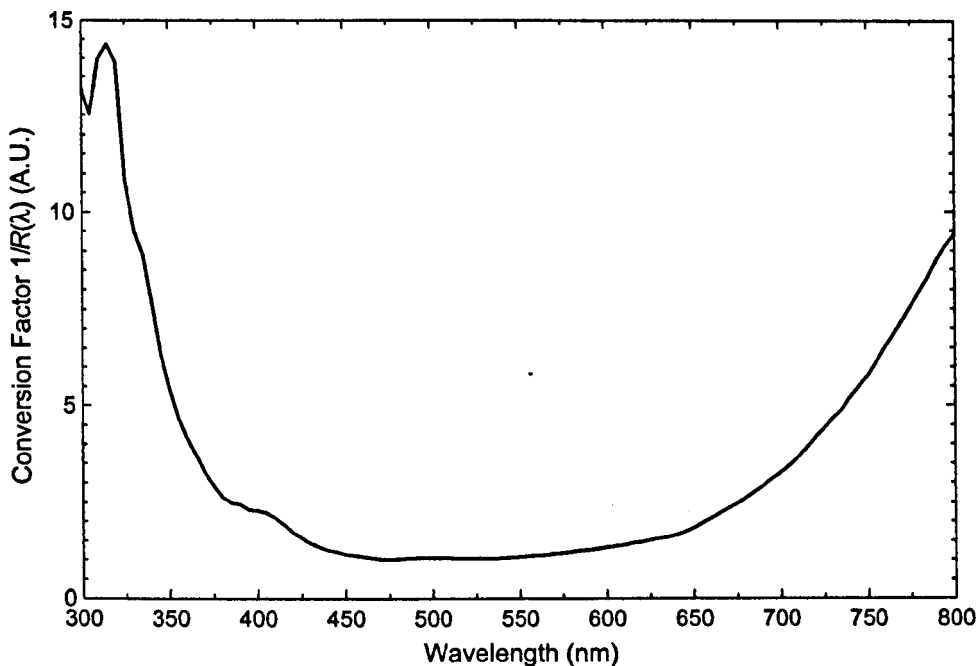


**Fig. 2.6:** Conversion factor ( $1/R(\lambda)$ ) used to calibrate the photoluminescence quantum yield measurement. Larger values toward the UV and red parts of the spectrum are representative of a reduction in sensitivity at these wavelengths.

when there was no sample present in the sphere. This was used to determine the flux of laser light prior to absorption,  $L$ , by integrating the spectrum with respect to wavelength. Here, the integration limits,  $\lambda_1$  and  $\lambda_2$  were chosen to encompass the entire wavelength range of the excitation source without impinging on the sample fluorescence.

$$L = \int_{\lambda_1}^{\lambda_2} \lambda \frac{S(\lambda)}{R(\lambda)} d\lambda \quad (2.6)$$

The second measurement was taken with the sample mounted inside the sphere. This spectrum contains both the emitted fluorescence and the laser light that has not been absorbed. Integrating this data between the limits of excitation,  $\lambda_1$  and  $\lambda_2$ , yields the flux of unabsorbed laser light  $L_S$ . The amount of light absorbed by the sample is therefore given by  $L - L_S$ . The flux of light resulting

from photoluminescence ( $PL$ ) is measured by integrating between the limits of emission,  $\lambda_2$  and  $\lambda_3$ . Hence, the photoluminescence quantum yield is calculated from

$$\eta_{PL} = \frac{PL}{L - L_S} \quad (2.7)$$

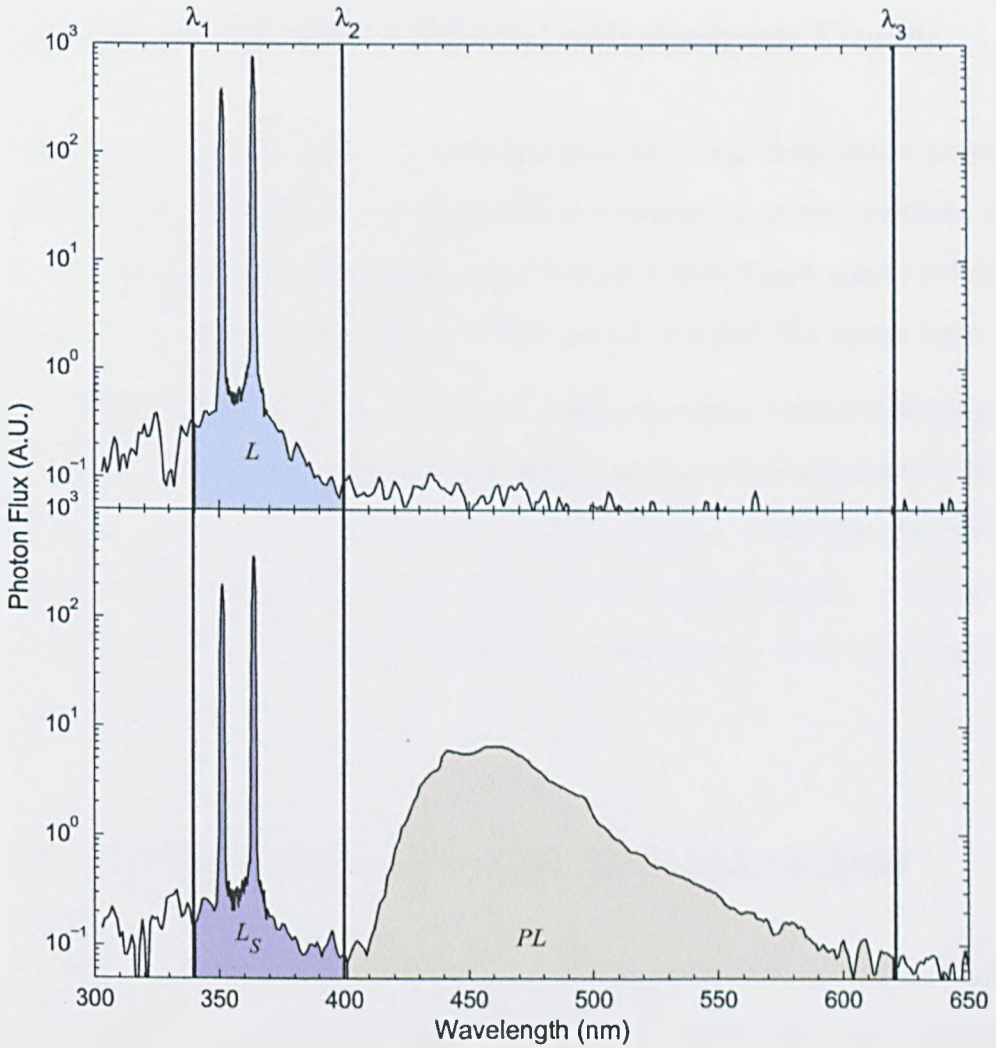


**Fig. 2.7:** Photoluminescence quantum yield measurement of a TFB thin film. Spectra have been plotted on a semi-log scale. **(Above)** The excitation spectrum taken with no sample. **(Below)** The PL spectrum and the remaining unabsorbed laser light. The integrals  $L$ ,  $L_S$  and  $PL$  are demonstrated, along with their defining limits  $\lambda_1$ ,  $\lambda_2$  and  $\lambda_3$ .

Figure 2.7 illustrates the integration limits described above. It should be noted that this method does not distinguish between emission that results from directly absorbed photons and emission caused by secondary absorption of the scattered laser. It is assumed that both mechanisms of photoluminescence are equivalent and that the quantum yield can be calculated using equation 2.7.<sup>37</sup>

## 2.5 Time-Resolved Photoluminescence Decay

Photoluminescence lifetime measurements were obtained from dilute polymer solutions. The samples were dissolved in either toluene or dichloromethane at a concentration of 0.1 mg/ml and were placed in 1 mm path length quartz cuvettes. Excitation at 380 nm was provided by a frequency-doubled Ti:Sapphire laser.

Measurement of the PL decay was achieved using the time-correlated single photon counting technique (TCSPC). Sample fluorescence was coupled into a SPEX 270M scanning monochromator and detected using an avalanche photodiode. The data was recorded using a Becker & Hickl SPC-830 module. Concurrent measurement of the time-integrated spectrum was used to detect any degradation of the polymer.

## 2.6 Device Fabrication and Characterisation

The LEDs discussed in this work were all fabricated using a standard set of processes. Device fabrication was a stepwise procedure that can be broadly categorised into four main processes, namely substrate preconditioning, polymer deposition, cathode evaporation and encapsulation.

The standard device structure that was used in this work is depicted in figures 2.8 and 2.9. The whole substrate can accommodate six individually addressable LEDs. Each of the device areas is defined by the overlap between the isolated anodes and the common cathode. Sandwiched between the two sets of electrodes are

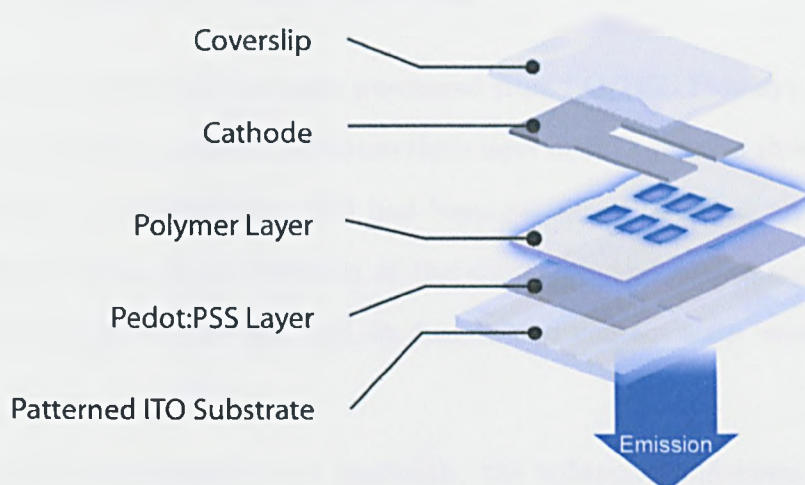


**Fig. 2.8:** Diagram depicting the layered structure of a typical polymer light-emitting diode.

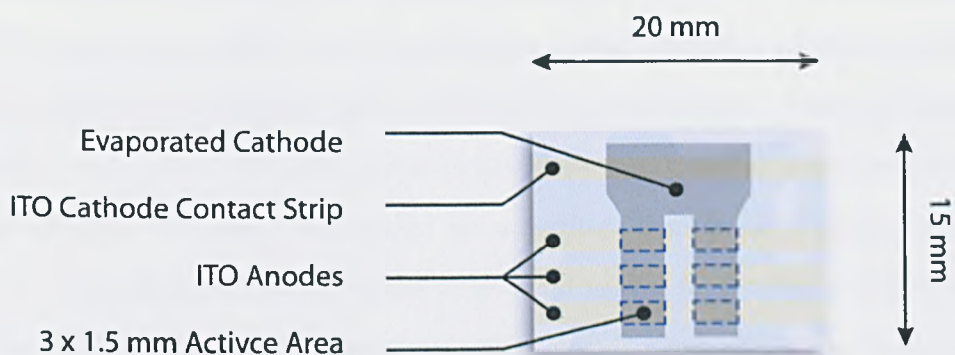


**Fig. 2.9:** Diagram showing how the active area of each device is defined by the overlap of the common cathode with the ITO fingers.

the organic layers. This structure is commonly referred to as 'bottom-emitting'. That is, emission from the device occurs primarily through the underside of the substrate.



## 2.6.1 Substrate Preconditioning

ITO coated glass substrates were purchased from LC-TEC Displays. They were  $20 \times 15 \times 1.1$  mm in size with a 110 nm thick layer of ITO giving a sheet resistance of  $20 \Omega/\square$ . As received, the ITO had been patterned to define three separate fingers protruding from each side of the substrate, and a continuous cathode contact strip across the top. All six fingers and contact strip were 1.5 mm in width.

Prior to the deposition of any materials, the substrate underwent a series of wet cleaning processes. Firstly, a lint-free cloth was doused with acetone and run across its surface, ensuring the removal of any large, strongly adhered contaminants. The substrate was then submerged in a 2% v/v aqueous solution of Hellmanex II, heated to 50 °C and sonicated for 10 minutes. A custom-made PTFE cradle was used to hold the substrate upright during sonication such that any dislodged particulates would fall away from its surface. Residual cleaning solution was rinsed off under a flow of deionised water, before the substrate was submerged in DI water and heated for a further 10 minutes. Finally, the substrate was transferred into a beaker of IPA and heated for 5 minutes before being dried under a pressurised flow of air. This cleaning procedure was based upon the method that has been recommended by H.C. Stark, the makers of Baytron P VP CH 8000 (now using the brand name Clevios<sup>TM</sup>).<sup>38</sup>

## 2.6.2 Device Fabrication

All of the LEDs discussed in this thesis are composed of multiple polymeric layers. The devices were fabricated by depositing each layer in sequence.

Additional to the electroluminescent layer, the typical device structure also incorporated a hole injection and transport layer adjacent to the anode. The intrinsically conducting complex formed from poly-(3,4-ethylenedioxythiophene) and

polystyrene sulfonic acid (PEDOT:PSS) was used for this purpose. A low conductivity grade of the material, Baytron P VP CH 8000, was purchased from H.C Stark. It was received as a dark blue aqueous solution suitable for spin-coating. The solution was dispensed directly onto the substrate through a 0.45  $\mu\text{m}$  PVDF syringe mounted filter and spun at 5000 rpm for 30 s. The thickness of the resulting film was approximately 50 nm. Immediately after the film was spun, a cotton bud wetted with DI water was used to wipe clean the cathode contact strip.

The film was dried by annealing it at 150 °C for 15 minutes under a  $\text{N}_2$  atmosphere. It has been shown that the removal of water from the PEDOT:PSS film can result in an increase in its conductivity.<sup>39</sup> Subsequent layers were spun in air. However, due to the hygroscopic nature of PEDOT:PSS, the films were stored under nitrogen until the deposition of the next layer.

The electroluminescent layer was deposited using the methods outlined in sections 2.3.1 and 2.3.2. Polymer solutions were prepared from toluene at a concentration of 10 to 20 mg/ml. Using a spin speed of between 1500 rpm and 3000 rpm would result in a film thickness of 50-100 nm. The exact parameters used to fabricate each device are detailed in the results section of this thesis. Again, the film was removed from the cathode contact using a cotton bud, this time wetted with toluene.

After the deposition of the organic layers, the device was transferred into a  $\text{N}_2$  filled integrated glovebox-evaporator system. This allowed for the handling of reactive materials to be carried out under oxygen and moisture deficient conditions (typically less than 1 ppm in both cases). The cathode was thermally evaporated using a Kurt J. Lesker thin film deposition system. A shadow mask was used to pattern the electrode. The material to be evaporated was placed into a suitable crucible, which in turn was fitted into a tungsten heater. The evaporator could accommodate three thermal sources, making it possible to deposit a tri-layer cathode without the need to break vacuum. A base pressure of  $< 1 \times 10^{-6}$  mbar

was reached prior to the evaporation.

The evaporation procedure was computer automated, with film thickness monitored using a quartz crystal microbalance. Depending upon the configuration of the top electrode, various materials were used. Aluminium and silver were deposited at a rate of 1 Å/s, calcium at a rate of 0.8 Å/s and lithium fluoride at a rate of 0.1 Å/s.

The device was encapsulated with a glass coverslip and UV curing epoxy prior to being removed from the glovebox. The epoxy was exposed for 10 minutes using a UV light box.

### 2.6.3 LED Characterisation

Electrical connection was made via a 2.54 mm pitch dual in line (DIL) edge-clip leadframe (see figure 2.10). As depicted, the top contact connects to the common cathode and the bottom three contacts connect to the ITO anodes on each side of the substrate. A test fixture, made from two ZIF (Zero Insertion Force) sockets mounted onto Veroboard could then be used to create a temporary electrical connection to the device.

A Keithley 237 integrated source-measure unit was used to both drive the device with a DC voltage and determine the resulting current flow. The luminance was measured simultaneously using a photodiode placed in close proximity to the emitting surface. The current from the photodiode was amplified prior to being recorded by a Keithley 2000 digital multimeter. Current-voltage-luminance (I-V-L) measurements were computer automated through a GPIB interface.

This measurement allows for the sensitive detection of low light levels. However, data recorded by the photodiode is not directly representative of the device's brightness. To obtain a photopically calibrated measurement that accounts for the spectral response of the human eye, a Topcon BM-8 luminance meter was used. For each device a calibration factor was determined. This factor was

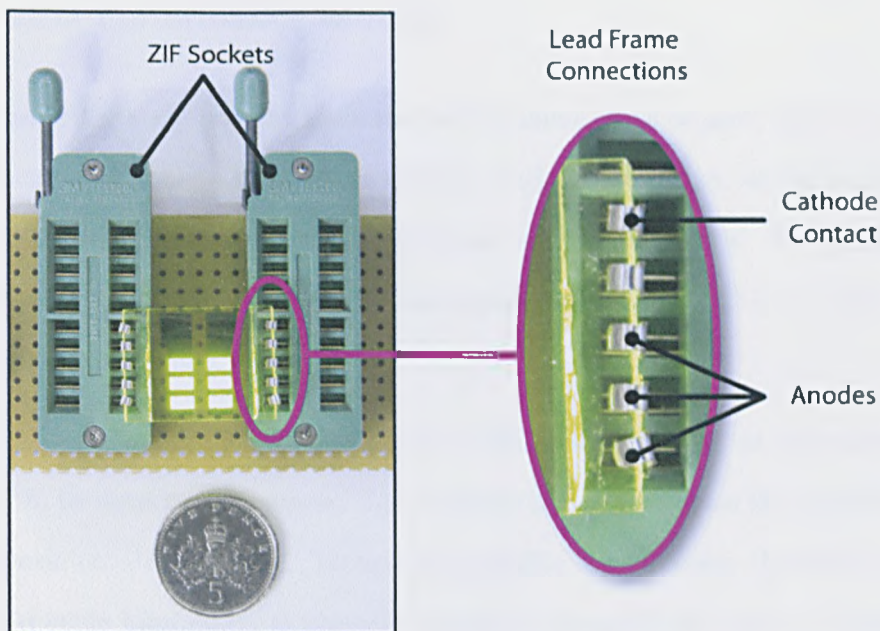


**Fig. 2.10:** Photograph of an operational LED, connected via a custom-made test fixture. All six devices are being driven in parallel.

then used to convert the current that was output from the photodiode into a corresponding luminance, expressed in candelas per square meter ( $\text{cd}/\text{m}^2$ ).

A conversion factor was obtained by measuring each device with both the photodiode and the luminance meter. To calculate an accurate value, it is important that the emission from the device is consistent in both measurements. This was best achieved under constant current operation. However, in some cases a lack of device stability meant that a reliable conversion factor could not be obtained. Consequently, these devices were measured directly with the luminance meter. This method however, has a reduced sensitivity.

Emission spectra were also obtained under constant current operation. Light was collected by a Lumatec liquid lightguide coupled to an Oriel Multispec 125 Spectrograph containing a 400  $\text{ln}/\text{mm}$ , 500 nm blaze grating. The spectrum was detected by an Andor DB 420 CCD, cooled to  $-40^\circ\text{C}$ . All spectra have been corrected for the combined response of the instrument.

## 2.6.4 LED Performance Metrics

A variety of criteria are used to assess the performance of an organic LED. These tend to focus on the aspects that are relevant to its application, which in most cases is as an electroluminescent emitter in an electronic display. To this end, two of the most frequently cited performance metrics for an OLED is the turn-on voltage and the efficiency.

The turn-on voltage can be broadly defined as the lowest voltage at which luminescence can be detected. However, this is clearly dependent upon the sensitivity of the experimental apparatus. To avoid ambiguity, an emission threshold, defined at a specific luminance, is typically reported alongside the turn-on voltage.

The metrics used to characterise the efficiency of a device are most commonly defined in photometric units. The luminance efficiency, expressed in  $\text{cd}/\text{A}$ , relates the brightness of the device to the current that flows through it and is determined from  $\eta_L = LA/I$  where  $L$  is the luminance,  $A$  is the active area, and  $I$  is the device current. This metric is usually measured at normal incidence to the plane of the substrate.

Assuming that the LED is a Lambertian emitter, the net luminous flux  $\phi$  emitted from the forward hemisphere is calculated from  $\phi = \pi I$  where  $I$  is the luminous intensity in candelas.<sup>40</sup> The luminance efficiency can then be used to calculate the luminous power efficiency from

$$\eta_P = \frac{\pi \eta_L}{V} \quad (2.8)$$

where  $V$  is the drive bias.<sup>41</sup> This quantity is used to express device efficiency in terms of the total amount of visible light emitted from the device and the electrical power dissipated within it.

Photometric quantities are useful for evaluating OLED performance, particularly with regard to their applicability in the displays industry. However, these

measurements can be misleading when used to analyse the underlying physics of the device. In this respect, a more telling quantity is the external quantum efficiency  $\eta_{\text{EQE}}$ , defined as the fraction of photons that are emitted from the device for every electron that flows through it. Although not as accurate as measuring the efficiency using an integrating sphere,<sup>41</sup> this quantity can be calculated from the device's emission spectrum, luminance efficiency and the assumption of Lambertian emission.<sup>36</sup> In this work, the external quantum efficiency has been calculated using

$$\eta_{\text{EQE}} = \frac{\pi e}{hc} \eta_L \left[ \frac{\int F(\lambda) d\lambda}{\int (1/\lambda) F(\lambda) y(\lambda) d\lambda} \right] \quad (2.9)$$

where  $F$  is the emission spectrum of the device,  $y$  is the photopic response curve in lm/W and  $\lambda$  is the wavelength. Note that this equation does not require absolute values for the emission spectrum. It is sufficient that the spectra are merely proportional to the power spectral distribution of the device. Where calculated in this thesis, the external quantum efficiency was derived from normalised spectra.

## 2.7 Time-of-Flight Photocurrent

Charge carrier mobility was determined using the time-of-flight photocurrent technique. This measurement monitors the drift of a thin layer of photogenerated charge carriers under an applied bias. To achieve this, the polymer under test was deposited between two electrodes using the same techniques described in section 2.6.2. However, this measurement requires that only photo-excited charge carriers contribute to the current flowing through the device. As a consequence, it is necessary that the bias is applied using non-injecting contacts. With a work function of 4.28 eV, aluminium provides a substantial barrier to the injection of both holes and electrons for the materials that were tested. As such, aluminium was used to provide both electrodes.

Evaporated onto the glass substrate, a 20 nm thick layer of aluminium provided a semi-transparent contact through which the film could be optically excited. As a film thickness of several hundred nanometers was required for this measurement, concentrated solutions ranging from 60-80 mg/ml were used for spin-coating. A 50 nm layer of Al was deposited to form the top contact.

All time-of-flight photocurrent measurements were carried out at Queen Mary University of London by Dr. Theo Kreouzis. The devices were fabricated at Sheffield. Figure 2.11 illustrates the experimental arrangement used to carry out the measurements.

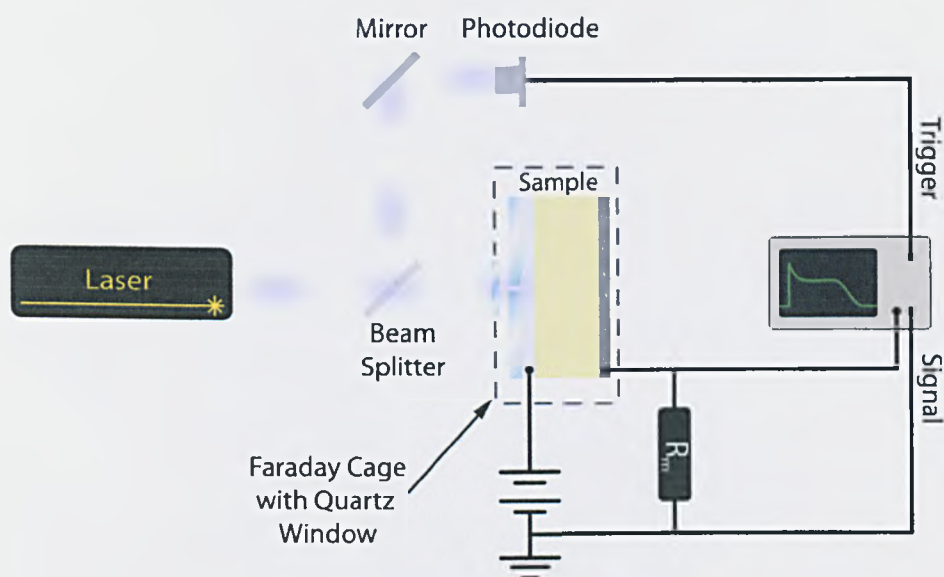


**Fig. 2.11:** Experimental arrangement of the time-of-flight photocurrent measurement.

The devices were excited by the 337 nm line of a Lambda Physik  $N_2$  laser. A variable bias was applied to the device, and the resulting photocurrent was measured from the voltage drop across the resistor. The data was recorded by an Agilent Infinium digital storage oscilloscope, triggered by the signal from a photodiode. Typically, the data would be averaged over 50-70 measurements.

Interference from the laser was a substantial source of noise. The background

signal was recorded by placing a beam stop in the path of the laser to prevent illumination of the sample. This could then be subtracted from subsequent photocurrent measurements.



## References

- [1] Burroughes, J. H., Bradley, D. D. C., Brown, A. R., Marks, R. N., Mackay, K., Friend, R. H., Burns, P. L., and Holmes, A. B. *Nature* **347**(6293), 539–541 (1990).
- [2] Braun, D. and Heeger, A. J. *Appl. Phys. Lett.* **58**(18), 1982–1984 (1991).
- [3] Herold, M., Gmeiner, J., Riess, W., and Schworer, M. *Synth. Met.* **76**(1-3), 109–112 January (1996).
- [4] Ohmori, Y., Uchida, M., Muro, K., and Yoshino, K. *Jpn. J. Appl. Phys., Part 2* **30**(11B), L1941–L1943 November (1991).
- [5] Donat-Bouillud, A., Levesque, I., Tao, Y., D'Iorio, M., Beaupre, S., Blondin, P., Ranger, M., Bouchard, J., and Leclerc, M. *Chem. Mater.* **12**(7), 1931–1936 July (2000).
- [6] Drolet, N., Beaupre, S., Morin, J. F., Tao, Y., and Leclerc, M. *J. Opt. A-Pure Appl. Op.* **4**(6), S252–S257 (2002).
- [7] Leclerc, M. *J. Polymer Sci., Polymer Chem.* **39**(17), 2867–2873 (2001).
- [8] Scherf, U. and List, E. J. W. *Adv. Mater.* **14**(7), 477 April (2002).
- [9] Hoegl, H. *J. Phys. Chem.* **69**(3), 755 (1965).
- [10] Romero, B., Schaer, M., Leclerc, M., Ades, D., Siove, A., and Zuppiroli, L. *Synth. Met.* **80**(3), 271–277 (1996).
- [11] Blouin, N. and Leclerc, M. *Acc. Chem. Res.* **41**(9), 1110–1119 September (2008).
- [12] Morin, J. F. and Leclerc, M. *Macromolecules* **34**(14), 4680–4682 (2001).
- [13] Morin, J. F., Beaupre, S., Leclerc, M., Levesque, I., and D'Iorio, M. *Appl. Phys. Lett.* **80**(3), 341–343 (2002).
- [14] Iraqi, A. and Wataru, I. *Chem. Mater.* **16**(3), 442–448 (2004).
- [15] Iraqi, A., Pickup, D. F., and Yi, H. N. *Chem. Mater.* **18**(4), 1007–1015 February (2006).
- [16] Adachi, C., Tsutsui, T., and Saito, S. *Appl. Phys. Lett.* **55**(15), 1489–1491 (1989).
- [17] Kido, J., Shionoya, H., and Nagai, K. *Appl. Phys. Lett.* **67**(16), 2281–2283 (1995).
- [18] Huang, J. S., Hou, W. J., Li, J. H., Li, G., and Yang, Y. *Appl. Phys. Lett.* **89**(13), 133509 (2006).
- [19] Wu, F. I., Reddy, D. S., Shu, C. F., Liu, M. S., and Jen, A. K. Y. *Chem. Mater.* **15**(1), 269–274 January (2003).

- [20] Peng, Z. H., Bao, Z. N., and Galvin, M. E. *Adv. Mater.* **10**(9), 680-684 June (1998).
- [21] Song, S. Y., Jang, M. S., Shim, H. K., Hwang, D. H., and Zyung, T. *Macromolecules* **32**(5), 1482-1487 (1999).
- [22] Lee, S. J., Gallegos, J. R., Klein, J., Curtis, M. D., and Kanicki, J. *Synth. Met.* **155**(1), 1-10 (2005).
- [23] Mullen, K. and Scherf, U., editors. *Organic light emitting devices : synthesis, properties, and applications*. Weinheim : Wiley-VCH, (2006).
- [24] Mitschke, U. and Bauerle, P. *J. Mater. Chem.* **10**(7), 1471-1507 (2000).
- [25] Jacob, J., Zhang, J. Y., Grimsdale, A. C., Mullen, K., Gaal, M., and List, E. J. W. *Macromolecules* **36**(22), 8240-8245 November (2003).
- [26] Lux, A., Holmes, A. B., Cervini, R., Davies, J. E., Moratti, S. C., Gruner, J., Cacialli, F., and Friend, R. H. *Synth. Met.* **84**(1-3), 293-294 January (1997).
- [27] Assaka, A. M., Rodrigues, P. C., de Oliveira, A. R. M., Ding, L. M., Bin, H., Karasz, F. E., and Akcelrud, L. *Polymer* **45**(21), 7071-7081 September (2004).
- [28] Morteani, A. C., Dhoot, A. S., Kim, J. S., Silva, C., Greenham, N. C., Murphy, C., Moons, E., Cina, S., Burroughes, J. H., and Friend, R. H. *Adv. Mater.* **15**(20), 1708 October (2003).
- [29] Redecker, M., Bradley, D. D. C., Inbasekaran, M., Wu, W. W., and Woo, E. P. *Adv. Mater.* **11**(3), 241 February (1999).
- [30] Ego, C., Grimsdale, A. C., Uckert, F., Yu, G., Srdanov, G., and Mullen, K. *Adv. Mater.* **14**(11), 809-811 June (2002).
- [31] Norrman, K., Ghanbari-Siahkali, and Larsen, N. B. *Annu. Rep. Prog. Chem., Sect. C: Phys. Chem.* **101**, 174-201 (2005).
- [32] Lakowicz, J. R. *Principles of fluorescence spectroscopy*. New York : Springer, 3rd edition, (2006).
- [33] Greenham, N. C., Samuel, I. D. W., Hayes, G. R., Phillips, R. T., Kessener, Y. A. R. R., Moratti, S. C., Holmes, A. B., and Friend, R. H. *Chem. Phys. Lett.* **241**(1-2), 89-96 (1995).
- [34] deMello, J. C., Wittmann, H. F., and Friend, R. H. *Adv. Mater.* **9**(3), 230- & (1997).
- [35] Ariu, M., Lidzey, D. G., Sims, M., Cadby, A. J., Lane, P. A., and Bradley, D. D. C. *J. Phys.: Condens. Matter* **14**(42), 9975-9986 (2002).
- [36] Virgili, T., Lidzey, D. G., and Bradley, D. D. C. *Adv. Mater.* **12**(1), 58 (2000).

- 
- [37] Johnson, A. R., Lee, S. J., Klein, J., and Kanicki, J. *Rev. Sci. Instrum.* **78**(9), 096101 September (2007).
- [38] H. C. Stark - CLEVIOS Homepage, [www.clevios.com](http://www.clevios.com). Last accessed 02/07/2008.
- [39] Huang, J., Miller, P. F., de Mello, J. C., de Mello, A. J., and Bradley, D. D. C. *Synth. Met.* **139**(3), 569–572 (2003).
- [40] McCluney, W. R. *Introduction to radiometry and photometry*. Norwood, MA : Artech House, (1994).
- [41] Forrest, S. R., Bradley, D. D. C., and Thompson, M. E. *Adv. Mater.* **15**(13), 1043–1048 (2003).

## Chapter 3

# Thermal Stability of Polycarbazoles

### 3.1 Introduction

Issues relating to the stability of polymer LEDs have been a major contributing factor to the delayed commercialisation of the technology. In particular, wide energy gap, blue-emitting LEDs have suffered from shorter lifetimes owing to their relatively poor luminescent and spectral stabilities. With the benchmark operational lifetime of many applications residing in the tens of thousands of hours, the improvement of device longevity remains the focus of many research groups within the field. Improving our understanding of the mechanisms of polymer degradation is a critical step in the development of stable and efficient devices.

In this chapter, the thermal stability of the alkyl-substituted polymers **P1** - **P3** and the triarylamine substituted polymer **P6** has been investigated. Photoluminescence spectra were obtained from samples that had undergone a variety of heat treatments. These were used to assess the susceptibility of each material to thermally induced degradation. As there exists a large body of work on the degradation of polyfluorene, this material was also studied and used as a benchmark.

## 3.2 Degradation in Arylene-Type Polymers

It has been well established that many materials undergo strong spectral changes accompanied by a reduction in efficiency during prolonged device operation. An exemplary case is that of the polyfluorenes. These intrinsically blue-emitting materials exhibit a broad, low-energy emission band from 500 - 600 nm that evolves whilst the device is operating. For commercial applications where colour purity is essential, this is highly problematic.

The origin of this long-wavelength emission has been widely debated. Similar spectral features were observed from the ladder-type polymer, LPPP. Like polyfluorene, this material has a poly-*para*-phenylene (PPP) based molecular structure. However, the incorporation of bridging carbon atoms on consecutive phenyl units results in a rigid and highly planarised backbone with extended electronic conjugation (see figure 3.1). Photoluminescence studies of this polymer revealed that the solid-state emission incorporated a broad low-energy shoulder in addition to the short wavelength vibronic structure that was observed from the dilute solution.<sup>1</sup> As the LPPP molecules in solution are considered to be spatially isolated from each other, the blue emission band was assigned to the radiative decay of intramolecular fluorophores. Conversely, the closely packed nature of the solid film would enable the formation of low energy interchain excitations. Photoluminescence from the film could then be explained by a combination of both inter and intramolecular emission. Furthermore, the presence of a low-energy tail in the absorption spectrum of the thin film suggested that the intermolecular species were aggregates.<sup>2</sup> Unlike excimers and exciplexes,<sup>3</sup> aggregates are stable in the ground state, thus leaving a detectable signature in the materials absorption.

In light of these results, discovery of the long-wavelength emission band in the electroluminescence spectrum of polyfluorene was initially attributed to the decay of intermolecular excitations. Under certain conditions this emission, com-

monly referred to as the 'green band' or 'g-band', could also be observed during photocxcitation of the polymer film. Although its presence in the PL spectrum of pristine films was dependent upon the specific structural properties of the polyfluorene (for example, the size of its alkyl substituents or the nature of the chain-terminating end group), the green band emission could invariably be induced or intensified through either thermal or UV irradiative treatments carried out in air.<sup>4-8</sup> Bliznyuk *et al.* proposed that the broad, low-energy emission band was actually composed of several overlapping peaks.<sup>7</sup> These were assigned to intermolecular excitations with varying numbers of constituent chromophores, the long-wavelength tail resulting from electronic delocalisation over multiple chain segments. It was suggested that these excitations were excimeric in nature due to the lack of any detectable difference in the absorption spectrum associated with the grow-in of the green band.

Other publications have also supported the assignment of the g-band to aggregate or excimeric species. Zeng *et al.* reported the synthesis of a spirofluorene containing copolymer (see figure 3.1) that suppressed thermally induced changes to the emission spectrum.<sup>9</sup> It was noted that degradation was only evident when the films were heated above the material's glass transition temperature  $T_g$ . Above  $T_g$  the polymeric matrix is softened allowing for the reorientation and alignment of chromophores into the cofacial arrangement that is necessary for excimer formation. The improved stability observed in the spirofluorene containing polymer was thus attributed to its high glass transition temperature.

A similar argument was used to explain the improvement in stability found in high molecular weight poly(9,9'-dioctylfluorene).<sup>10</sup> It was proposed that the pristine material contained a fraction of small oligomeric molecules that possessed a sufficiently high mobility to allow chain realignment and induce aggregation. The removal of this fraction, via the technique of gel permeation chromatography, gave rise to a marked improvement in efficiency and colour purity of the light-emitting diode.

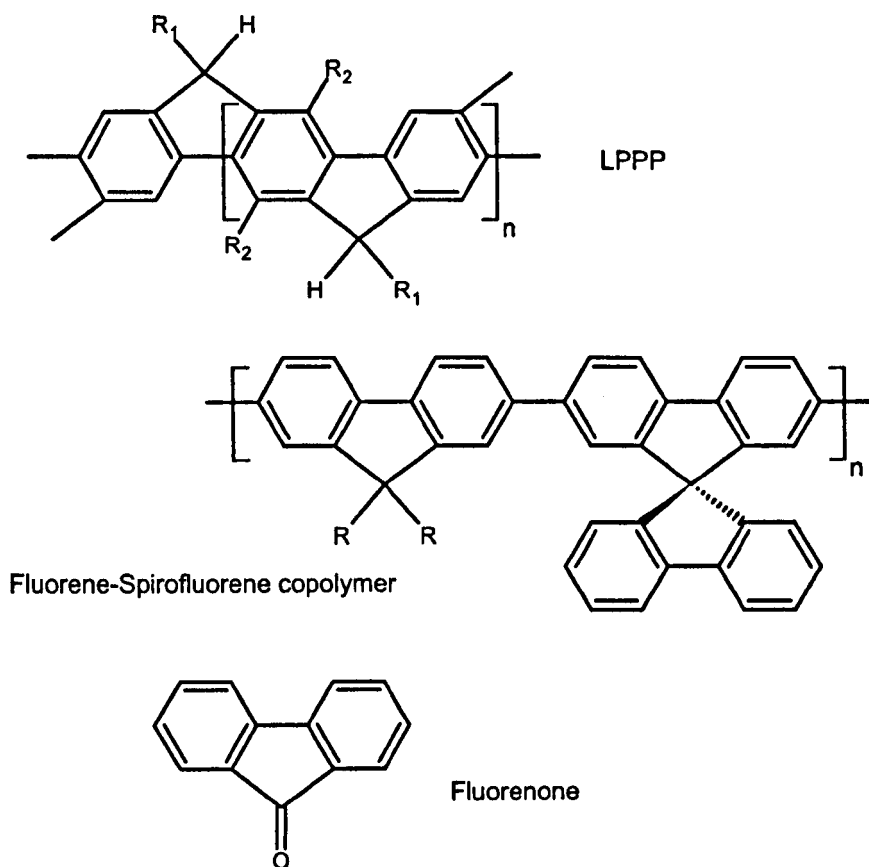


**Fig. 3.1:** The chemical structures of the ladder polymer LPPP, a spirofluorene copolymer and the fluorenone moiety.

An alternative theory, which is now more widely accepted over those discussed above, is that the green band is induced by the formation of chemical defects along the polyfluorene backbone. Infrared spectroscopy carried out on both photodegraded<sup>7</sup> and thermally degraded<sup>11</sup> samples revealed the presence of a  $1720\text{ cm}^{-1}$  absorption band that is consistent with the ketonic defect fluorenone (see figure 3.1). Both studies showed that the non-alkylated fluorene units used to terminate the dihexyl substituted polyfluorene backbone were highly susceptible to oxidation when the polymer was thermally/irradiatively treated in air. Further to this, a comparison of the spectroscopic properties of mono-substituted and di-substituted polyfluorenes highlighted the importance of fully protecting the bridging carbon atom via its functionalisation.<sup>12</sup>

Compelling evidence as to the important role of fluorenone in the spectral degradation of polyfluorenes was provided by the synthesis of a model compound in which a low concentration of the keto defect was introduced into the polymer backbone.<sup>13</sup> As little as 1% fluorenone content was sufficient to produce a predominant green emission during photoexcitation of the thin film, implying the occurrence of exciton migration to the low-energy defect. These results were a convincing reproduction of the spectra obtained from the photoluminescence of degraded polyfluorene. Interestingly, LEDs that were fabricated using the fluorenone copolymer exhibited only the low-energy green component with almost complete suppression of the characteristic polyfluorene blue band. Enhancement of the green emission during electroluminescence suggests that fluorenone defects act as charge carrier traps as well as centers for energy migration.

Exhaustive studies have led to a wide acceptance that the spectral degradation observed in polyfluorene based LEDs and the green emission band induced in the PL of oxidised films are caused by a common fluorenone defect. Although the devices are generally encapsulated or tested under an oxygen deficient environment it is possible that a trace amount of residual oxygen is present during the film deposition or cathode evaporation stages of fabrication. Gong *et al.* proposed that oxidation of the polyfluorene backbone is catalysed by the presence of calcium at the cathode interface.<sup>14</sup> Suppression of the long wavelength emission during electroluminescence has been achieved by incorporating a charge transporting buffer layer between the polyfluorene film and the reactive cathode metal.<sup>14,15</sup>

Although there is a general agreement that emission from the g-band is dependent upon the generation of fluorenone defects, the exact nature of the emissive species is still under dispute. By studying the behaviour of PFO when dissolved in an inert polystyrene matrix, Sims *et al.*<sup>16,17</sup> have suggested that inter-chain/inter-segment interactions are requisite for the appearance of the g-band. They therefore concluded that the characteristic low energy emission band observed from



photo-oxidised PFO is actually generated by a fluorenone excimer and that the fluorenone moiety by itself merely acts as a quenching site. In contradiction to this theory, Becker *et al.*<sup>18</sup> have used single-molecule PL measurements to detect fluorenone emission from isolated polyfluorene chains. They discounted the possibility of an intramolecular excimer forming between two fluorenone defects on a single molecule as the defect comprised only 1% of the copolymer that was studied.

### 3.2.1 Degradation Studies on Carbazole-Based Materials

Like fluorene, the carbazole moiety constitutes a biphenyl group bridged at the 9-position. As discussed above, it is oxidation of the bridging carbon in polyfluorene that is, at least in some part, responsible for its photoinduced, thermal and electrical degradation. However, as the carbazole moiety incorporates nitrogen at this bridging position an equivalent degradation mechanism is precluded.

There has been little published on the processes responsible for the degradation of carbazole based materials. In a study carried out on poly(*N*-vinylcarbazole), Rivaton *et al.* showed that a variety of decomposition products were formed as a result of its photo-oxidation.<sup>19</sup> These were evidenced by changes in both the absorption and emission spectra, as well as the formation of an insoluble fraction caused by cross-linking of the aliphatic backbone. The investigation of a 3,3'-linked carbazole dimer doped into a poly(methyl methacrylate) (PMMA) matrix has also revealed the occurrence of photodegradation when UV-irradiated in air.<sup>20</sup> Neither of these studies, however, have explored the oxidative stability of a main-chain polycarbazole.

In this section, the spectral stability of polymers **P1**, **P2**, **P3** and **P6** has been investigated. Having undergone a variety of thermal treatments, the PL spectra of all seven polymers was recorded. Due to its well studied mechanism of degradation and analogous structure, thin-films of PFO (poly(9,9-dioctylfluorene)) were

used as a representative 'benchmark' material.

### 3.3 Sample Preparation

All of the measurements described in this section were taken from polymer thin-films that were fabricated using the materials and methods discussed in Chapter 2. The films were spun from toluene onto 15 × 15 mm Spectrosil 2000 substrates. For each polymer that was under investigation, four samples were fabricated. The first sample was measured in its pristine, as-spun form. The second and third samples were annealed in air at 150 °C for 20 minutes and 2 hours respectively. The final set of samples were transferred to a nitrogen filled glove-box where the oxygen and water levels are constantly monitored and kept below 1 ppm. These were also thermally annealed at 150 °C for 2 hours. After this time, the samples were removed from the hotplate and left to reach room temperature for at least two hours prior to being removed from the glove-box.

### 3.4 Photoluminescence Measurements

Photoluminescence was generated by exciting the samples with the 325 nm line of a HeCd laser. The laser was attenuated to a power of 0.1 mW and defocused to a spot size of approximately 1 cm in diameter. The excitation beam was perpendicular to the plane of the substrate and incident upon the polymer coated surface. Fluorescence was collected from the same surface at an angle of approximately 45°. This geometry remained consistent for all measurements, allowing a direct comparison between the data collected.

### 3.5 Thermal Stability of PFO

Figure 3.2 shows the normalised PL spectra that were obtained from the four PFO samples. It should first be noted that all of the spectra discussed within this chapter have been background subtracted and have undergone correction for the response of the spectrometer. The data is presented such that the y-axis is proportional to the irradiance of the sample in  $\text{Wm}^{-2}\text{nm}^{-1}$  and not the photonic flux. The second order laser peak that occurs at 650 nm has also been removed from each data set.

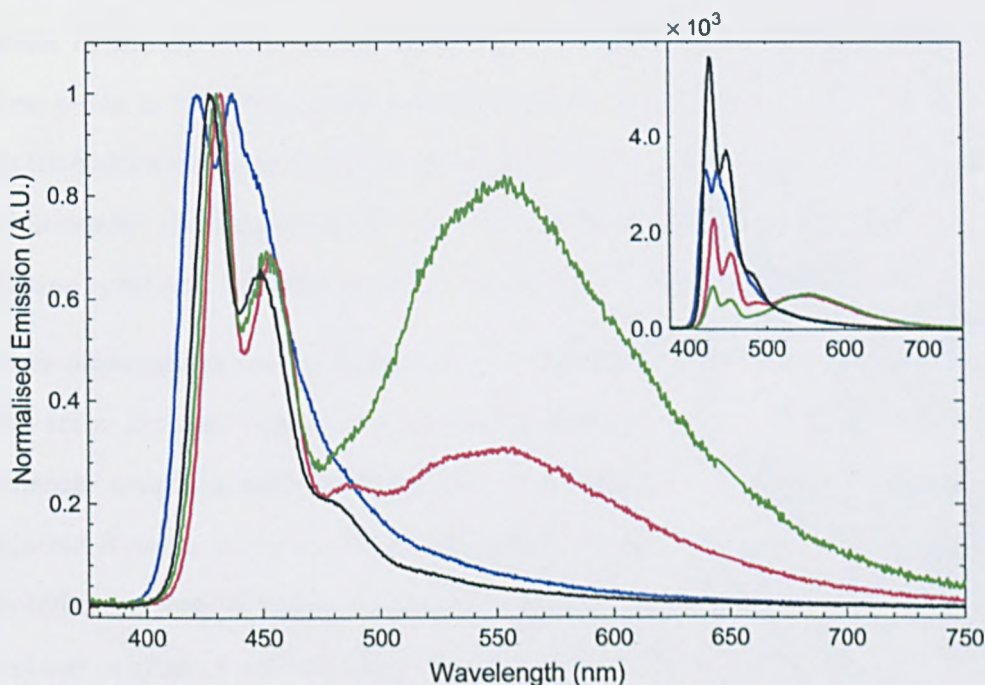


**Fig. 3.2:** The normalised PL spectra of PFO samples in its pristine form (blue) and after annealing at 150°C in air for 20 minutes (red), in air for 120 minutes (green) and under a nitrogen atmosphere for 120 minutes (black). Non-normalised data is presented in the inset to show the relative intensities of emission from the four samples.

All four samples have a highly structured emission spectrum between 400 and 500 nm. The pristine film exhibits two sharp, well resolved peaks, one located at 423 nm and the other 438 nm. Protruding from the latter peak there is a slight shoulder at around 446 nm. Beyond 500 nm, emission from the pristine film is

minimal.

The three annealed films also feature two narrow emission peaks between 400 and 500 nm. However, these spectra all exhibit a bathochromic shift relative to the pristine film. The sample annealed in air for 20 minutes shows the largest shift, peaking at 433 nm. The air baked film that was treated for 2 hrs was red-shifted by 8 nm, peaking at 431 nm. Finally the sample that was annealed under nitrogen for 2 hrs showed the smallest red-shift, peaking at 428 nm.

Notably, the relative intensities of the first and second peaks of all three annealed samples are very similar. These can be assigned to the 0-0 and 0-1 vibronic modes of the  $S_1 \rightarrow S_0$  transition in PFO. The large difference in intensity of these peaks is reflective of the varying strength of each transition. In contrast, the intensities of the first and second peaks of the pristine film are very similar. Additionally, the separation of these features is approximately  $780 \text{ cm}^{-1}$  in the pristine spectrum, whereas in all three annealed films it is around  $1,100 \text{ cm}^{-1}$ .

These observations can be explained by considering the presence of the  $\beta$ -phase. The term  $\beta$ -phase describes a spectrally distinct form of PFO in which the molecule adopts a planarised  $2_1$  helix (see figure 3.3). In this conformation, adjacent fluorene units are rotated by  $180^\circ$  relative to each other such that the phenyl rings form a highly conjugated coplanar arrangement. As a result, the  $\beta$ -phase exhibits a red-shifted emission spectrum with highly defined vibronic features, similar to that of the rigid ladder-type polymer LPPP.<sup>21</sup>

The  $\beta$ -phase can be induced from a glassy PFO matrix through a variety of treatments such as exposing the film to solvent vapour or slowly reheating it from liquid nitrogen temperature. It has also been shown that, when spun from certain solvents, the  $\beta$ -phase can form in the pristine film.<sup>22</sup> A recent study has shown that, on casting from toluene, the glassy phase is preferentially located next to the substrate whereas the  $\beta$ -phase forms at the free interface.<sup>23</sup>

From figure 3.3, it can be seen that the pristine PFO spectrum is composed of

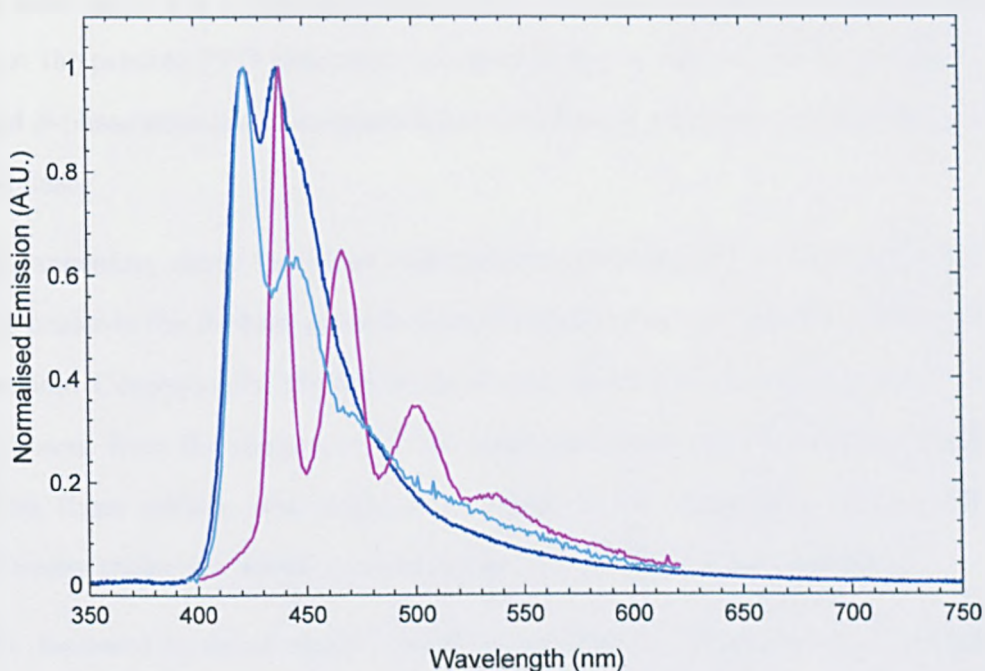


**Fig. 3.3:** The normalised PL spectrum of the pristine PFO film (blue), a film containing only the glassy phase (cyan) and a film containing approximately 11% of the  $\beta$ -phase (magenta). The glassy phase and  $\beta$ -phase spectra were obtained from Dr. W. C. Tsoi. The proposed structure of the  $\beta$ -phase of PFO is also illustrated

both glassy and  $\beta$ -phase features. For example, the second peak in the PL spectrum of the as-cast film (located at 438 nm) is coincident with the 0-0 transition of the  $\beta$ -phase. It is therefore possible to conclude that some portion of the pristine film has adopted the  $2_1$  helix conformation. The shoulder at 446 nm is therefore most likely a result of the 0-1 transition of the glassy phase.

Studies into the spectroscopic properties of PFO films that contain the  $\beta$ -phase have shown that energy transfer from the glassy matrix is highly efficient. Almost complete energy transfer to the lower energy  $\beta$ -phase chains is observed when

as little as 1-2% of the molecules adopt this conformation.<sup>24,25</sup> This suggests that the pristine PFO spectrum presented in figures 3.2 and 3.3 (in which glassy and  $\beta$ -phase emission is comparable) results from a very low concentration of the  $\beta$ -phase.

On annealing above the glass transition temperature ( $T_g \sim 75^\circ\text{C}$  for PFO<sup>21</sup>), molecules in the  $\beta$ -phase are able to structurally relax into the disordered conformation. Consequently, the 438 nm peak that signifies the presence of the  $\beta$ -phase is absent from the spectra of all three annealed films. The red-shifted emission from these samples also suggests a change in the morphology of the matrix, whereby molecules adopt a conformation with extended conjugation.

As discussed in detail above, the thermally induced oxidation of polyfluorene results in the appearance of an additional long wavelength emission band. The spectra reported in figure 3.2 typify this observation. Here, the g-band is observed above 500 nm in the emission spectra of both air annealed films. Relative to the intrinsic blue emission, it grows in intensity as the annealing time is increased. For the sample that was annealed for 2 hrs, emission from the g-band peaks at 555 nm and its tail extends beyond 750 nm. When annealed under nitrogen, the g-band is completely absent from the PL spectrum.

### 3.6 Thermal Stability of Poly(alkyl-carbazole)s

Figure 3.4 shows the normalised PL spectra obtained from pristine and annealed films of polymers **P1**, **P2**, and **P3**. Each of these polymers incorporate protecting methyl groups in the 3- and 6-positions. It has been shown that these features stabilise the molecules against irreversible oxidation during electrochemical characterisation.

The inset of each spectrum shows the non-normalised data. As the excitation power and collection geometry remained constant for each set of measurements, these data can be used to gauge the affect of annealing on the intensity of emission

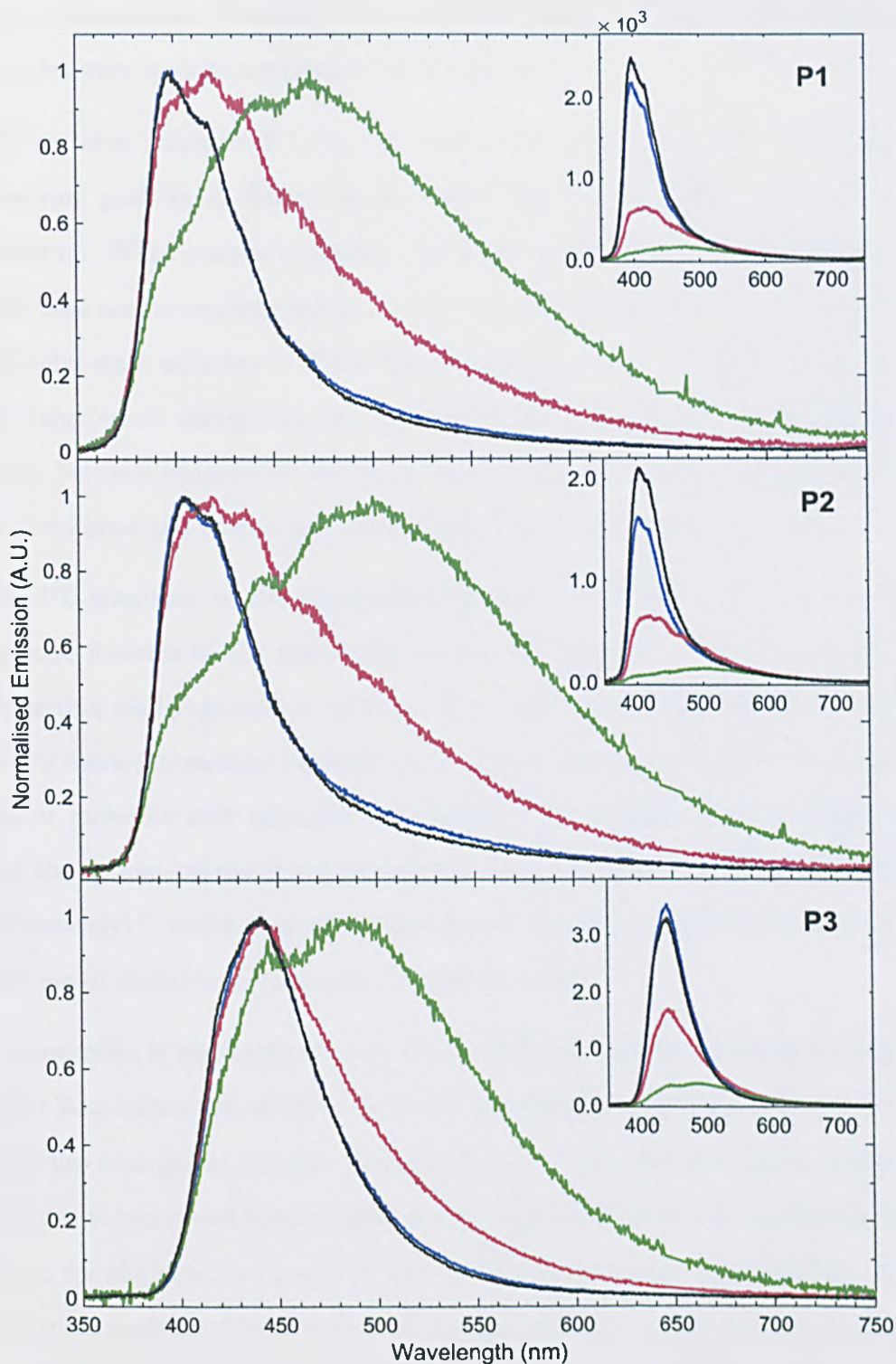


**Fig. 3.4:** The normalised PL spectra of polymers **P1**, **P2** and **P3** in their pristine form (blue) and after annealing at 150 °C in air for 20 minutes (red), in air for 120 minutes (green) and under a nitrogen atmosphere for 120 minutes (black). Non-normalised data are presented in the figure insets. These illustrate the relative intensities of the four spectra.

from the material. To allow a comparative analysis between each polymer, all samples were spun to a thickness of  $60 \pm 20$  nm.

Of the three polymers **P1** has the largest energy gap, its photoluminescence spectrum peaking at 400 nm in the deep violet region of the electromagnetic spectrum. When compared against a previously reported carbazole homopolymer that does not incorporate the protecting methyl groups in the 3 and 6-positions, the solid-state emission of **P1** is blue-shifted by 32 nm.<sup>26</sup> This is indicative of the large steric demand of the 3,6-substitutions. An increase in the dihedral angle between consecutive carbazole units limits electronic conjugation along the backbone and results in a substantial hypsochromic shift in emission.

The PL spectrum of the copolymer **P2** peaks at 403 nm. A redshift in the spectral features of the copolymer is expected to result from the omission of protecting methyl groups on alternating carbazole units. The consequent reduction of steric interactions between neighbouring monomers should lead to a more planar molecule with enhanced conjugation. This redshift is more apparent in the absorption spectra of polymers **P1** and **P2** (peaking at 318 nm and 350 nm respectively)<sup>27</sup> which may reflect the occurrence of energy transfer to a small fraction of chains with extended conjugation in **P1**.

On annealing in air, both polymers **P1** and **P2** show significant spectral changes. After 20 minutes, the emission from **P1** has substantially broadened and a new peak has emerged at 417 nm. Emission from the film that was annealed for 120 minutes is broadened further, with its full width half maximum increasing from 55 nm for the pristine sample to 168 nm for the thermally degraded film. This spectrum peaks at 470 nm with the bands at 417 nm and 400 nm still present as high energy shoulders. Similar observations were made for polymer **P2**.

The PL spectrum obtained from **P3** also underwent modification when the sample was thermally treated in air. However, when compared against the results from polymers **P1** and **P2**, its susceptibility to degradation appears to be reduced. After being annealed for 20 minutes, the emission peak remained at



441 nm and the FWHM increased only slightly. Once again, annealing for 120 minutes caused further degradation, shifting the PL peak to a broad emission band centered around 486 nm. However, even after a prolonged heat treatment, emission from the intrinsic blue band was still a prominent feature.

Significantly, there is no sign of spectral changes from any of the films that were annealed under an inert N<sub>2</sub> atmosphere. This observation is inconsistent with a morphologically induced degradation mechanism such as the enhanced formation of intermolecular species and would seem to imply the occurrence of thermally induced oxidation.

The above results demonstrate that the emissive properties of all three alkyl substituted polymers can be modified by heating them in the presence of oxygen. As was seen with the polyfluorene samples, the degraded spectrum is significantly broadened, with the majority of emission occurring in the green. However, on inspection of the non-normalised data (see the figure insets), it is apparent that these changes result from the preferential quenching of the short-wavelength features, whilst the low-energy tail is sustained but does not increase in intensity. This is in contrast to the results obtained from PFO where an increase in emission above 500 nm is clearly seen alongside quenching of the blue features.

One possible interpretation of these observations is that the thermal degradation of polymers **P1 - P3** results from the formation of a non-emissive quenching site. The concentration of this quenching species increases with the anneal time, causing a reduction in photoluminescence. Emission that occurs within the long wavelength tail however, appears unaffected by its presence. This may be a result of exciton trapping at low energy defect sites that are intrinsic to the pristine polymer. Excitons that migrate to these sites become localised and immobile and therefore, further migration to quenching centers would be inhibited.

The formation of non-emissive quenchers has also been considered as a degradation mechanism in polyfluorene. MALDI-TOF spectrometry was used to identify both fluorenone and alkyl ketone degradation products from photo-oxidised flu-

orene trimers.<sup>28</sup> It was proposed that the alkyl ketone component would act as a site for quenching emission. On the investigation of a model system, composed of a tertiary blend of polyfluorene, fluorenone and an alkyl ketone quenching species (shown in figure 3.5), it was found that when low concentrations of fluorenone were present, PL emission from the blue polyfluorene matrix would be preferentially quenched over emission from the green band.<sup>29</sup> These findings are in agreement with the above proposed mechanism of degradation in the alkyl substituted polycarbazoles.

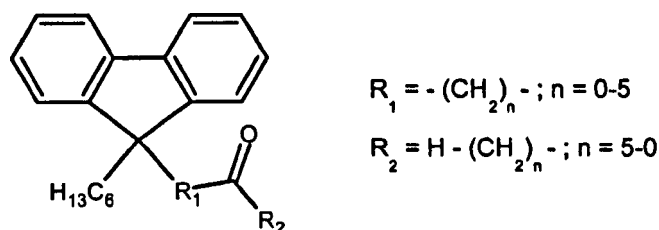
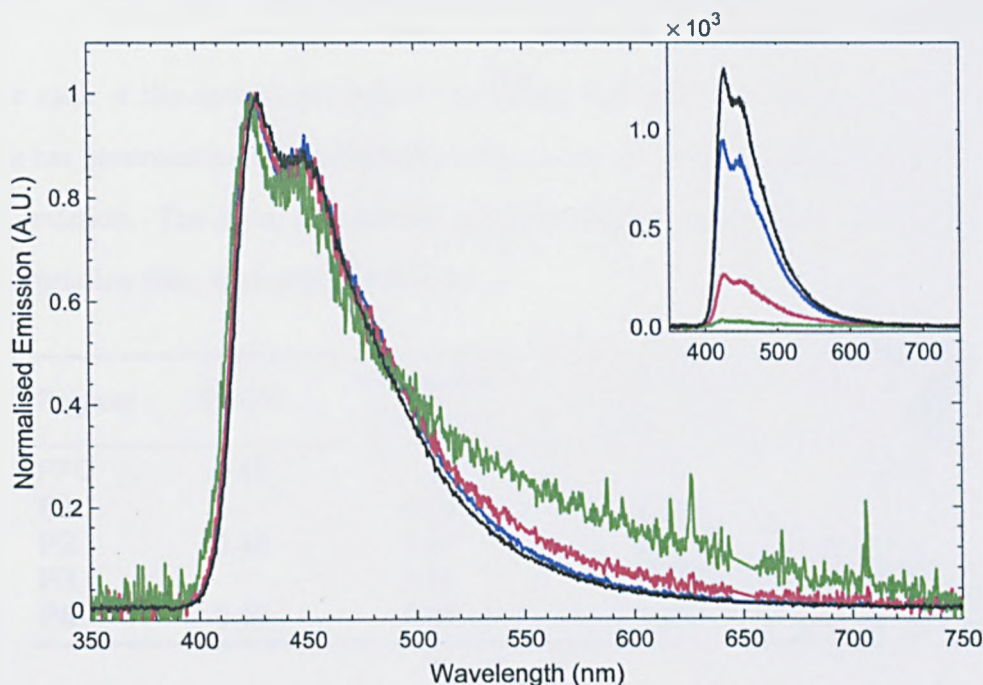


Fig. 3.5: An alkyl ketone containing product of photo-oxidised fluorene.<sup>28</sup>

### 3.7 Thermal Stability of Poly(aryl-carbazole)s

Figure 3.6 presents the PL spectra obtained from pristine and thermally annealed films of the triarylamine-substituted homopolymer **P6**. With emission occurring predominantly in the blue part of the electromagnetic spectrum, its photoluminescence peaks at 428 nm with a second feature, probably of vibronic origin at 450 nm. Regardless of the thermal history of the film, the normalised PL spectra acquired from all four samples are similar in both shape and position. Their emission maxima are all located at the same wavelength, whilst the FWHM remains in the range of 60-75 nm, with the small variations being attributable to the presence of noise. Only when the film is annealed for 120 minutes in air is there a notable difference in the spectrum, with a slight increase in significance

of the low-energy tail.



**Fig. 3.6:** The normalised PL spectra of **P6** samples in its pristine form (blue) and after annealing at 150 °C in air for 20 minutes (red), in air for 120 minutes (green) and under a nitrogen atmosphere for 120 minutes (black). The intensity (in counts) of the four spectra can be seen in the inset.

In comparison to the results obtained from both PFO and the alkyl-substituted polycarbazoles, polymer **P6** shows a marked improvement in the stability of its normalised emission spectrum. This is an important property for blue-emitting polymers which have traditionally suffered from poor colour stability and spectral impurity. However, on inspection of the non-normalised data, it is clear that the total emission from the polymer is considerably diminished when the sample is annealed in air. These results suggest that the quenching of emission must occur equally across the entire spectrum. With reference to the discussion regarding the alkyl-substituted polymers, this would appear to indicate an absence of emissive exciton traps in the pristine film. When a non-emissive defect is introduced through thermal oxidation, emission from the single species is quenched equally across all wavelengths.

### 3.8 Comparison of Emission Intensities

For each of the spectra presented (including both pristine and annealed films), the net photoluminescence intensity was calculated by integrating over the limits of emission. The data, represented as a fraction of the emission intensity from the pristine film, is shown in table 3.1.

Polymer	PLQY	Air Annealed (20 mins)	Air Annealed (120 mins)	N <sub>2</sub> Annealed (120 mins)
PFO	0.45	0.83	0.61	1.20
<b>P1</b>	-	0.50	0.18	1.11
<b>P2</b>	0.16	0.67	0.21	1.26
<b>P3</b>	-	0.61	0.23	0.94
<b>P6</b>	0.29	0.30	0.05	1.32

**Table 3.1:** A comparison of the optical power of samples that have undergone different heat treatments. The values represent the net power emitted from each sample relative to that of the pristine film (which by definition has a relative power of 1). Where measured, the PLQY of the polymer film is included for reference.

Of the five polymers discussed in this chapter, PFO has shown the smallest reduction in photoluminescence on annealing in air. Despite the spectral stability observed from **P6**, this polymer undergoes the greatest reduction in emission.

On comparison of the results from polymers **P1** and **P2**, there is no clear improvement in thermal stability afforded by the full protection of the homopolymer over the alternating protection of the copolymer. Indeed, these results seem to suggest that the copolymer is the more stable of the two materials. However, this is only marginal and may result from experimental or analytical inaccuracies. Nevertheless, these measurements do not emulate the improvement in electrochemical stability observed due to the presence of the 3,6- protecting methyl groups.<sup>27</sup> This may infer that separate mechanisms are responsible for the thermal and electrolytic degradation of polycarbazole.

Interestingly, all of the polymers except **P3** have shown an increase in emission

when annealed under nitrogen. This behaviour has been previously observed from polyfluorene in the absence of ketonic defects.<sup>30</sup> Significantly, it appears that any morphological changes that are induced by the process of annealing do not result in the formation of emission-quenching interchain excitations.

### 3.9 Conclusions

All of the carbazole-based polymers that were investigated have undergone significant degradation when annealed in air. In the alkyl-substituted polymers this was manifest by a large increase in the spectral bandwidth and a redshift in peak emission. However, this was proven to result from uneven quenching across the broad emission spectrum and not from the formation of a new emissive species as was observed in PFO. In contrast, the triarylamine-substituted polymer showed extreme colour stability on annealing, despite suffering from a large reduction in overall emission.

These findings suggest that the general mechanism of degradation in polycarbazoles involves the formation of a non-emissive quenching species. The absence of degradation when annealed under an inert atmosphere implies that this species may result from thermally induced oxidation of the polymer. In addition, it has been noted that the oxidation of alkyl side-chains has been identified as a source of non-emissive defects in polyfluorene. An increase in photoluminescence was observed from most of the polymers when annealed under nitrogen. This may result from morphological changes that occur during annealing, although further studies are required to investigate this possibility.

## References

- [1] Stampfl, J., Graupner, W., Leising, G., and Scherf, U. *J. Lumin.* **63**(3), 117–123 February (1995).
- [2] Lemmer, U., Heun, S., Mahrt, R. F., Scherf, U., Hopmeier, M., Siegner, U., Gobel, E. O., Mullen, K., and Bassler, H. *Chem. Phys. Lett.* **240**(4), 373–378 June (1995).
- [3] Jenekhe, S. A. and Osaheni, J. A. *Science* **265**(5173), 765–768 August (1994).
- [4] Pei, Q. B. and Yang, Y. *J. Am. Chem. Soc.* **118**(31), 7416–7417 August (1996).
- [5] Kreyenschmidt, M., Klaerner, G., Fuhrer, T., Ashenhurst, J., Karg, S., Chen, W. D., Lee, V. Y., Scott, J. C., and Miller, R. D. *Macromolecules* **31**(4), 1099–1103 February (1998).
- [6] Klarner, G., Davey, M. H., Chen, W. D., Scott, J. C., and Miller, R. D. *Adv. Mater.* **10**(13), 993 September (1998).
- [7] Bliznyuk, V. N., Carter, S. A., Scott, J. C., Klarner, G., Miller, R. D., and Miller, D. C. *Macromolecules* **32**(2), 361–369 (1999).
- [8] Teetsov, J. and Fox, M. A. *J. Mater. Chem.* **9**(9), 2117–2122 (1999).
- [9] Zeng, G., Yu, W. L., Chua, S. J., and Huang, W. *Macromolecules* **35**(18), 6907–6914 August (2002).
- [10] Weinfurtner, K. H., Fujikawa, H., Tokito, S., and Taga, Y. *Appl. Phys. Lett.* **76**(18), 2502–2504 (2000).
- [11] Lee, J. I., Klaerner, G., and Miller, R. D. *Chem. Mater.* **11**(4), 1083–1088 April (1999).
- [12] List, E. J. W., Guentner, R., de Freitas, P. S., and Scherf, U. *Adv. Mater.* **14**(5), 374–378 (2002).
- [13] Gong, X., Moses, D., Heeger, A. J., and Xiao, S. *Synth. Met.* **141**(1-2), 17–20 March (2004).
- [14] Gong, X. O., Iyer, P. K., Moses, D., Bazan, G. C., Heeger, A. J., and Xiao, S. S. *Adv. Funct. Mater.* **13**(4), 325–330 (2003).
- [15] Chen, Z. Y. and Ma, D. G. *Mater. Sci. Eng. B-Solid State Mater. Adv. Technol.* **141**(1-2), 71–75 June (2007).
- [16] Sims, M., Bradley, D. D. C., Ariu, M., Koeberg, M., Asimakis, A., Grell, M., and Lidzey, D. G. *Adv. Funct. Mater.* **14**(8), 765–781 August (2004).
- [17] Ferenczi, T. A. M., Sims, M., and Bradley, D. D. C. *J. Phys.: Condens. Matter* **20**(4), 045220 January (2008).

- [18] Becker, K., Lupton, J. M., Feldmann, J., Nehls, B. S., Galbrecht, F., Gao, D. Q., and Scherf, U. *Adv. Funct. Mater.* **16**(3), 364–370 February (2006).
- [19] Rivaton, A., Mailhot, B., Derderian, G., Bussiere, P. O., and Gardette, J. L. *Macromolecules* **36**(15), 5815–5824 July (2003).
- [20] Castex, M. C., Olivero, C., Pichler, G., Ades, D., and Siove, A. *Synth. Met.* **156**(9-10), 699–704 May (2006).
- [21] Grell, M., Bradley, D. D. C., Ungar, G., Hill, J., and Whitehead, K. S. *Macromolecules* **32**(18), 5810–5817 September (1999).
- [22] Khan, A. L. T., Sreearunothai, P., Herz, L. M., Banach, M. J., and Kohler, A. *Phys. Rev. B: Condens. Matter Mater. Phys.* **69**(8), 085201 February (2004).
- [23] Azuma, H., Asada, K., Kobayashi, T., and Naito, H. *Thin Solid Films* **509**(1-2), 182–184 June (2006).
- [24] Ariu, M., Lidzey, D. G., Sims, M., Cadby, A. J., Lane, P. A., and Bradley, D. D. C. *J. Phys.: Condens. Matter* **14**(42), 9975–9986 (2002).
- [25] Ariu, M., Sims, M., Rahn, M. D., Hill, J., Fox, A. M., Lidzey, D. G., Oda, M., Cabanillas-Gonzalez, J., and Bradley, D. D. C. *Phys. Rev. B: Condens. Matter Mater. Phys.* **67**(19), 195333 (2003).
- [26] Iraqi, A. and Wataru, I. *Chem. Mater.* **16**(3), 442–448 (2004).
- [27] Iraqi, A., Pickup, D. F., and Yi, H. N. *Chem. Mater.* **18**(4), 1007–1015 February (2006).
- [28] Liu, L. L., Tang, S., Liu, M. R., Xie, Z. Q., Zhang, W., Lu, P., Hanif, M., and Ma, Y. G. *J. Phys. Chem. B* **110**(28), 13734–13740 July (2006).
- [29] Liu, L. L., Lu, P., Xie, Z. Q., Wang, H. P., Tang, S., Wang, Z. M., Zhang, W., and Ma, Y. G. *J. Phys. Chem. B* **111**(36), 10639–10644 September (2007).
- [30] Rozanski, L. J., Cone, C. W., Ostrowski, D. P., and Bout, D. A. V. *Macromolecules* **40**(13), 4524–4529 June (2007).

## Chapter 4

# Charge Transport in Triarylamine-Substituted Polycarbazoles

### 4.1 Introduction

The process of charge carrier transport is fundamental to the operation of an organic light-emitting diode. One of the many requirements for the attainment of efficient electroluminescence is the balanced flow of charge carriers. Accordingly, the characterisation of charge transport is instrumental in the development of new electroluminescent materials and subsequent device optimisation.

Triarylamine-functionalised materials are widely recognised for their high hole mobilities and low ionisation potentials. These properties make them ideal for the injection and transport of holes in multilayer or composite blend device structures. The small molecular material TPD was measured to have a hole mobility over  $1 \times 10^{-3} \text{ cm}^2/\text{Vs}$  (with an applied field of between 0.4 and 0.6 MV/cm) in its amorphous glassy phase.<sup>1</sup> Recent studies on the fluorene-based copolymer TFB have revealed its hole mobility to be as high as  $1 \times 10^{-2} \text{ cm}^2/\text{Vs}$  (between 0.2 and 0.5 MV/cm).<sup>2</sup> It has been suggested that the low ionisation potential of these triarylamine-containing materials makes them less susceptible to the formation of deep traps within the manifold of hole transport states.<sup>3,4</sup> As such, high mobilities can still be achieved, even with the presence of defects and impurities.



The following sections report upon the characterisation of charge transport in the triarylamine-substituted polymers **P6** and **P7**. Whereas the homopolymer **P6** was expected to exhibit a high hole mobility owing to its triarylamine side-chain, the oxadiazole copolymer **P7** was synthesised to promote ambipolar transport. Through time-of-flight photoconductivity measurements, carrier drift mobilities for both materials have been derived. A field dependent mobility was observed and analysed in terms of a Poole-Frenkel-type relationship. All of the measurements discussed in this chapter were carried out by Dr. Theo Kreouzis at Queen Mary University of London. The samples were fabricated at Sheffield using the methods described in chapter 2.

## 4.2 Transient Photocurrents

The term ‘time-of-flight’ (TOF) describes a generic methodology whereby the time taken for an entity to traverse a known distance is measured. The photocurrent variant of this technique is commonly used in the characterisation of charge carrier transport in organic semiconductors.<sup>5-9</sup> The diagram presented in figure 4.1 illustrates the principle of this measurement.

The samples used in this measurement consist of a thin layer of polymer deposited between two electrodes. To allow photoexcitation of the polymer, one of the electrodes is semitransparent. A thin layer of excitons is generated at the surface of the sample by exciting it with a pulsed laser. The duration of the pulse must be significantly shorter than the timescale of the measurement and the repetition rate low enough to allow the photocurrent to decay between excitations.

Under the influence of an applied electric field, the excitons dissociate into mobile charge carriers which are free to drift within the sample. The motion of these charge carriers causes a displacement current to flow in the external circuit which is monitored as a voltage drop across the measurement resistor.<sup>10</sup> If the bias is defined relative to the illuminated electrode, a hole transient is measured when

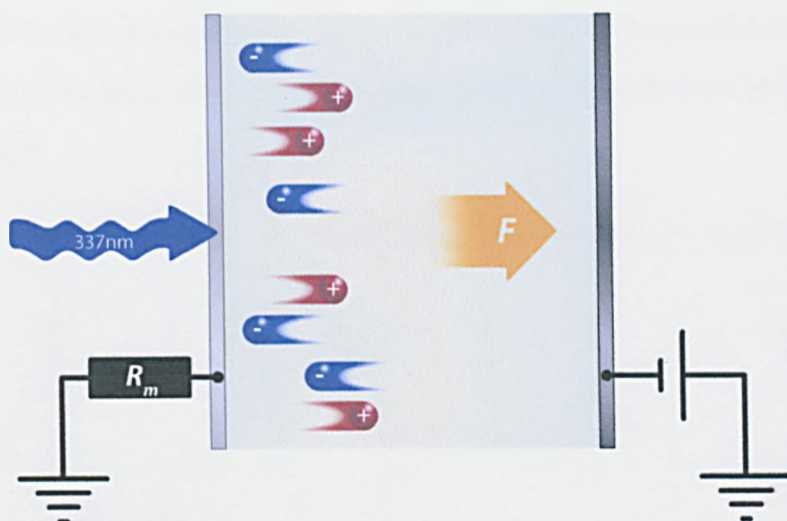


**Fig. 4.1:** Illustration of carrier generation and transport in a time-of-flight sample. Excitation occurs through a semi-transparent electrode and the generated carriers drift under the influence of an applied electric field  $F$ . In this example, the device is biased to measure the transit of holes.

a positive bias is applied (as depicted). Conversely, an electron transient is measured under negative bias.

Figure 4.2 shows a hole photocurrent transient that was obtained from the fluorene-based copolymer TFB. Some of the important features have been highlighted and labeled. The initial current spike, seen within the first hundred nanoseconds of the transient, is caused by the immediate collection of n-type carriers at the illuminated electrode. Once these have been removed from the sample, the remaining hole current reaches a constant level. This plateau is indicative of non-dispersive transport, whereby the sheet of charge carriers travels at a constant mean velocity across the sample. When the carriers have traversed the full thickness of the sample, they are collected at the counter electrode and no longer contribute to the photocurrent. The resulting inflexion in the photocurrent, labeled  $t_0$  is typically used to define the transit time of the fastest

carriers. When a clear plateau region can be observed it is possible to define the transit time  $t_{1/2}$  at which point the photocurrent reaches half the value of its constant level. This represents the time taken for half of the generated carriers to reach the collecting electrode and is thus a closer representation of the mean transit time.<sup>11</sup>

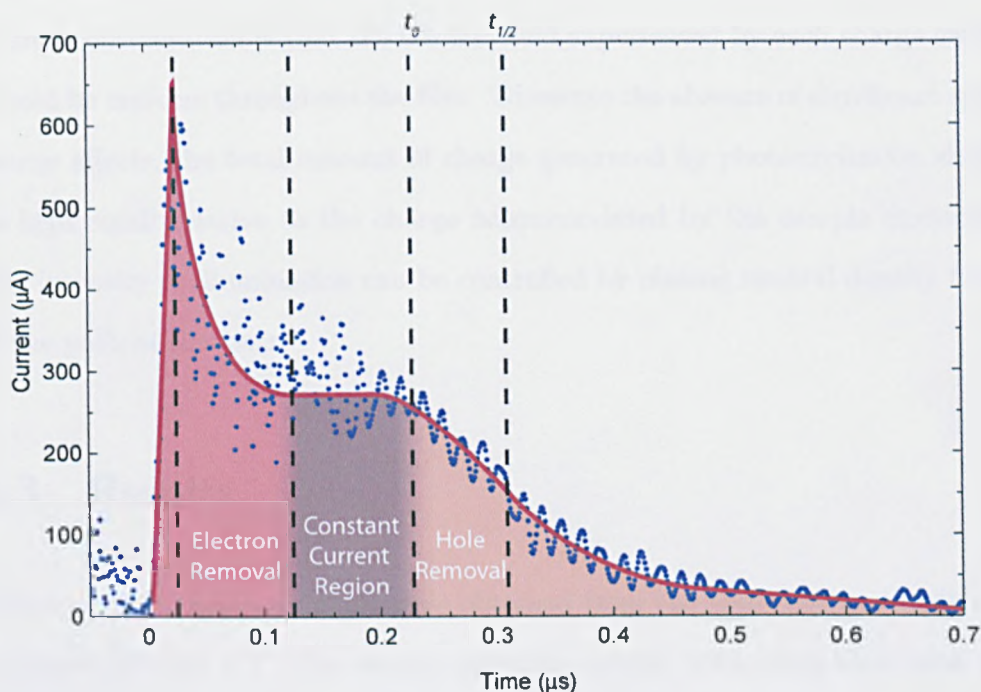


**Fig. 4.2:** Hole photocurrent trace from a TFB sample. The curve provides a guideline, illustrating the shape of a typical non-dispersive transient.

There are a number of conditions that must be met to ensure that the measured photocurrent is a true representation of charge transport within the sample. Firstly, it is important that the photoexcitations are generated close to the illuminated electrode. This ensures that the measured transit time results from carriers that have traversed the full width of the sample. Therefore, the total thickness of the sample must be much larger than the penetration depth of the excitation radiation. This is defined as the distance at which the intensity of the excitation is reduced to  $1/e$  of its initial value and is equal to the reciprocal of the absorption coefficient.

It is also important that the shape of the transient photocurrent is not modified by the response of the measurement circuit. The RC time constant must therefore be kept significantly shorter than the transit time of the charge carriers. In practice, this requirement results in a trade off between temporal response and signal strength, which is controlled by the size of the load resistor.

A final consideration is that the electric field experienced by each charge carrier should be uniform throughout the film. To ensure the absence of significant space charge effects, the total amount of charge generated by photoexcitation should be kept small relative to the charge accommodated by the sample electrodes. The intensity of illumination can be controlled by placing neutral density filters in the path of the laser.

### 4.3 Results

Photocurrent transient signals were obtained from the triarylamine-substituted polymers **P6** and **P7**. The details regarding sample fabrication have been discussed in chapter 2. Polymer **P6** was spun to a thickness of 1.07  $\mu\text{m}$  and **P7** to a thickness of 0.55  $\mu\text{m}$ . To evaluate any field-dependent variations in mobility, several transient signals were recorded at a variety of voltages for each sample.

As discussed, it is necessary to ensure that the RC response of the time-of-flight circuit is significantly smaller than the transit time  $t_0$ . The total resistance of the circuit was predominantly determined by the presence of the load resistor. Depending upon the size of the photocurrent, this was varied between 50-200  $\Omega$ . As the samples typically had a capacitance of around 0.2 nF, a time-constant  $\tau \approx 40$  ns can be calculated for the high sensitivity measurements. This is substantially faster than the observed transit times.

The penetration depth at 337 nm (the wavelength of the  $\text{N}_2$  laser) was calculated from the absorption spectra of the two polymers. At this wavelength, the absorption coefficient of polymer **P7** was  $1.01 \times 10^5 \text{ cm}^{-1}$ , corresponding to a

depth of 99 nm, less than 20% of the film thickness. The sample fabricated from P6 had a penetration depth equivalent to 11% of the overall film thickness. The total amount of photogenerated charge, calculated by integrating the photocurrent transients, was typically 10 - 20% of the charge (CV) stored on the device electrodes.

### 4.3.1 Time-of-Flight Photocurrents

Figure 4.3 presents the TOF transient from polymer P6 when a 0.51 MV/cm electric field was applied to the device. The sample was biased such that the measured signal resulted from the drift of positively charged carriers. This data is representative of the photocurrents obtained throughout the full range of field strengths.

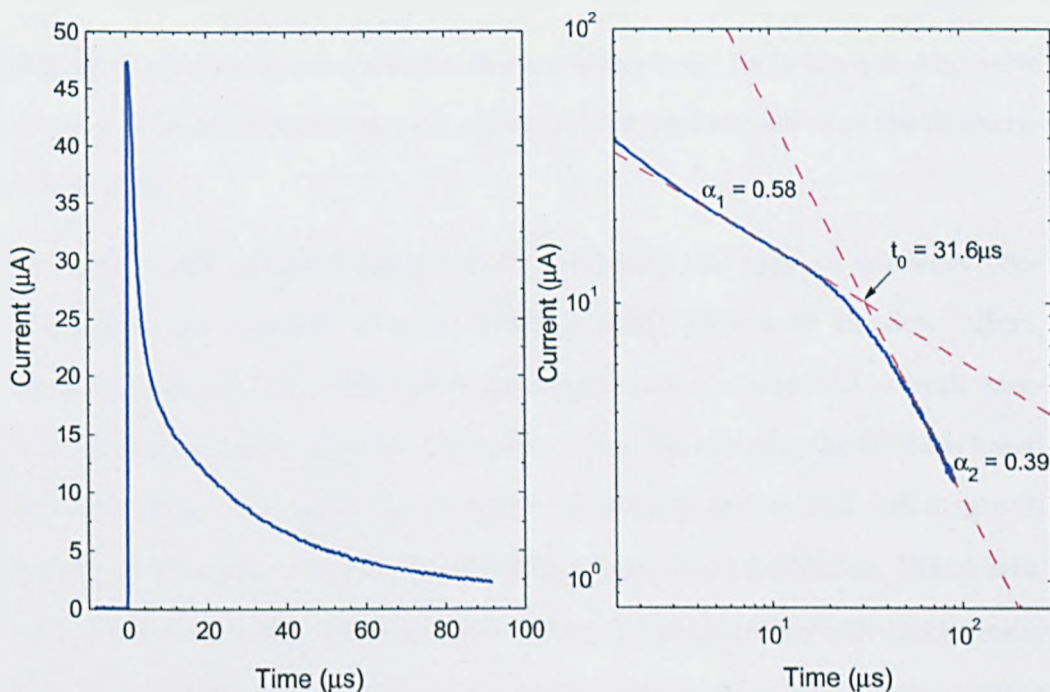


**Fig. 4.3:** The photocurrent transient for holes obtained from polymer P6. An electric field of 0.51 MV/cm was held across the polymer film. Plotting the data on a log-log scale reveals an inflexion point indicating the transit time of the fastest carriers,  $t_0$ .

In contrast to the transient obtained from the TFB sample, this data exhibits

a continuous decrease in current with no distinguishable plateau region. This form of photocurrent is common among many amorphous materials and is associated with dispersive transport. The absence of any plateau region reflects the continual decrease in the mean velocity of the charge carriers.

The analysis of these dispersive photocurrent transients was based upon the method of Scher and Montroll.<sup>12</sup> By plotting the data on a double log scale, two linear regions can be identified, the first being associated with the pre-transit photocurrent, and the second, steeper region, indicating the absorption of carriers at the counter electrode. These two regions were fitted using

$$\begin{aligned}
 I &= A_1 t^{-(1-\alpha_1)}; & [t < t_0] \\
 I &= A_2 t^{-(1+\alpha_2)}; & [t > t_0]
 \end{aligned}
 \tag{4.1}$$

allowing (as depicted) extrapolation to an intercept,  $t_0$ . As in the non-dispersive transient, this indicates the time at which the first carriers arrive at the discharging electrode.

The most widely adopted formalism for analysing this type of transient photocurrent is the Gaussian Disorder Model (GDM) derived by Bässler.<sup>13</sup> Here, the charge carriers are considered to propagate across a manifold of both energetically and spatially disparate transport states. Specifically, the GDM is based upon the assumption that the energetic (diagonal) and spatial (off-diagonal) disorder of these states can be described by a Gaussian distribution. When arbitrarily generated within this density-of-states, a charge carrier will energetically relax by initiating a series of hopping events until eventually reaching a mean energy level below the center of the distribution.<sup>14</sup> Dispersive transport occurs when the transit time of the carriers is shorter than the time required to reach energetic equilibrium within the manifold of transport states. Simulations have shown this to be dependent upon the degree of energetic disorder, defined by the standard deviation of the distribution  $\sigma$ .<sup>15</sup>

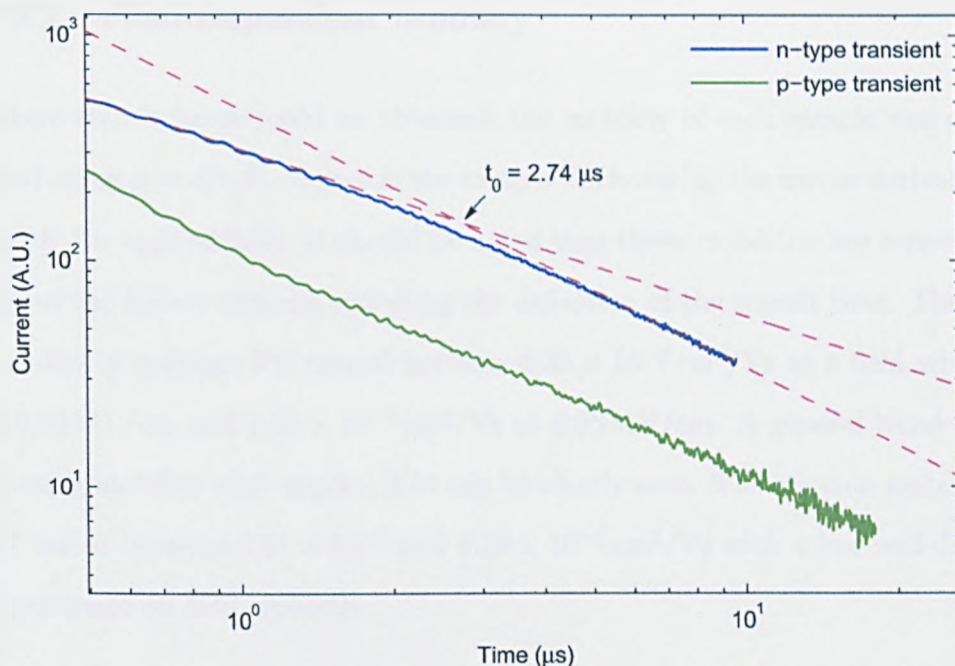


**Fig. 4.4:** Photocurrent transients obtained from polymer **P7**. The electron transient was obtained with an applied field of  $-0.84$  MV/cm and the hole transient at an applied field of  $+0.11$  MV/cm.

The photocurrent transient for electrons, obtained by applying a negative bias relative to the illuminated electrode, was also obtained from **P6** at a variety of voltages. However, these transients were extremely dispersive, possibly indicating from the presence of deep traps for n-type carriers. Determination of the transit time from these measurements was prohibited as there was no discernable transition, even when plotted on a double log scale.

Figure 4.4 shows the transient photocurrent obtained from polymer **P7** when both positive and negative biases are applied. Although both transient signals are highly dispersive, a gradual inflexion in the electron photocurrent can be identified, allowing the determination of the transit time. No such feature can be found in the hole transient. This is in contrast to the results obtained from **P6** where the electron photocurrents were significantly more dispersive than the hole photocurrents, suggesting that the incorporation of the oxadiazole moiety may indeed alter the balance of charge transport in a bipolar device.

### 4.3.2 Field-Dependent Mobility

Where transit times could be obtained, the mobility of each sample was calculated using  $\mu = d/t_0E$ . Here  $d$  is the sample thickness,  $t_0$  the carrier arrival time and  $E$  the applied field. It should be noted that these mobilities are representative of the fastest carriers, reflecting the definition of the transit time. The hole mobility of polymer **P6** ranged between  $6.35 \times 10^{-6} \text{ cm}^2/\text{Vs}$  at a field strength of  $0.53 \text{ MV/cm}$  and  $2.86 \times 10^{-5} \text{ cm}^2/\text{Vs}$  at  $0.95 \text{ MV/cm}$ . A general trend of increasing mobility with applied field can be clearly seen. The electron mobility of **P7** varied between  $2.51 \times 10^{-5}$  and  $4.36 \times 10^{-5} \text{ cm}^2/\text{Vs}$  with a less well-defined dependence on field strength.

For amorphous organic materials, the variation of mobility with field strength is often analysed in terms of a Poole-Frenkel-like dependence.<sup>16</sup> This describes an exponential relationship between  $\mu$  and the square root of the applied field.

$$\mu = \mu_0 \exp(\gamma\sqrt{E}) \quad (4.2)$$

In this format, the temperature dependence has been neglected such that any value derived for the zero field mobility  $\mu_0$  and the Poole-Frenkel coefficient  $\gamma$  is only valid at room temperature. When compared against the expression for mobility derived from the Gaussian Disorder Model, equivalence can be attained by incorporating a temperature dependence.<sup>13</sup>

$$\mu(E, \hat{\sigma}, \Sigma) = \mu_0 \exp \left[ - \left( \frac{2}{3} \hat{\sigma} \right)^2 \right] \times \begin{cases} \exp [C(\hat{\sigma}^2 - \Sigma^2)\sqrt{E}]; & \Sigma \geq 1.5 \\ \exp [C(\hat{\sigma}^2 - 2.25)\sqrt{E}]; & \Sigma < 1.5 \end{cases} \quad (4.3)$$

Here, the energetic disorder parameter  $\hat{\sigma}$  is defined by the standard deviation of the gaussian distribution,  $\sigma$ , and the temperature,  $T$ , such that  $\hat{\sigma} = \sigma/k_B T$ . The term  $\Sigma$  represents the off-diagonal disorder which is also described by a gaussian



distribution.

Figure 4.5 shows the field dependent mobility of holes for polymer **P6** and electrons for polymer **P7**. When plotted on a logarithmic scale, the hole mobility of **P6** shows a linear trend with the square root of the applied field. This is indicative of the field dependent behaviour described by equation 4.2. Fitting the data to this expression yielded values of  $\mu_0 = 1.33 \times 10^{-7} \text{ cm}^2/\text{Vs}$  for the zero field hole mobility of **P6** with  $\gamma = 5.5 \pm 0.9 \times 10^{-3} \text{ (cm/V)}^{1/2}$  for the Poole-Frenkel coefficient.

The variation of electron mobilities calculated for polymer **P7** is much smaller, despite being measured over a wider range of field strengths. No clear field dependence was observed from this material.

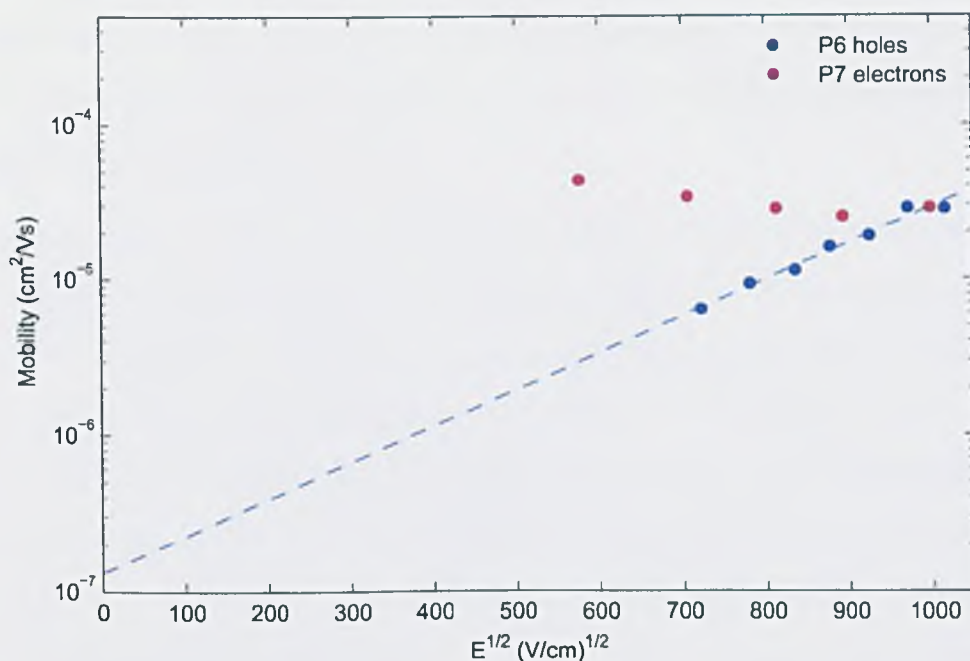


**Fig. 4.5:** Electric field dependence of hole mobility of polymer **P6** and the electron mobility of polymer **P7**. Data has been plotted as  $\mu$  vs  $\sqrt{E}$  on a semi-log scale to identify Poole-Frenkel-like behaviour.

In the general context of organic semiconductors, the carrier mobilities measured for both polymers **P6** and **P7** are quite low. These results, in conjunction with the observation of highly dispersive transport, suggest the existence of a wide

distribution of transport states. This supposition could be further investigated by studying the temperature dependence of mobility.

The observation of low mobility and dispersive transport has also been associated with the presence of deep traps below the intrinsic transport manifold. Charge carriers become immobilised within the trap states and will no longer contribute to the flow of current until thermally released. This results in the observation of both decreased currents and increased transit times. Simulations have shown that, within the Gaussian Disorder Model, the presence of trap states can be accounted for by an effective increase in the energetic disorder parameter, the magnitude of which is dependent upon the concentration and depth of the traps.<sup>17</sup> It is therefore possible for an intrinsically non-dispersive material to exhibit dispersive behaviour if a sufficient concentration of trapping species are present. This situation will occur when the effective width of the density of states becomes greater than the critical width at which the non-dispersive - dispersive transition occurs.<sup>15</sup>

Experimentally, this phenomenon has been observed in a model system of small molecular materials.<sup>18</sup> To simulate the presence of traps, various concentrations of a low ionisation potential material (1-NaphDATA) were doped into an  $\alpha$ -NPD host layer. Time-of-flight photocurrent measurements were used to show that the hole mobility of a film that incorporated a low concentration of the dopant was up to two orders of magnitude lower than that of the pristine sample. Furthermore, under an increased dopant concentration the sample underwent a transition from being intrinsically non-dispersive, to exhibiting dispersive behaviour, as predicted by the simulations.

## 4.4 Conclusion

Photocurrent transients have been obtained from the triarylamine-substituted polycarbazoles **P6** and **P7**. The homopolymer **P6** displayed dispersive transport

characteristics for both holes and electrons. However, a much greater degree of dispersion was observed from the electron transients, possibly indicating the presence of deep trapping states below the LUMO. The featureless nature of the electron photocurrents, even after plotting on a double logarithmic scale, prohibited determination of the carrier transit time. The opposite trend was observed from the oxadiazole-containing copolymer **P7**. For this material, the photocurrents obtained from the transit of electrons were less dispersive than those from the transit of holes.

On investigation of the field dependence, the hole mobilities obtained from polymer **P6** were in good agreement with a Poole-Frenkel-type relationship. A value of  $\mu_0 = 1.33 \times 10^{-7} \text{ cm}^2/\text{Vs}$  was obtained for the zero-field hole mobility with a Poole-Frenkel coefficient of  $\gamma = 5.5 \pm 0.9 \times 10^{-3} (\text{cm}/\text{V})^{1/2}$ . The electron mobilities obtained from the copolymer **P7** showed little field dependence.

The results from this study suggest that electron transport in triarylamine-substituted polycarbazoles can be improved through the incorporation of oxadiazole into the main-chain. Further work is needed to investigate the dependence of mobility upon film thickness and to obtain electron and hole mobilities for polymers **P6** and **P7** respectively.

---

## References

- [1] Stolka, M., Yanus, J. F., and Pai, D. M. *J. Phys. Chem.* **88**(20), 4707–4714 (1984).
- [2] Fong, H. H., Papadimitratos, A., and Malliaras, G. G. *Appl. Phys. Lett.* **89**(17), 172116 October (2006).
- [3] Redecker, M., Bradley, D. D. C., Inbasekaran, M., and Woo, E. P. *Appl. Phys. Lett.* **73**(11), 1565–1567 September (1998).
- [4] Redecker, M., Bradley, D. D. C., Inbasekaran, M., Wu, W. W., and Woo, E. P. *Adv. Mater.* **11**(3), 241 February (1999).
- [5] Kepler, R. G., Beeson, P. M., Jacobs, S. J., Anderson, R. A., Sinclair, M. B., Valencia, V. S., and Cahill, P. A. *Appl. Phys. Lett.* **66**(26), 3618–3620 June (1995).
- [6] Campbell, I. H., Smith, D. L., Neef, C. J., and Ferraris, J. P. *Appl. Phys. Lett.* **74**(19), 2809–2811 (1999).
- [7] Redecker, M., Bradley, D. D. C., Inbasekaran, M., and Woo, E. P. *Appl. Phys. Lett.* **74**(10), 1400–1402 March (1999).
- [8] Malliaras, G. G., Shen, Y. L., Dunlap, D. H., Murata, H., and Kafafi, Z. H. *Appl. Phys. Lett.* **79**(16), 2582–2584 October (2001).
- [9] Lee, S. H., Yasuda, T., and Tsutsui, T. *J. Appl. Phys.* **95**(7), 3825–3827 April (2004).
- [10] Kepler, R. G. *Phys. Rev.* **119**(4), 1226–1229 (1960).
- [11] Campbell, A. J., Bradley, D. D. C., and Antoniadis, H. *Appl. Phys. Lett.* **79**(14), 2133–2135 October (2001).
- [12] Scher, H. and Montroll, E. W. *Phys. Rev. B: Condens. Matter Mater. Phys.* **12**(6), 2455–2477 (1975).
- [13] Bassler, H. *Phys. Status Solidi B* **175**(1), 15–56 January (1993).
- [14] Bassler, H., Schonherr, G., Abkowitz, M., and Pai, D. M. *Phys Rev B: Condens Matter Mater Phys* **26**(6), 3105–3113 (1982).
- [15] Borsenberger, P. M., Pautmeier, L. T., and Bassler, H. *Phys. Rev. B: Condens. Matter Mater. Phys.* **46**(19), 12145–12153 November (1992).
- [16] Gill, W. D. *J. Appl. Phys.* **43**(12), 5033–5040 (1972).
- [17] Wolf, U., Bassler, H., Borsenberger, P. M., and Gruenbaum, W. T. *Chem. Phys.* **222**(2-3), 259–267 October (1997).
- [18] Fleissner, A., Schmid, H., Melzer, C., and von Seggern, H. *Appl. Phys. Lett.* **91**(24), 242103 December (2007).

## **Chapter 5**

# **Optoelectronic Characterisation of 'Single-Component' LEDs**

### **5.1 Introduction**

This chapter reports upon the fabrication and characterisation of polycarbazole-based light-emitting diodes. Each of the seven polymers were incorporated into 'single-component' devices whereby the emissive polycarbazole was deposited directly between the anode and cathode and no other active materials were present. The devices were evaluated with regard to their electronic and luminescent properties.

## 5.2 Device Structure

All of the devices discussed in this chapter were fabricated with a basic anode/polymer/cathode structure. In this simple OLED architecture, electroluminescence is generated via the direct injection of carriers into the semiconducting polymer. Such a device can be optimised through an appropriate choice of electrode materials and deposition parameters. These factors are discussed herein.

### 5.2.1 The Conducting Polymeric Anode

Poly(3,4-ethylenedioxythiophene) (PEDOT) is a low energy-gap (around 1.6–1.7 eV),<sup>1</sup> stable derivative of polythiophene. When synthesised in conjunction with a polystyrene sulfonic acid (PSS) electrolyte, it forms an ionic complex which has proven to have many desirable properties. These include high conductivity, optical transparency, high work function, environmental stability and solution processability making it of particular importance with regard to application in organic LEDs.

Structurally, the PEDOT:PSS complex forms from the ionic bonding of low molecular weight PEDOT<sup>+</sup> cations onto segments of the much larger, anionic PSS<sup>-</sup> molecule.<sup>2</sup> Synthesised in an aqueous dispersion, these molecules coalesce with an excess of the PSS<sup>-</sup> species to form negatively charged colloidal gel particles. Although effectively insoluble, these gel particles exist as a solution processable suspension in water. When deposited as a thin film, this particulate structure is manifest by the resulting granular morphology, the nature of which strongly influences the film's electronic properties.<sup>3–5</sup> The lack of solubility of the PEDOT:PSS complex in organic solvents facilitates its use in the standard PLED device structure.

In a conventional device, the conducting polymer functions more as an anode modification than as a complete replacement for the ITO alloy. Indeed, attempts

to fabricate a fully solution processable anode using PEDOT:PSS alone were unsuccessful as the conductivity of the material was proven to be too low. Devices that were fabricated using this structure required a high operating voltage owing to the large drop in potential across the resistive electrode.<sup>6</sup> The incorporation of an ITO underlayer is thus required to provide a sufficiently high conductivity whilst maintaining optical transparency.

The incorporation of the PEDOT:PSS conducting layer has numerous benefits over a conventional ITO anode. Firstly, it functions as a buffer layer between the polymeric semiconductor and the ITO. The surface of ITO can feature large spikes which under device operation can act to enhance the electric field, forming localised channels that sustain abnormally high current densities. Resistive heating melts the polymer, causing the formation of micro-shorts and the appearance of non-emissive regions or 'dark spots'.<sup>7</sup> The layer of PEDOT:PSS is known to form a smoother interface with the polymeric film, reducing the formation of electrical shorts and improving device stability<sup>8</sup>.

In addition to this, the polymeric buffer layer can also provide a barrier to chemical degradation by separating the semiconductor from the ITO anode. FTIR measurements have been used to show that oxygen extraction from ITO is a possible degradation mechanism, particularly when other sources (such as atmospheric oxygen) have been excluded.<sup>9</sup> The improved device stability observed on inclusion of a polymeric injection layer (when polyaniline was used as well as PEDOT:PSS) was consequently attributed to the removal of the ITO/emitter interface.<sup>10</sup>

One of the main functions of the PEDOT:PSS layer is to facilitate enhanced hole injection into the semiconducting polymer. This is of particular importance in materials with a high ionisation potential such as polyfluorene, where an injection barrier of approximately 1 eV can exist. The work function of a PEDOT:PSS layer has been indirectly measured through the use of electroabsorption spectroscopy. Here, the magnitude of the built-in field was seen to

increase by 0.5 eV relative to a device that did not include the polymeric conductor but was otherwise identical.<sup>11</sup> Assuming the work function of ITO to be between 4.7-4.8 eV, the incorporation of PEDOT:PSS increased the work function to between 5.2-5.3 eV. In addition, the work function of PEDOT:PSS, as measured by UV photoemission spectroscopy, was found to be around 5.15 eV, which is still consistent with a reduced injection barrier for holes.<sup>12</sup> There is also evidence that the injection barrier is reduced further by electron trapping at the PEDOT:PSS interface which may lead to ohmic injection in some materials.<sup>13</sup>

All of the devices reported in this work incorporated the ITO/PEDOT:PSS bilayer anode. When the PEDOT layer was absent, devices suffered from very short lifetimes and instability. Importantly, it was found that their characterisation lacked repeatability and was inconsistent, even when comparing two diodes that had been fabricated on the same substrate. Devices that included the bilayer anode showed a marked improvement in this regard, allowing characterisation that was a true representation of the diode's properties.

A low conductivity grade, aqueous solution of PEDOT:PSS, Clevios P CH8000, was supplied by H. C. Stark and deposited as received. Specifically, this corresponds to a blend ratio of 1:20 PEDOT:PSS by weight and a particle diameter predominantly below 35 nm. This particular blend was specifically developed for use in matrix addressed displays where crosstalk between neighbouring pixels would be enhanced in a higher conductivity form of the material.

### **5.2.2 Active Layer Thickness**

Of the many parameters that can be adjusted and optimised in the fabrication of organic LEDs, the thickness of the constituent layers is perhaps one of the most fundamental. However, the derivation of a relationship between film thickness and device characteristics is not trivial and is dependent upon the properties of the system as a whole. Consequently, the process of device optimisation is



unique to each polymer and only applicable to a specific device structure.

When the thickness of the active semiconducting layer is varied, it influences both the electronic and optical properties of the device. Electronically, by decreasing the film thickness, a larger electric field is induced at a given applied bias. The operating voltage, and consequently the power efficiency  $\eta_P$ , can therefore be reduced by using thinner layers. The derivation of an exact relationship between film thickness and the electronic properties of a device is more complicated and is dependent upon the nature of the system. Although equations for space charge limited and injection limited currents do describe a thickness dependence, it should be reiterated that these are approximations and do not account for the flow of a bipolar current.

The thickness of the constituent layers can also have a profound influence on the optical properties of the device. The simplest of considerations in this regard is the effect of self absorption, caused by the overlap of the semiconductor's emission and absorption spectra. Typically, this will be manifest by a reduction in short-wavelength emission that is dependent upon the position of the recombination zone within the organic layer. In a conventional bottom-emitting structure, where emission is extracted through the ITO anode, this effect is most prominent when exciton generation occurs near the cathode. As the thickness of the emitting layer is increased, the influence of self absorption becomes more significant, particularly in materials which exhibit a small Stokes shift.

A more complex analysis will consider the occurrence of cavity modes between the highly reflective cathode and the partially reflective anode,<sup>14</sup> metal-dipole interactions near the cathode,<sup>15</sup> and waveguiding within the semiconductor. Each of these processes will be dependent upon the film thickness and, in combination, can vastly alter the emissive properties of the organic layer.<sup>16</sup> A particularly effective demonstration of the optical cavity effect revealed that a single polymeric emitter (LPPP) could be used in the fabrication of red, green and blue LEDs simply by varying the thickness of the active layer.<sup>17</sup> Thus, by controlling the

thickness of the constituent layers, the efficiency of emission from the device can be optimised.<sup>18</sup>

Investigation into the thickness dependent properties of organic LEDs is complicated further in solution processed polymeric systems. Here, the deposition process can itself influence the electronic and optical properties of the device. When the polymeric semiconductor is deposited by spin casting, thickness variations are achieved by controlling the concentration (and resulting viscosity) of the solution and the angular velocity of the spinning process. However, these factors alone can change the photophysical properties of the polymer film, irrespective of a change in thickness. In their study of MEH-PPV, Yang and coworkers suggested that the presence of molecular agglomerates, formed in solution but persistent in the thin film, was responsible for changes in the emission spectra between samples fabricated with different deposition parameters.<sup>19</sup> In addition, they showed that deposition induced morphological variations can also influence the electronic properties of a device.<sup>20</sup>

In all, these considerations necessitate an experimental optimisation for each polymer in each of its device configurations. However, given the limitations on material and time, this proved to be impractical. Therefore the semiconducting layer was spun to a target thickness of between 50 nm and 100 nm. This ensured that the device operating voltage was minimised whilst the occurrence of shorts resulting from film defects was negligible.

### **5.2.3 Cathode**

To facilitate electron injection, a low work-function Ca cathode has been used in this study. Some devices also incorporated a thin layer of lithium fluoride at the cathode/polymer interface. This layer has been found to improve electronic injection from both aluminium and calcium.<sup>21,22</sup> Although electroabsorption measurements have identified a reduction in the cathodic work function on

the incorporation of the LiF layer, the exact mechanism by which this occurs is unknown.<sup>22</sup> Various phenomena have been proposed such as charge confinement at the interface<sup>23,24</sup> and the liberation of low work function lithium.<sup>22,25</sup>

All cathodes were capped with a 100 nm of silver. This layer not only functions to protect the underlying calcium, but also reflects any light that is emitted toward the rear surface of the device.

### 5.3 Electrochemical Characterisation

Of the many factors that determine the operational characteristics of an organic light-emitting diode, the positioning of the component energy levels is considered to be amongst the most influential. As such, the determination of a material's ionisation potential and electron affinity is of great importance in understanding its function in a working device.

Cyclic voltammetry, an electrochemical technique, is frequently used for this purpose. Here, the organic material is deposited onto the working electrode and placed into an electrolyte solution. In the conventional 3-electrode configuration a bias is applied across the working electrode and a standard reference electrode and is linearly cycled between two switching potentials. The onset of current flow between the working and counter electrodes is then used to determine the oxidation and reduction potentials of the sample relative to the reference. As the potential of the reference electrode relative to the vacuum level is a known quantity, the ionisation potential or electron affinity of the organic material can be estimated.

As a consequence of their low electron affinity, it was often not possible to observe a reduction wave (n-type doping) from the polycarbazoles that were investigated in this study. Difficulty in obtaining a direct measurement of the reduction potential in such materials is not an uncommon occurrence. Consequently, it has become standard practice to estimate the electron affinity by subtracting an op-

tically determined band gap from the material's ionisation potential.<sup>26</sup> Although frequently adopted, the accuracy of this method is limited. The optical gap is most often calculated from the onset of absorption, representing the low-lying energy states that are involved in the vast majority of electronic transitions in a device. However, the 'single particle energy gap' (as would be determined from electrochemical means alone), is typically larger than the optical gap as a result of the exciton binding energy ( $\epsilon_b$ ).<sup>27</sup> Values in excess of  $\epsilon_b = 1.0$  eV have been reported in some conjugated materials.<sup>28</sup> This can result in a sizeable error in the estimation of a material's electron affinity if the exciton binding energy is neglected.

In the absence of an electrochemically derived electron affinity, the 'optical gap' technique has been used to complete the energy level diagrams for the polymers discussed here. However, based upon the above argument, it must be emphasised that the calculated electron affinity should only be considered as an estimate. Although a study carried out on PFO suggested that this methodology can be prone to sizeable errors,<sup>29</sup> measurements carried out on a 2,7-linked polycarbazole have shown the electrochemical and optical band gap to be equivalent.<sup>30</sup>

It should be noted that any electrochemical data discussed in this section was acquired by members of the Department of Chemistry at the University of Sheffield prior to receipt of the material.

## 5.4 Results

### 5.4.1 Alkyl-Substituted Polymers

Single layer devices incorporating the alkyl-substituted polymers, **P1**, **P2** and **P3** as the active layer, were fabricated. All three of these polymers bear protecting methyl substitutions at the 3 and 6 positions to improve their stability. Cyclic voltammetry studies have revealed that without these protecting groups, the

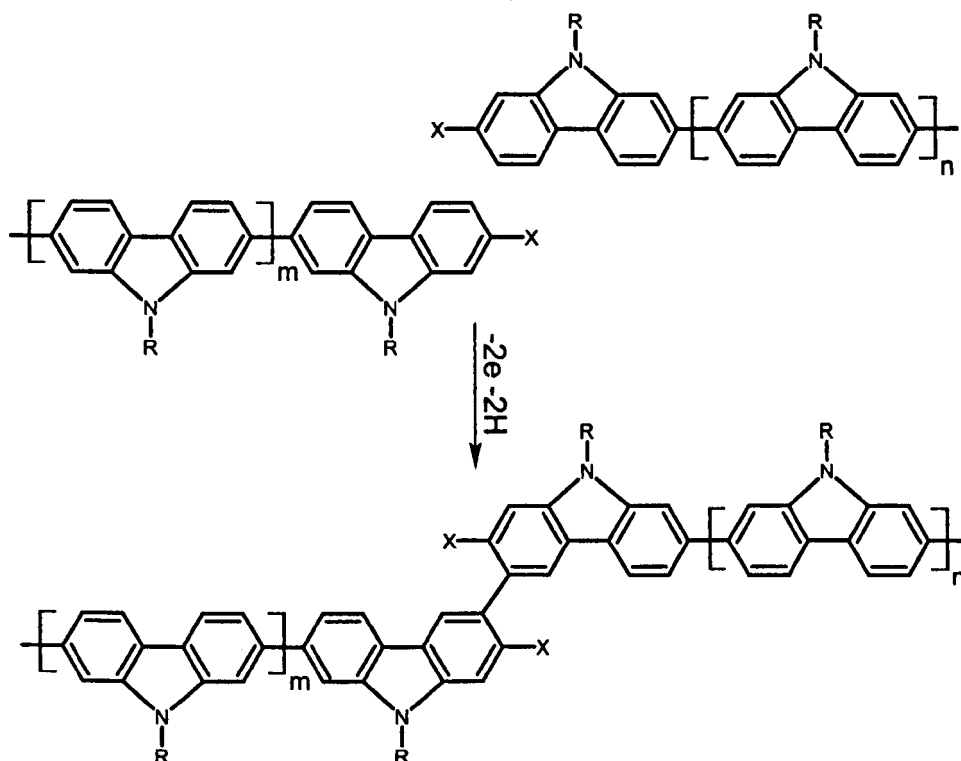


**Fig. 5.1:** The cross-linking of adjacent chain-terminating carbazole units upon oxidation. This scheme has been reproduced from reference 30.

alkyl substituted homopolymer (poly(9-alkyl-9H-carbazole-2,7-diyl)) is unstable under electrochemical oxidation. This was manifest by the emergence of a new, low-energy oxidation peak that could be observed on repeated scanning.<sup>31</sup>

In a separate study, Zotti *et al.* also detected the irreversible formation of new absorption bands that were induced during oxidation.<sup>30</sup> Furthermore, this treatment also caused the material to become insoluble. Given the evidence available to them, the authors proposed that when oxidised, this material would cross-link at the 3 and 3' positions of chain-terminating carbazole units. This process is depicted in figure 5.1.

In an effort to inhibit degradation in this class of material, the 3,6-methyl protected polymers **P1** and **P2** were synthesised. An initial investigation into their electrochemical properties was carried out prior to this work.<sup>32</sup> The cyclic voltam-

mograms revealed that in contrast to the previously reported polyalkylcarbazoles, both materials underwent reversible oxidation. These results suggested that the incorporation of 3,6-protection should afford the material an enhanced stability in working devices.

The ionisation potentials ( $I_p$ ) of the two materials, obtained from the onset of oxidation, were found to be 5.5 eV for **P1** and 5.2 eV for **P2**. When compared against the electrochemical properties of poly(9,9-dioctylfluorene) (PFO), this represents a decrease in  $I_p$  of 0.3-0.6 eV. Using their optical band gap, the electron affinities ( $E_a$ ) of **P1** and **P2** were calculated as 2.3 eV and 2.2 eV respectively. These values have been used to construct the band diagram presented in figure 5.2.

Due to its high electron affinity, materials that incorporate an oxadiazole ring are often found to be efficient at injecting and transporting electrons. At the same time, their high ionisation potential inhibits the transport of holes. Several groups have reported the synthesis of biphenyl oxadiazole-containing polymers which exhibit improved electron transporting/hole blocking properties.<sup>33-37</sup> On its incorporation into the main-chain of an alkoxy substituted PPV the oxadiazole moiety was found to lower the operating voltage and increase the efficiency of single layer devices with an air stable aluminium cathode.<sup>33</sup> The enhancement in device performance was attributed to the improved injection and transport in electrons. As the PPV homopolymer was expected to primarily transport holes, it was suggested that, on incorporation of the biphenyl oxadiazole unit the copolymer could more efficiently accommodate a balanced bipolar current.

From its electrochemical properties, the ionisation potential of **P3** was found to be 5.4 eV, between that of the homopolymer **P1** and the copolymer **P2**. Significantly however, a band gap of 3.0 eV was determined from the onset of optical absorption. This suggests that the electron affinity of **P3** is higher than that of both **P1** and **P2**, resulting in a reduction in the electronic injection barrier from a calcium cathode.

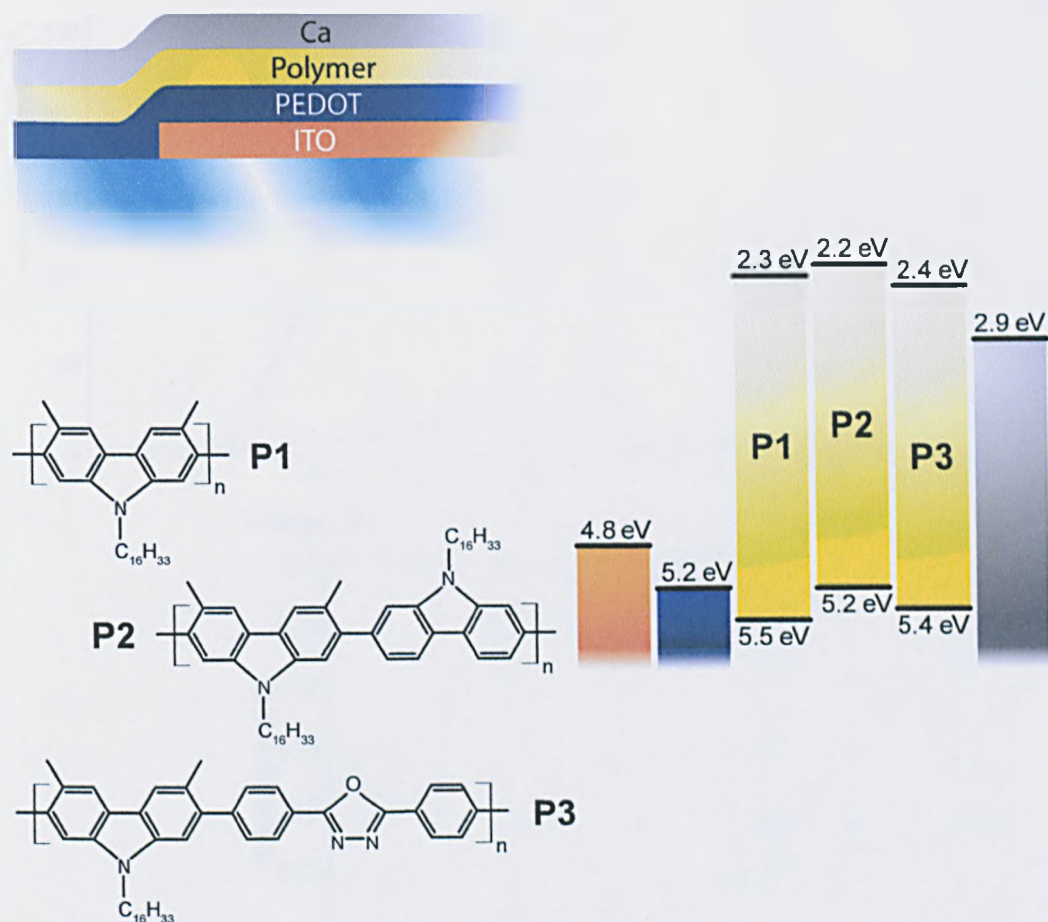


**Fig. 5.2:** The device structure and corresponding energy level diagram of single layer devices containing polymers **P1**, **P2** and **P3**. The chemical structures of the three polymers have been included for reference.

### Device Characteristics

Figure 5.3 presents the I-V-L characteristics of the three single layer devices fabricated from polymers **P1**, **P2** and **P3**. The thickness of the semiconducting layers were 70 nm, 70 nm and 80 nm respectively. It should be noted that the voltage-luminance characteristics of **P1** and **P2** were measured using a Topcon BM-8 luminance meter as described in Chapter 2. Consequently, the data collected from these two devices was noisier than that of the spectrally stable **P3** device which was measured using a photodiode. The two measurement techniques were

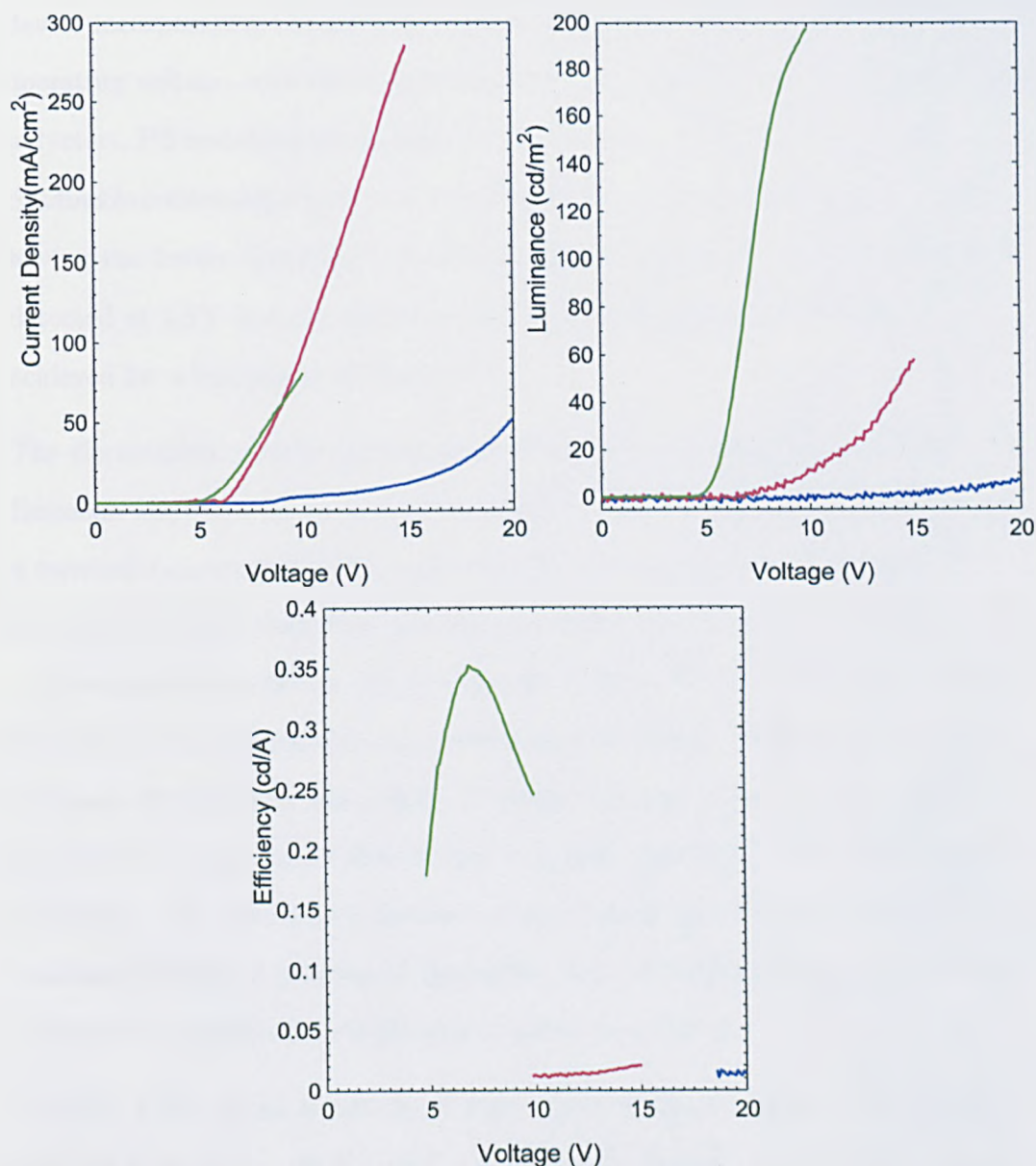


**Fig. 5.3:** The voltage dependence of current density, luminance and current efficiency of the three alkyl substituted polymers **P1** (blue), **P2** (red) and **P3** (green).

checked against each other to ensure consistency.

Of the three polymers, **P1**, the fully methyl-protected homopolymer, shows the highest operating voltage. Electroluminescence from this device structure could be detected at an applied bias of 7.4 V. However, light emission remained low up to a maximum applied bias of 20 V, giving a luminance of 8 cd/m<sup>2</sup>. The



device incorporating the partially methyl-protected copolymer **P2** had a lower operating voltage, with electroluminescence being detected at 5 V. Of the three polymers, **P2** sustained the highest current density of 280 mA/cm<sup>2</sup> at 15 V. The oxadiazole containing copolymer, **P3**, showed the most promising characteristics, having the lowest operating voltage and highest efficiency. Light emission was detected at 3.5 V and the maximum luminance efficiency ( $\eta_L$ ) of 0.35 cd/A was achieved for a luminance of 78 cd/m<sup>2</sup>.

The electroluminescence spectra of the three polymers are shown in figure 5.4. Emission was collected at normal incidence to the device whilst it was driven at a constant-current of 0.5 mA (equivalent to a current density of 11.1 mA/cm<sup>2</sup>). It should be noted that these spectra were taken from pristine devices that had not been previously driven and as such, they reflect the initial state of the device. The spectra would subsequently evolve during operation. It was found that using polymers **P1** and **P2**, this change in emission colour would occur rapidly over the first 5 seconds before slowing and eventually stabilising after 30 seconds of operation. The spectral evolution of **P3** occurred at a much slower rate and continued beyond 2 minutes of operation. The photoluminescence spectrum is presented alongside each set of data to allow comparison.

The EL of **P1** seems to consist of three main emission bands. The first band, peaking at 414 nm, coincides with the photoluminescence spectrum of the pristine film. The absence of vibronic features from both PL and EL may reflect a substantial amount of energetic disorder. A second emission peak, located at 475 nm can also be resolved. The third emission band, which seems to be structured from three or more unresolved features, occurs between 600-800 nm. Interestingly, the intensity of this long wavelength feature reduces with time.

Although the intensities are redistributed, qualitatively, the same three emission bands can be seen in the EL spectrum of polymer **P2**. As with **P1**, emission from the green feature would grow in intensity as the device was operated before the spectrum stabilised. Notably, polymer **P2** retained a greater fraction of the

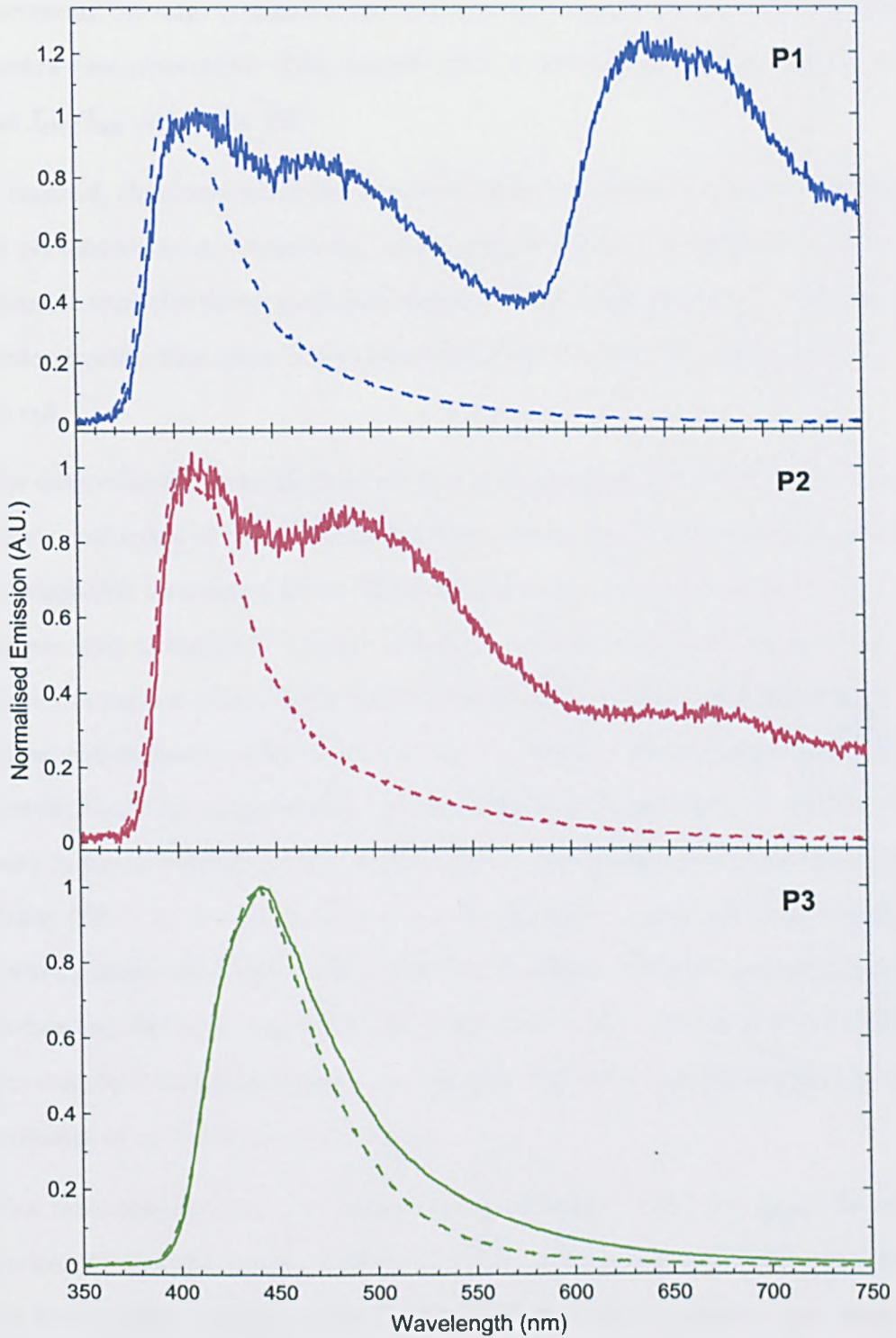


**Fig. 5.4:** The electroluminescence spectra of polymers **P1**, **P2**, and **P3** incorporated into single layer devices (solid line). The thin-film photoluminescence spectra are included for reference (dashed line).

intrinsic blue emission after being driven for 2 minutes. This is illustrated by calculating the ratio of emission intensities at 415 nm and 500 nm of the degraded spectra (not presented). This analysis gives a value of  $I_{415}/I_{500} = 0.28$  for P1 and  $I_{415}/I_{500} = 0.51$  for P2.

In contrast, the electroluminescence spectrum from polymer P3 closely resembles its photoluminescence spectrum, albeit with a slight increase in the FWHM. Emission from this device gradually changed whilst it was operated, but remained predominantly blue after being driven for 2 minutes with a constant current of 0.5 mA.

The data collected from all three devices is summarised in table 5.1. A colourimetric evaluation of the materials has been carried out by calculating their CIE (Commission Internationale de l'Eclairage) chromaticity coordinates. These values are used to represent a unique colour in an internationally recognised colour space. Being the most widely adopted standard, the 'CIE 1931 Standard Observer' colour matching functions were used in the calculation of the chromaticity coordinates.<sup>38</sup> As a benchmark, the recommended chromaticity of the blue primary in the new HDTV format, as listed by the International Telecommunication Union (ITU), is  $x_b = 0.15$  and  $y_b = 0.06$ . However, these values are targeted toward plasma and liquid crystal display technologies. A more appropriate comparison can be made against a 'state-of-the-art' blue-emitting polymer OLED, reported by Cambridge Display Technologies (CDT) as having chromaticity coordinates of  $x_b = 0.14$  and  $y_b = 0.18$ .<sup>39</sup>

This table also lists the maximum external quantum efficiency ( $\eta_{EQE}$ ) for each device. These values were obtained using the method that was outlined in chapter 2. For each polymer, the initial emission spectrum (prior to the onset of degradation) was used for the calculation. As the validity of this approach is dependent upon the emission spectrum from each device remaining constant throughout the I-V-L measurement, these values should only be considered as an approximation.

		<b>P1</b>	<b>P2</b>	<b>P3</b>
Thickness (nm)		70	70	80
Voltage at (V)	1 cd/m <sup>2</sup>	- <sup>a</sup>	- <sup>a</sup>	4.8
	10 cd/m <sup>2</sup>	- <sup>b</sup>	9.8	5.5
	100 cd/m <sup>2</sup>	- <sup>b</sup>	- <sup>b</sup>	7.3
Max Luminance (cd/m <sup>2</sup> )		8	58	198
Current Density at 10 V (mA/cm <sup>2</sup> )		4	96	81
Max Efficiency	(cd/A)	0.02	0.02	0.35
	(% <i>ph/e</i> )	0.02	0.01	0.33
CIE	x	0.33	0.26	0.18
	y	0.28	0.30	0.15
Injection Barrier (eV)	$\Delta E_h$	0.3	0	0.2
	$\Delta E_e$	0.6	0.7	0.5

**Table 5.1:** A list of the key performance metrics for single layer LEDs fabricated using the alkyl-substituted polymers **P1**, **P2** and **P3**.

The devices that were fabricated from polymers **P1** and **P2** suffer from a high operating voltage and low efficiency. It is particularly notable that the current density of the **P1** device remains low, even when driven by a 20 V potential difference, equivalent to an electric field of 2.9 MV/cm. **P2** on the other hand, exhibits a significantly higher current density at a reduced bias. These results clearly indicate an improvement in charge injection and/or transport in **P2**, the 3,6-protected-unprotected alternating copolymer.

Consideration of the energy levels can provide a partial explanation for the disparity between the two polymers. From the band diagram presented in figure 5.2 it can be seen that an energy barrier to the injection of holes of 0.3 eV exists at the PEDOT:PSS/**P1** interface. **P2** on the other hand presents no injection barrier to holes, thus forming an ohmic contact in this device structure. The barrier for electron injection from a Ca cathode is similar in both materials with **P1** presenting a 0.6 eV barrier and **P2**, a 0.7 eV barrier. These values suggest that the improvement in I-V characteristics observed in polymer **P2** may result

<sup>a</sup>Below the detection limit.

<sup>b</sup>Above the maximum luminance.

from an increase in the hole current. Verification of this statement could be achieved by studying the electronic characteristics of single carrier devices. The substantial barrier to electron injection in both materials is likely to cause an imbalance in the flow of carriers resulting in a large leakage current. The low efficiency observed from both of these materials will, in part, result from this.

Aside from their I-V-L characteristics, these two devices also exhibit poor colour purity and stability. The electroluminescence spectra obtained from both polymers **P1** and **P2** contain multiple anomalous emission bands that are either absent or non-resolvable during photoexcitation of the pristine film. As a result, EL emission from the polymers appears white in colour, in contrast to the intrinsic blue emission that is observed from PL.

Due to their wide band gap, blue-emitting materials are particularly susceptible to colour conversion either by energy transfer to, and/or charge trapping on lower energy defect states. These states may result from the presence of chemical defects and impurities that are intrinsic to the pristine material, perhaps as a byproduct of the polymer's synthesis or from its subsequent degradation during storage. However, the rapid evolution of the emission spectrum on the initial operation of each device indicates that these polymers are highly susceptible to electrical degradation. Similar observations have been reported in polyfluorene based devices whereby the oxidation of fluorene at the bridging carbon atom results in the formation of an emissive fluorenone defect. This defect acts as a center for energy transfer as well a site for charge trapping and subsequent recombination, causing a shift in the predominant colour of emission from blue to green.<sup>40</sup> Gong *et al.* discovered that the inclusion of a buffer layer, separating the polyfluorene emitter from the Ca cathode, significantly reduced the occurrence of degradation during device operation.<sup>41</sup> This led to the supposition that the oxidation of polyfluorene is catalysed by the presence of Ca, which diffuses into the polymer film on deposition.

Colour instability has also been studied in a poly(*para*-phenylene) (PPP) based

conjugated polymer. By incorporating the material into an air stable ITO/PE-DOT:PSS/polymer/Al device structure, Mauthner *et al.* were able to study the spectral degradation of the material under different environmental conditions.<sup>42</sup> Based upon the observation of two distinct spectral signatures, they concluded that this polymer formed differing degradation products when operated under an ambient atmosphere and an inert atmosphere. It was suggested that the defect species that was formed under an inert environment resulted from a chemical/electrochemical reaction between the semiconducting polymer and the aluminium cathode. However, on incorporation into a light-emitting electrochemical cell (LEC) structure, the stability of the electroluminescence spectrum from this material was found to improve considerably. Here, an ionic salt is added to the semiconducting polymer such that on the application of a bias, n- and p-type doping of the polymer occurs next to the negatively and positively charged electrodes respectively.<sup>43</sup> It was speculated that the increased spectral stability afforded by the LEC device occurred as a result of a shift in the recombination zone, away from the aluminium induced defects near the cathode.<sup>42</sup>

The **P3** device shows a marked improvement in performance when compared against the other two alkyl-substituted polymers. Although this is most notably manifest by an order of magnitude increase in the luminance efficiency, the device also exhibits a lower electroluminescence threshold voltage. It is this observation in particular that is symptomatic of the increase in electron affinity afforded by the biphenyl oxadiazole unit of polymer **P3**. The reduction in the injection barrier to minority n-type carriers in this device facilitates the initiation of a bipolar current and subsequent recombination and emission at a lower applied bias. Although the observed increase in efficiency is also expected to result from an improvement in the balance of charge carriers, other factors, such as variations in the radiative efficiency of the three polymers will also influence this performance metric.

The improvement in stability observed from the electroluminescence spectrum

of **P3** is also a significant result. There may be several reasons for this. When comparing the optical and electronic properties of an alternating PPV-oxadiazole copolymer against those of the PPV homopolymer, Peng *et al.* also observed a reduced susceptibility to degradation.<sup>33</sup> On studying the IR spectra of UV irradiated films they noted that when both materials were exposed to identical treatments, fewer carbonyl groups (known to be a source of luminescence quenching) were formed in the oxadiazole-containing copolymer. This led them to conclude that the incorporation of oxadiazole into the polymer backbone caused a redistribution of electronic density away from the oxidation-susceptible vinyl bond thus stabilising the material against degradation.

The aforementioned work carried out by Mauthner *et al.* also suggested that spectral instability can be dependent upon the position of the recombination zone within the device.<sup>42</sup> As **P3** has a higher electron affinity than the other alkyl-substituted polymers, recombination is likely to occur further away from the Ca cathode, providing an alternative explanation for the increased stability observed from this polymer.

It should be noted that the observation of low energy defect emission may be associated with a decrease in the radiative efficiency of the material. Such species may also act as charge traps, inhibiting carrier transport across the device. It is therefore possible that the superior I-V-L performance of the **P3** device is more a reflection upon the materials enhanced stability than its intrinsic injection and transport properties.

#### 5.4.2 Aryl-Substituted Polymers

The formation of ground and excited state intermolecular species (aggregates and excimers/exciplexes respectively) has been observed in many conjugated materials. Their presence is frequently cited as a cause of poor radiative efficiency, redshifted emission and thermal instability. A popular strategy for inhibiting

the formation of these states in conjugated polymers involves the attachment of bulky side chains protruding from the molecular backbone. The additional steric hinderance causes, on average, an increase in the separation of the chromophoric species and a reduction in their electronic coupling. To this end, aryl-containing side-chains have been successfully introduced into PPV<sup>44</sup>, PPP<sup>45</sup> and PF<sup>46,47</sup> type materials, improving their solid state emissive properties whilst maintaining solubility. This form of electronic encapsulation can however have a detrimental influence on the mobility of charge carriers in an electroluminescent device.

Alternatively, Jacobs *et al.* suggested that the improvement in performance observed from the phenyl substituted ladder-type polymer polyindeno[1,2-b]fluorene,<sup>48</sup> and later polypentaphenylene,<sup>49</sup> was a consequence of its improved resistance to the formation of chemical defects. Electroluminescent devices that were fabricated from these materials showed a considerable enhancement in stability along with the suppression of a low energy emission band that has been associated with the generation of ketonic defects. Thermal studies, in which the absence of oxidative degradation was observed from the phenyl-substituted polymer, when it had been prevalent in an identically treated alkyl-substituted analog, also supported their proposition.

The two devices discussed in this section were both fabricated using polycarbazoles bearing alkoxy-substituted aryl pendant groups, attached at the nitrogen position of the main-chain. Polymer P4 also differs from the aforementioned poly(alkylcarbazole)s in that it incorporates no substitutions at the reactive 3,6-positions of the carbazole monomer.

The ionisation potential of this polymer, as determined from the onset of electrochemical oxidation, was found to be 5.4 eV. However, the absence of an associated reduction wave, accompanied by the loss of electroactivity on repeated cycling, showed that the oxidation process was irreversible. As was found in the unprotected poly(alkylcarbazole)s,<sup>31</sup> this behaviour may indicate the formation of new linkages at the 3,6-positions. From the optical bandgap, the electron affinity was



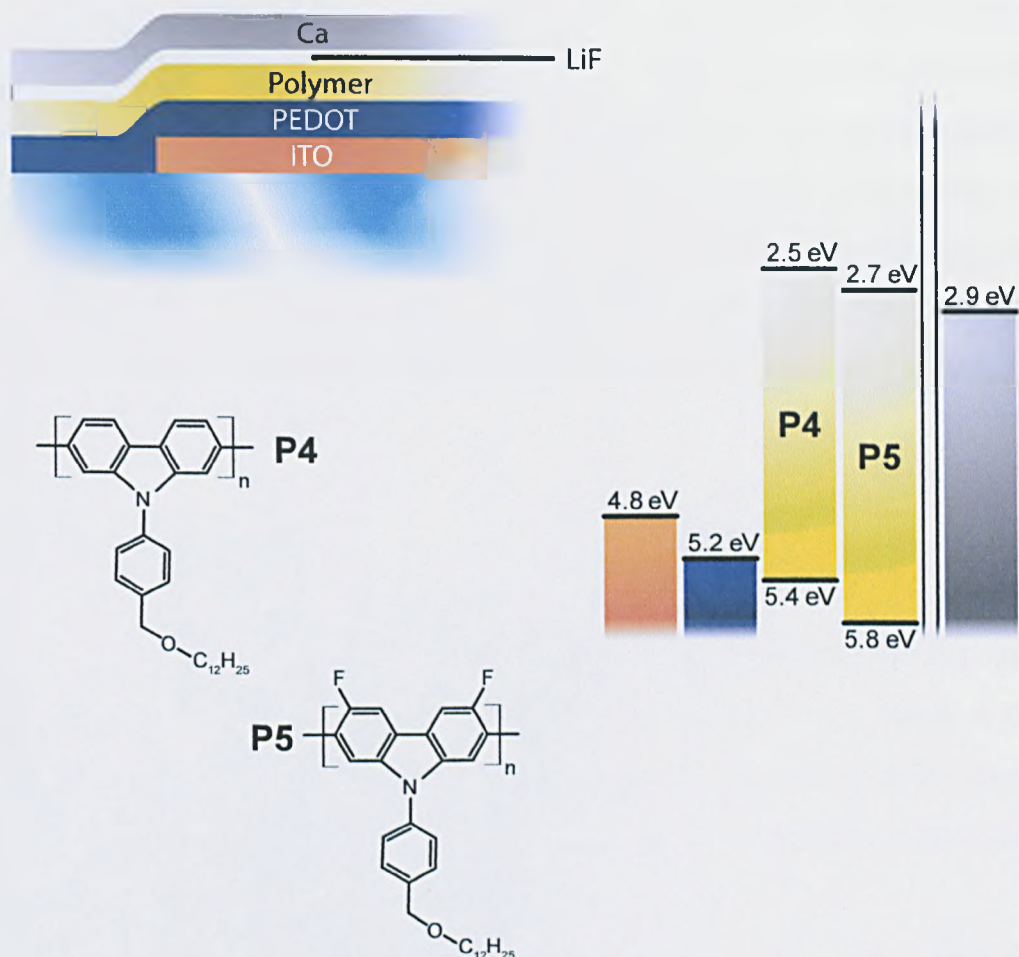


**Fig. 5.5:** The device structure and corresponding energy level diagram of single layer devices containing polymers **P4** and **P5**. The chemical structures of the two polymers have been included for reference.

calculated to be 2.5 eV.

The aryl-substituted carbazole **P5** incorporates fluorine at the 3,6-positions. These substitutions provide a dual functionality, protecting the polymer against electrolytic degradation whilst altering the electronic density of the polymer backbone. Due to its high electronegativity, the incorporation of fluorine into a conjugated molecule will generally result in an increase in its electron affinity. In this way, conjugated polymers have been synthesised with an enhanced ability to accommodate n-type carriers.<sup>50,51</sup>

Again, cyclic voltammetry was carried out on a drop-cast thin film of **P5** prior to receipt of the material. From this data, its ionisation potential was determined to be 5.8 eV. Perhaps more significantly, a reduction peak was observed from the cationic state, implying a reversible oxidation process. This observation further supports the functionalisation of the 3,6-positions as an affective strategy in stabilising the electrochemical properties of 2,7-linked polycarbazoles. From its optical band gap, the electron affinity of **P5** was calculated to be 2.7 eV. An energy level diagram that represents single-layer devices incorporating **P4** and **P5** is presented in figure 5.5.

### Device Characteristics

The I-V-L characteristics of single layer LEDs fabricated from the two aryl-substituted polymers **P4** and **P5** are shown in figure 5.6. The thickness of the electroluminescent layer in these two devices were 70 nm and 60 nm respectively. Both of the devices that are discussed in this section incorporated a 3 nm thick layer of lithium fluoride beneath the Ca cathode.

Electroluminescence was observed from the **P4** device when a bias of 5.8 V was applied. Emission continued to increase with voltage up to a maximum bias of 15 V, at which point a luminance of 113 cd/m<sup>2</sup> and current density of 415 mA/cm<sup>2</sup> was recorded. The operating voltage of the fluorine protected **P5** device was significantly reduced, with a bias of only 3.6 V required to detect emission. Maxima were recorded in both the I-V and L-V curves, indicating the occurrence of device degradation under a high electric field. This phenomenon was generally observed from all of the polymers under the application of an extreme bias. A maximum current density of 190 mA/cm<sup>2</sup> was sustained at a voltage of 12.7 V, and the peak luminance, 184 cd/m<sup>2</sup>, was recorded at 12.5 V. The luminance efficiency of **P5** peaked at low voltages with a maximum value of 0.21 cd/A. As the bias was increased, the efficiency of this device was reduced, but remained higher than that of the **P4** device (with a peak efficiency of 0.03 cd/A) throughout the full

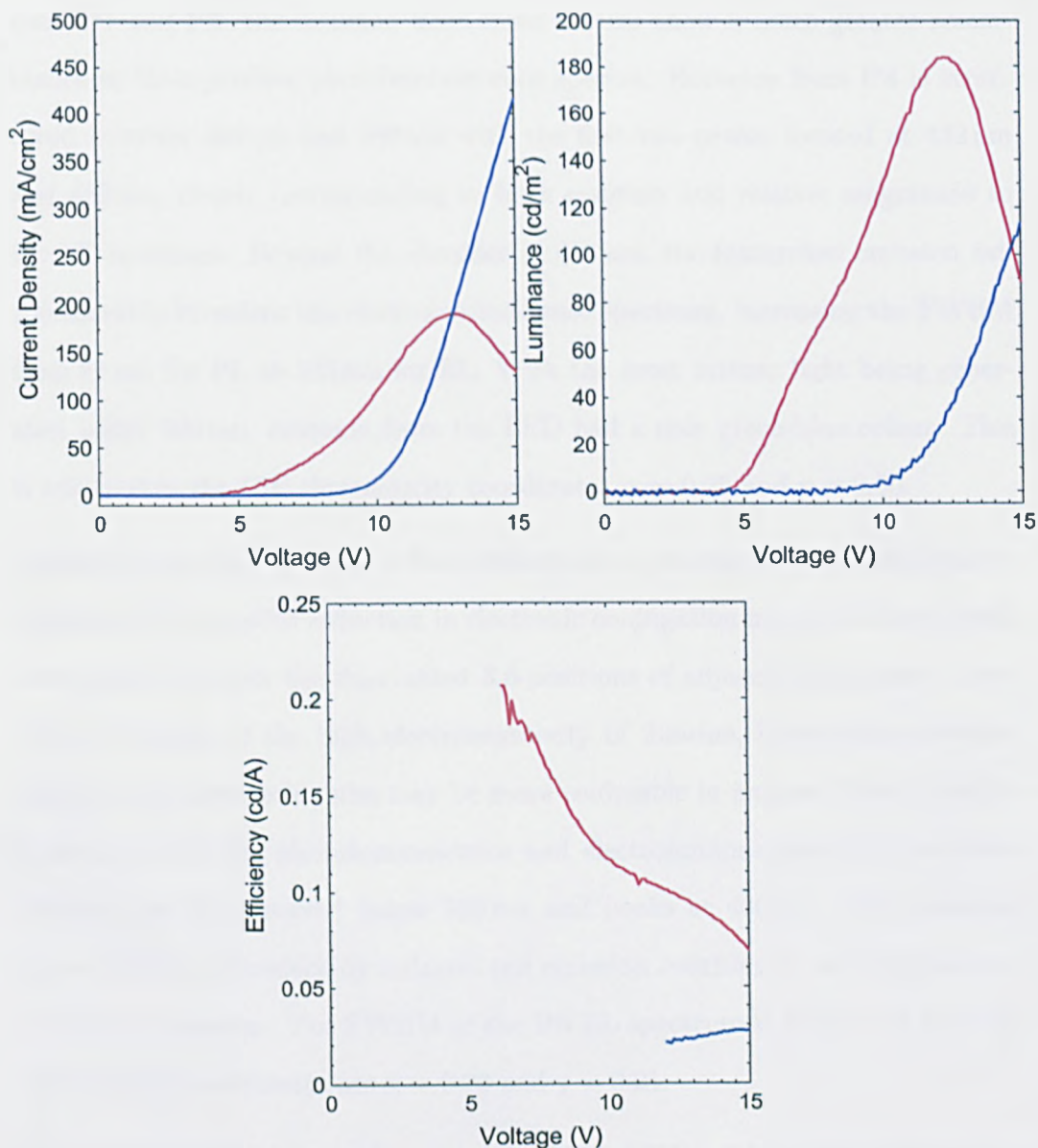


**Fig. 5.6:** The voltage dependence of current density, luminance and current efficiency of the two aryl substituted polymers **P4** (blue), **P5** (red).

measurement range. This data clearly shows a reduction in operating voltage, an increase in current flow (at lower voltages, below the onset of degradation) and a substantial increase in the maximum luminance efficiency from the fluorine protected polymer.

The electroluminescence spectra of the two devices are presented in figure 5.7. In contrast to the EL spectra that were obtained from the alkyl-substituted poly-

mers **P1** and **P2**, the emission from these devices show a much greater resemblance to their pristine photoluminescence spectra. Emission from **P4** is structured between 400 nm and 500 nm with the first two peaks, located at 432 nm and 458 nm, closely corresponding in both position and relative magnitude to the PL spectrum. Beyond the shoulder at 486 nm, the featureless emission tail considerably broadens the electroluminescence spectrum, increasing the FWHM from 81 nm for PL to 135 nm for EL. With the most intense light being generated below 500 nm, emission from the LED had a pale green-blue colour. This is reflected in the CIE chromaticity coordinates,  $x = 0.25$  and  $y = 0.30$ .

Emission from the **P5** device is blue-shifted relative to the unprotected polyaryl-carbazole. The implied reduction in electronic conjugation may result from steric interactions between the fluorinated 3,6-positions of adjacent monomers. However, in respect of the high electronegativity of fluorine, interactions between neighbouring carbazole units may be more coulombic in nature. This blue-shift is seen in both the photoluminescence and electroluminescence spectra where emission can be observed below 390 nm and peaks at 430 nm. This material also exhibits a considerably reduced tail emission resulting in an improvement in colour saturation. The FWHM of the **P5** EL spectrum is 91 nm and the CIE chromaticity coordinates are  $x = 0.23$  and  $y = 0.21$ .

Key results obtained from the polymers **P4** and **P5** can be found in table 5.2. From these devices it is apparent that the incorporation of fluorine protection at the 3,6-positions is beneficial to the electroluminescent properties of this class of material. This was not only demonstrated by the lower operating voltage and higher efficiency of the **P5** device, but also by the improvement in spectral purity and stability.

On consideration of the energy levels of the two polymers, it is clear that the fluorine substitutions of polymer **P5** has afforded this material an enhanced ability to accommodate n-type carriers. It is therefore possible to interpret these results

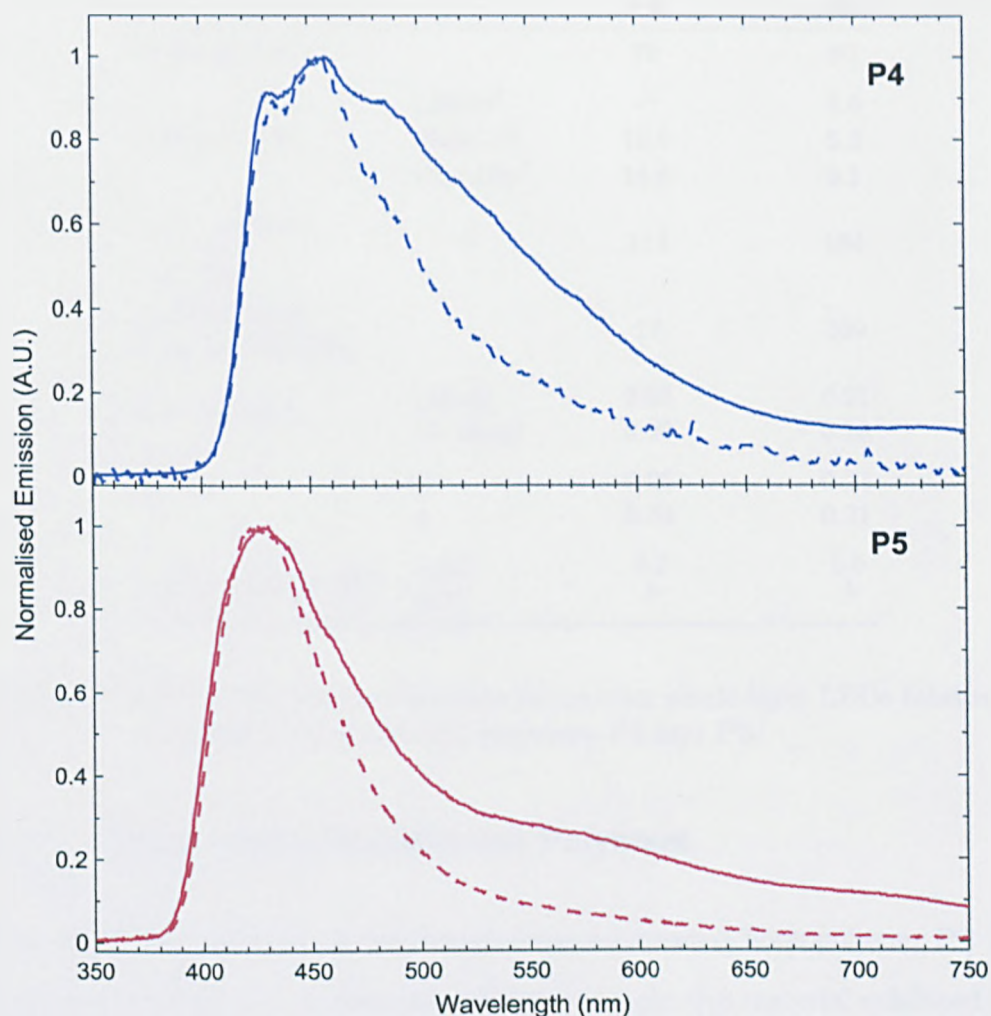


**Fig. 5.7:** The electroluminescence spectra of polymers **P4** and **P5** incorporated into single layer devices (solid line). The thin-film photoluminescence spectra are included for reference (dashed line).

as evidence for a deficiency in electron injection/transport in the **P4** device. However, electrochemical measurements have shown that this material is also susceptible to irreversible oxidation. Hole injection and transport will therefore be inhibited as the material degrades. Further investigation is required to identify the exact mechanism by which the fluorine protecting groups of polymer **P5** enhance its electroluminescent properties.

		P4	P5
Thickness (nm)		70	60
Voltage at (V)	1 cd/m <sup>2</sup>	– <sup>a</sup>	4.6
	10 cd/m <sup>2</sup>	10.9	5.3
	100 cd/m <sup>2</sup>	14.6	9.1
Max Luminance (cd/m <sup>2</sup> )		113	184
Current Density at 10 V (mA/cm <sup>2</sup> )		17	109
Max Efficiency	(cd/A)	0.03	0.21
	(% ph/e)	0.02	0.18
CIE	x	0.25	0.23
	y	0.30	0.21
Injection Barrier (eV)	$\Delta E_h$	0.2	0.6
	$\Delta E_e$	– <sup>b</sup>	– <sup>b</sup>

**Table 5.2:** A list of the key performance metrics for single layer LEDs fabricated using the aryl-substituted polymers P4 and P5.

### 5.4.3 Triarylamine-Substituted Polymers

The ionisation potential of the triarylamine substituted homopolymer P6 was determined using cyclic voltammetry.<sup>52</sup> Interestingly, this material exhibited two resolvable oxidation peaks. When the switching potentials (the limits between which the voltage is swept) were chosen to encompass only the first oxidation peak, a reversible redox wave was observed. This behaviour was sustained over multiple cycles. However, when the switching potential was increased to incorporate the higher energy oxidation peak, a loss of reversibility was observed. This was manifest by an absence of the reduction peak in the reverse scan and a loss of electroactivity on repeated cycling.

Based upon these observations, it was suggested that two isolated oxidation events were occurring.<sup>52</sup> The lower energy peak was assigned to p-type doping of the triarylamine pendant group. The ionisation potential of P6, determined from the onset of this low energy oxidation peak, was 5.0 eV. This is the smallest

<sup>a</sup>Below the detection limit.

<sup>b</sup>Cathode injection barrier may be modified by LiF.

value obtained from all of the polycarbazoles discussed in this thesis and should lead to the barrier-free injection of holes from a PEDOT:PSS anode. The second oxidation event, the peak of which is located at +0.4 V relative to the first, was associated to electron transfer from the polycarbazole backbone. The irreversible nature of this process mirrors that of the other main-chain polycarbazoles that bear no protecting substituents at the 3,6-positions.

The proposed electronic structure of **P6** is illustrated in figure 5.8. From the onset of absorption at 420 nm, the optical energy gap of this polymer was calculated to be 3.0 eV. If it is assumed that this process results in the formation of an intrachain excited state that is localised to the polymer backbone, and that the preceding interpretation of the electrochemical data is correct, then the electron affinity of the main-chain is estimated at 2.4 eV. These energy levels are identical to those of an analogous alkyl-substituted polycarbazole,<sup>31</sup> supporting the hypothesis that the triarylamine side-group and the main-chain retain their own distinct electronic properties.

Similar observations have been made from a triarylamine-substituted polyfluorene copolymer.<sup>53</sup> Again, cyclic voltammetry measurements detected two resolvable oxidation processes, the lower of which was assigned to the oxidation of the side-group and the higher, assigned to the polymer backbone. The ionisation potential of this material was estimated at 5.3 eV. In this case, the triphenylamine pendant moieties bore no substituent groups. The lower ionisation potential observed from **P6** may therefore be linked to the presence of the two electron-donating alkoxy substitutions on the pendant side-chain.

From the electrochemical analysis of **P7**, it was possible to observe both the oxidation and reduction of the neutral molecule. As was the case with **P6**, two oxidation peaks were detected. These were located at identical potentials to the homopolymer, corresponding to a main-chain ionisation potential of 5.4 eV, and pendant group ionisation potential of 5.0 eV. Again, the polymer exhibited irreversible oxidation at high potentials, but was otherwise stable. From the onset

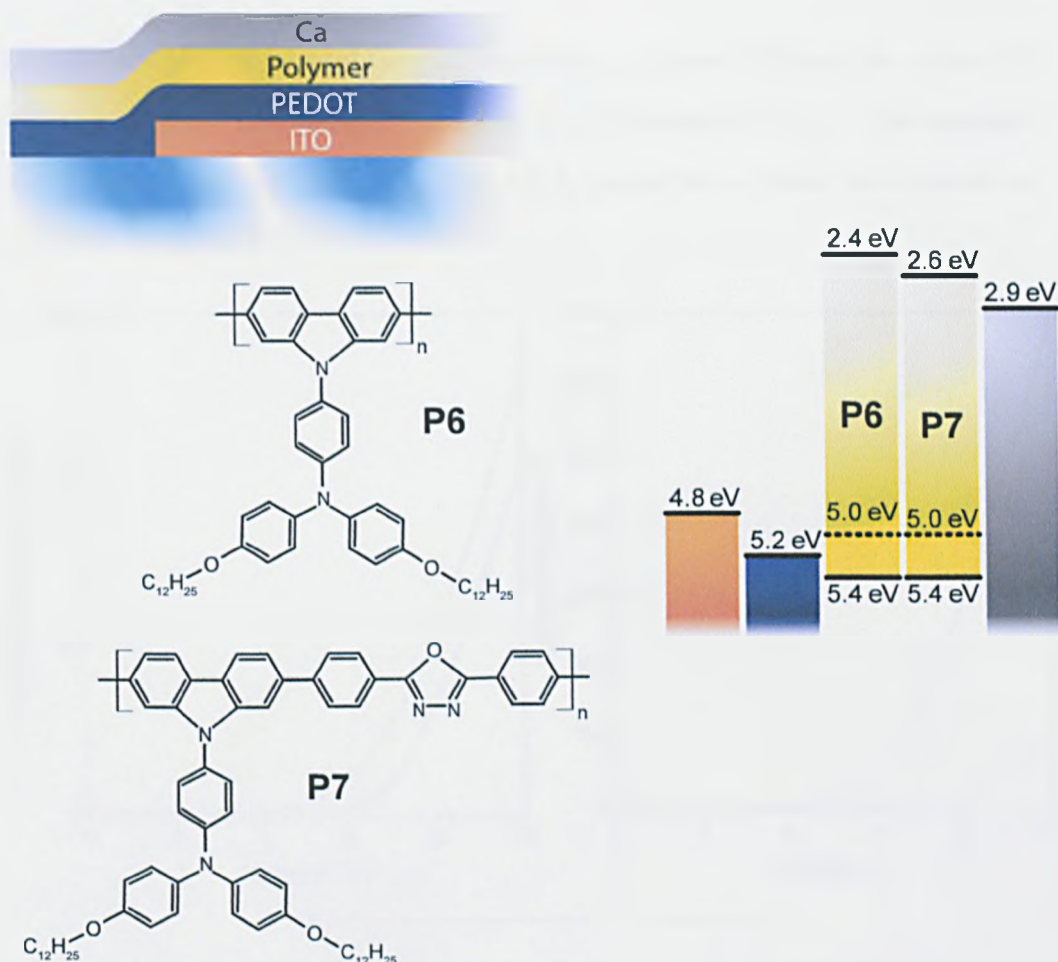


**Fig. 5.8:** The device structure and corresponding energy level diagram of single layer devices containing polymers **P6** and **P7**. The low-energy  $I_p$ , associated with the oxidation of the pendant group, is represented by the dashed lines. The optically determined  $E_a$  of **P7** is reported here. The chemical structures of the two polymers have been included for reference.

of reduction, the electron affinity of **P7** is estimated at 2.4 eV, also identical to that of the homopolymer **P6**. It should be noted however, that the optically derived band gap of this polymer was 2.8 eV, suggesting an exciton binding energy of 0.2 eV. It is therefore likely that the incorporation of the electron accepting oxadiazole moiety into the main-chain of **P7** has resulted in an increase in its electron affinity relative to the homopolymer **P6**.



## Device Characteristics

Two devices were fabricated, one incorporating polymer **P6**, and the other **P7**. In both cases, the active layer was spun to a thickness of 70 nm. The standard Ca/Ag bilayer cathode was used. The I-V-L properties of these two devices are presented in figure 5.9.

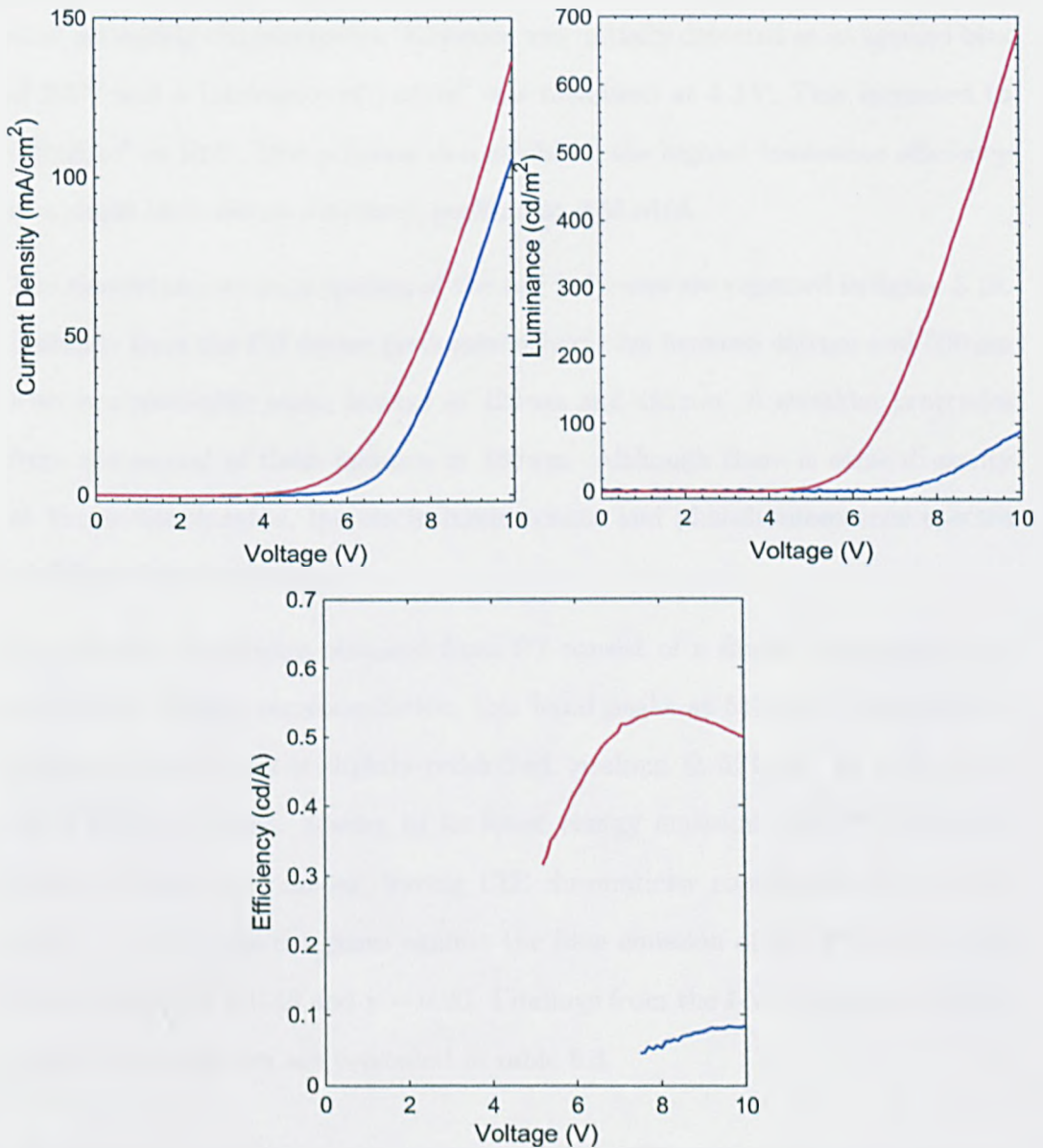


**Fig. 5.9:** The voltage dependence of current density, luminance and current efficiency of the two triarylamine substituted polymers **P6** (blue), **P7** (red).

Electroluminescence from the **P6** device was detected when a bias of 4.5 V was applied. The luminance increased to a value of 90 cd/m<sup>2</sup> at 10 V. The luminance efficiency showed a general trend of increasing with voltage, reaching a maximum value of 0.08 cd/A at 10 V. The data suggests however, that this value is close to the maximum attainable efficiency for this device.

Of all of the single layer LEDs discussed in this thesis, the **P7** device shows the most promising characteristics. Emission was initially detected at an applied bias of 2.9 V and a luminance of 1 cd/m<sup>2</sup> was measured at 4.3 V. This increased to 680 cd/m<sup>2</sup> at 10 V. This polymer also exhibited the highest luminance efficiency in a single layer device structure, peaking at 0.53 cd/A.

The electroluminescence spectra of the two polymers are reported in figure 5.10. Emission from the **P6** device predominantly occurs between 400 nm and 500 nm with two resolvable peaks located at 428 nm and 452 nm. A shoulder protrudes from the second of these features at 480 nm. Although there is some disparity at longer wavelengths, the electroluminescence and photoluminescence spectra of **P6** are largely similar.

In contrast, the spectra obtained from **P7** consist of a single, featureless emission band. During photoexcitation, this band peaks at 513 nm. The electroluminescence spectrum is slightly redshifted, peaking at 521 nm. In both cases, the FWHM is 90 nm. Owing to its lower energy emission, the **P7** device appeared blue-green in colour, having CIE chromaticity coordinates of  $x = 0.29$  and  $y = 0.55$ . This compares against the blue emission of the **P6** device with coordinates of  $x = 0.19$  and  $y = 0.20$ . Findings from the I-V-L data and electroluminescence spectra are presented in table 5.3.

As a general observation, both polymers **P6** and **P7** exhibit a lower operational voltage than their alkyl or aryl substituted analogues. This is perhaps a consequence of their low ionisation potential, allowing the facile injection of holes from the PEDOT:PSS anode. However, the precise nature of charge injection and

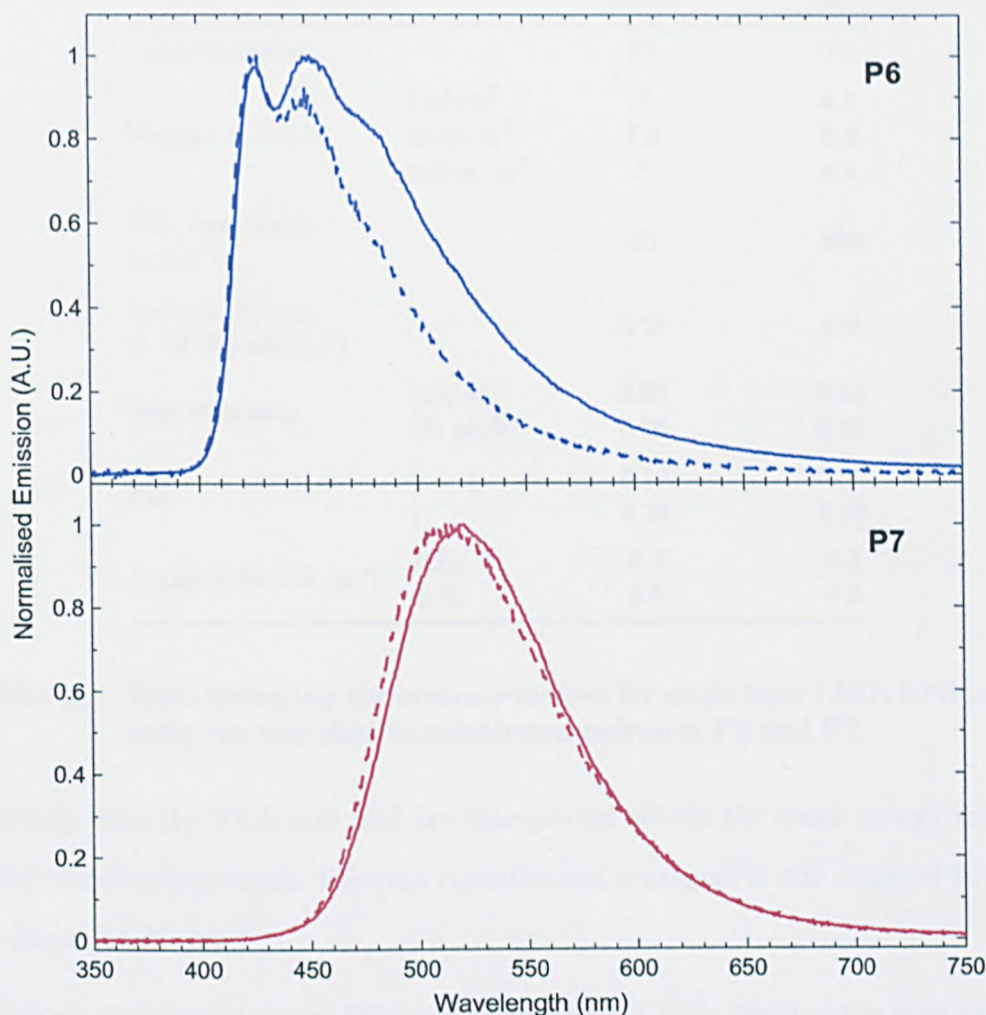


**Fig. 5.10:** The electroluminescence spectra of polymers **P6** and **P7** incorporated into single layer devices (solid line). The thin-film photoluminescence spectra are included for reference (dashed line).

transport in this class of material remains unclear. From the cyclic voltammetry data, there is evidence that the triarylamine (TAA) group exists as an electronically isolated species, separate from the delocalised  $\pi$ -system of the main chain. If this assumption is correct, the low ionisation potential pendant groups may be expected to act more as a molecular dopant, uniformly dispersed throughout the matrix of the polycarbazole main chain. Indeed, as a result of its high concentration, carrier hopping between adjacent side-groups may be the predominant hole transport mechanism in these materials. In this scenario, holes are injected

		P6	P7
Thickness (nm)		70	70
Voltage at (V)	1 cd/m <sup>2</sup>	- <sup>a</sup>	4.3
	10 cd/m <sup>2</sup>	7.6	5.2
	100 cd/m <sup>2</sup>	- <sup>b</sup>	6.7
Max Luminance (cd/m <sup>2</sup> )		90	680
Current Density at 10 V (mA/cm <sup>2</sup> )		106	136
Max Efficiency	(cd/A)	0.08	0.53
	(% <i>ph/e</i> )	0.06	0.17
CIE	x	0.19	0.29
	y	0.20	0.55
Injection Barrier (eV)	$\Delta E_h$	0.2	0.2
	$\Delta E_e$	0.5	0.3

**Table 5.3:** Table listing key performance metrics for single layer LEDs fabricated using the triarylamine-substituted polymers **P6** and **P7**.

directly into the TAA unit and are transported within the lower energy manifold of side-group states. Electron injection and transport is still confined to the polymer backbone.

The emissive properties of **P7** are notably distinct from those of the homopolymer. Namely, its spectrum is broader, structureless and peaks at a significantly lower energy. All of these features are symptomatic of a charge-transfer (CT) excited state. CT structures are usually formed between two entities, one which acts as an electron donor and the other as an electron acceptor. The strength of the donor-acceptor interaction determines the size of the band gap of the combined system. The formation of a CT structure is usually signified by the emergence of a low-energy absorption band, located at a longer wavelength than either of the two component spectra.<sup>54</sup> Interestingly, such a feature is absent from the absorption spectrum of **P7**, which peaks at 380 nm, coincident with the absorption maximum of the homopolymer. Nevertheless, the generation of a charge-transfer state would seem likely given the donor-acceptor nature of this

<sup>a</sup>Below the detection limit.

<sup>b</sup>Above the maximum luminance.

material. Specifically, the presence of the low-ionisation potential triarylamine group may facilitate this interaction with the oxadiazole-carbazole acceptor.

## 5.5 Conclusions

Light-emitting diodes incorporating each of the seven polycarbazoles have been fabricated using a single-component device structure. Despite their improved electrochemical stability (evidenced from cyclic voltammetry measurements), the methyl-protected polyalkylcarbazoles **P1** and **P2** were susceptible to degradation under electroluminescence. Both of the devices required a high operating voltage and suffered from low efficiency. Although an intrinsic blue emission was observed from both polymers during photoluminescence, their EL spectra were broad and featured multiple emission bands. Interestingly, of the two materials, it was the partially protected copolymer **P2** that suffered the least from these issues. These results suggest the existence of alternative degradation mechanisms to those previously identified in polyalkylcarbazoles.

The electroluminescent stability of this class of material is greatly improved upon its copolymerisation with a biphenyl oxadiazole unit. On its initial operation, emission from the **P3** device was deep blue in colour, closely resembling its thin-film photoluminescence spectrum. Furthermore, this device required a lower operating voltage and exhibited a higher EL efficiency than the other polyalkylcarbazole LEDs.

Devices incorporating the aryl-substituted polymers **P4** and **P5** showed that the electroluminescent properties of these materials are enhanced by the incorporation of fluorine substitutions at the 3- and 6-positions. The addition of these protecting groups serves two functions. Firstly, as was observed from the methyl-protected polymers, the electrochemical stability of the material is enhanced. It is believed that degradation via the cross-linking of adjacent molecules is inhibited by the incorporation of these protecting groups. The second function of the

fluorine substituent is to increase the electron affinity of the polymer backbone. A consequent enhancement in electron injection should therefore be realised.

Electrochemical analysis of the triarylamine-substituted polymers **P6** and **P7** revealed that both of these materials exhibited two oxidation peaks. These results were interpreted as evidence of electronic decoupling between the main-chain and the pendant group, with the low energy feature being associated with the triarylamine moiety and the high energy feature with the backbone. Devices fabricated from both polymers operated at low biases, perhaps as a consequence of ohmic injection into their low-lying HOMO. The combination of electrochemical and time-of-flight data suggests that a majority hole current will flow through the single-component **P6** device. Large leakage currents are therefore likely to limit the efficiency of this structure. In contrast, electron injection and transport should be enhanced in the copolymer, owing to its high-electron affinity biphenyl-oxadiazole group. The enhanced efficiency observed from the **P7** device supports this proposition. However, emission from this device is shifted to lower energies, away from the blue region of the visible spectrum. This was attributed to the formation of a charge-transfer species. The absence of CT-type emission from the alkyl-substituted copolymer **P3** suggests that the low ionisation potential triarylamine donor group must be present for this state to be energetically favourable .

---

## References

- [1] Groenendaal, B. L., Jonas, F., Freitag, D., Pielartzik, H., and Reynolds, J. R. *Adv. Mater.* **12**(7), 481–494 April (2000).
- [2] Kirchmeyer, S. and Reuter, K. *J. Mater. Chem.* **15**(21), 2077–2088 (2005).
- [3] Greczynski, G., Kugler, T., and Salaneck, W. R. *Thin Solid Films* **354**(1-2), 129–135 October (1999).
- [4] Jonsson, S. K. M., Birgersson, J., Crispin, X., Greczynski, G., Osikowicz, W., van der Gon, A. W. D., Salaneck, W. R., and Fahlman, M. *Synth. Met.* **139**(1), 1–10 August (2003).
- [5] Vacca, P., Petrosino, M., Miscioscia, R., Nenna, G., Minarini, C., Della Sala, D., and Rubino, A. *Thin Solid Films* **516**(12), 4232–4237 April (2008).
- [6] Carter, S. A., Angelopoulos, M., Karg, S., Brock, P. J., and Scott, J. C. *Appl. Phys. Lett.* **70**(16), 2067–2069 April (1997).
- [7] Liu, G., Kerr, J. B., and Johnson, S. *Synth. Met.* **144**(1), 1–6 July (2004).
- [8] Elschner, A., Bruder, F., Heuer, H. W., Jonas, F., Karbach, A., Kirchmeyer, S., and Thurm, S. *Synth. Met.* **111**, 139–143 June (2000).
- [9] Scott, J. C., Kaufman, J. H., Brock, P. J., DiPietro, R., Salem, J., and Goitia, J. A. *J. Appl. Phys.* **79**(5), 2745–2751 March (1996).
- [10] Scott, J. C., Carter, S. A., Karg, S., and Angelopoulos, M. *Synth. Met.* **85**(1-3), 1197–1200 February (1997).
- [11] Brown, T. M., Kim, J. S., Friend, R. H., Cacialli, F., Daik, R., and Feast, W. J. *Appl. Phys. Lett.* **75**(12), 1679–1681 September (1999).
- [12] Hwang, J. and Kahn, A. *J. Appl. Phys.* **97**(10), 103705 May (2005).
- [13] Lane, P. A., Brewer, P. J., Huang, J. S., Bradley, D. D. C., and deMello, J. C. *Phys. Rev. B: Condens. Matter Mater. Phys.* **74**(12), 125320 September (2006).
- [14] Cimrova, V. and Neher, D. *J. Appl. Phys.* **79**(6), 3299–3306 March (1996).
- [15] Becker, H., Burns, S. E., and Friend, R. H. *Phys. Rev. B: Condens. Matter Mater. Phys.* **56**(4), 1893–1905 (1997).
- [16] Bulovic, V., Khalfin, V. B., Gu, G., Burrows, P. E., Garbuzov, D. Z., and Forrest, S. R. *Phys. Rev. B: Condens. Matter Mater. Phys.* **58**(7), 3730–3740 August (1998).
- [17] Cimrova, V., Scherf, U., and Neher, D. *Appl. Phys. Lett.* **69**(5), 608–610 July (1996).
- [18] Cao, Y., Parker, I. D., Yu, G., Zhang, C., and Heeger, A. J. *Nature* **397**(6718), 414–417 (1999).

- [19] Shi, Y., Liu, J., and Yang, Y. *J. Appl. Phys.* **87**(9), 4254–4263 (2000).
- [20] Liu, J., Shi, Y. J., Ma, L. P., and Yang, Y. *J. Appl. Phys.* **88**(2), 605–609 July (2000).
- [21] Hung, L. S., Tang, C. W., and Mason, M. G. *Appl. Phys. Lett.* **70**(2), 152–154 (1997).
- [22] Brown, T. M., Friend, R. H., Millard, I. S., Lacey, D. J., Burroughes, J. H., and Cacialli, F. *Appl. Phys. Lett.* **79**(2), 174–176 (2001).
- [23] Kim, Y. E., Park, H., and Kim, J. J. *Appl. Phys. Lett.* **69**(5), 599–601 July (1996).
- [24] Zhang, S. T., Ding, X. M., Zhao, J. M., Shi, H. Z., He, J., Xiong, Z. H., Ding, H. J., Obbard, E. G., Zhan, Y. Q., Huang, W., and Hou, X. Y. *Appl. Phys. Lett.* **84**(3), 425–427 January (2004).
- [25] Hung, L. S. and Chen, C. H. *Mat. Sci. Eng. R* **39**(5-6), 143–222 December (2002).
- [26] Micaroni, L., Nart, F. C., and Hummelgen, I. A. *J. Solid State Electrochem.* **7**(1), 55–59 December (2002).
- [27] Conwell, E. M. *Synth. Met.* **83**(2), 101–102 November (1996).
- [28] Knupfer, M. *Appl. Phys. A: Mater. Sci. Process.* **77**(5), 623–626 October (2003).
- [29] Janietz, S., Bradley, D. D. C., Grell, M., Giebeler, C., Inbasekaran, M., and Woo, E. P. *Appl Phys Lett* **73**(17), 2453–2455 (1998).
- [30] Zotti, G., Schiavon, G., Zecchin, S., Morin, J. F., and Leclerc, M. *Macromolecules* **35**(6), 2122–2128 March (2002).
- [31] Iraqi, A. and Wataru, I. *Chem. Mater.* **16**(3), 442–448 (2004).
- [32] Iraqi, A., Pickup, D. F., and Yi, H. N. *Chem. Mater.* **18**(4), 1007–1015 February (2006).
- [33] Peng, Z. H., Bao, Z. N., and Galvin, M. E. *Adv. Mater.* **10**(9), 680–684 June (1998).
- [34] Song, S. Y., Jang, M. S., Shim, H. K., Hwang, D. H., and Zyung, T. *Macromolecules* **32**(5), 1482–1487 (1999).
- [35] Song, S. Y., Jang, M. S., Shim, H. K., Song, I. S., and Kim, W. H. *Synth. Met.* **102**(1-3), 1116–1117 (1999).
- [36] Chen, J. P., Markiewicz, D., Lee, V. Y., Klaerner, G., Miller, R. D., and Scott, J. C. *Synth. Met.* **107**(3), 203–207 December (1999).
- [37] Zhan, X. W., Liu, Y. Q., Wu, X., Wang, S. A., and Zhu, D. B. *Macromolecules* **35**(7), 2529–2537 March (2002).



- [38] '1931 CIE Standard Colourimetric Observer Data':Munsell Color Science Laboratory, [www.cis.rit.edu/mcsl/online/cie/php](http://www.cis.rit.edu/mcsl/online/cie/php). Last accessed 31/03/2009.
- [39] Fyfe, D. 'Printed P-OLEDs Move to Commercialisation':Presented at SID 2008 - Los Angeles. Available from [www.cdtltd.co.uk](http://www.cdtltd.co.uk). Last accessed 24/03/2009.
- [40] Gong, X., Moses, D., Heeger, A. J., and Xiao, S. *Synth. Met.* **141**(1-2), 17–20 March (2004).
- [41] Gong, X. O., Iyer, P. K., Moses, D., Bazan, G. C., Heeger, A. J., and Xiao, S. S. *Adv. Funct. Mater.* **13**(4), 325–330 (2003).
- [42] Mauthner, G., Collon, M., List, E. J. W., Wenzl, F. P., Bouguettaya, M., and Reynolds, J. R. *J. Appl. Phys.* **97**(6), 063508 (2005).
- [43] Smith, D. L. *J. Appl. Phys.* **81**(6), 2869–2880 March (1997).
- [44] Hsieh, B. R., Yu, Y., Forsythe, E. W., Schaaf, G. M., and Feld, W. A. *J. Am. Chem. Soc.* **120**(1), 231–232 January (1998).
- [45] Kim, Y. H., Ahn, J. H., Shin, D. C., and Kwon, S. K. *Polymer* **45**(8), 2525–2532 April (2004).
- [46] Setayesh, S., Grimsdale, A. C., Weil, T., Enkelmann, V., Mullen, K., Meghdadi, F., List, E. J. W., and Leising, G. *J. Am. Chem. Soc.* **123**(5), 946–953 February (2001).
- [47] Pogantsch, A., Wenzl, F. P., List, E. J. W., Leising, G., Grimsdale, A. C., and Mullen, K. *Adv. Mater.* **14**(15), 1061 August (2002).
- [48] Jacob, J., Zhang, J. Y., Grimsdale, A. C., Mullen, K., Gaal, M., and List, E. J. W. *Macromolecules* **36**(22), 8240–8245 November (2003).
- [49] Jacob, J., Sax, S., Gaal, M., List, E. J. W., Grimsdale, A. C., and Mullen, K. *Macromolecules* **38**(24), 9933–9938 November (2005).
- [50] Lux, A., Holmes, A. B., Cervini, R., Davies, J. E., Moratti, S. C., Gruner, J., Cacialli, F., and Friend, R. H. *Synth. Met.* **84**(1-3), 293–294 January (1997).
- [51] Assaka, A. M., Rodrigues, P. C., de Oliveira, A. R. M., Ding, L. M., Bin, H., Karasz, F. E., and Akcelrud, L. *Polymer* **45**(21), 7071–7081 September (2004).
- [52] Yi, H. N., Iraqi, A., Stevenson, M., Elliott, C. J., and Lidzey, D. G. *Macromol. Rapid Commun.* **28**(10), 1155–1160 May (2007).
- [53] Shu, C. F., Dodda, R., Wu, F. I., Liu, M. S., and Jen, A. K. Y. *Macromolecules* **36**(18), 6698–6703 September (2003).
- [54] Yamamoto, T., Zhou, Z. H., Kanbara, T., Shimura, M., Kizu, K., Maruyama, T., Nakamura, Y., Fukuda, T., Lee, B. L., Ooba, N., Tomaru, S., Kurihara, T., Kaino, T., Kubota, K., and Sasaki, S. *J. Am. Chem. Soc.* **118**(43), 10389–10399 October (1996).

## Chapter 6

# Optoelectronic Characterisation of Heterojunction LEDs

### 6.1 Introduction

In the most basic OLED structure, a single organic material is deposited directly between two injecting electrodes. Although simple to fabricate, such devices can be inefficient owing to an imbalance in charge injection and transport. To redress this imbalance, heterojunction structures have been developed. By incorporating two or more organic components with complimentary properties, a significant improvement in device performance can be effected.

This chapter reports upon the characterisation of a series of heterojunction devices. A predominantly n-type (electron transporting) molecular material was used in the fabrication of two different structures, namely distributed and planar heterojunctions. Devices incorporating polymers **P4** and **P6** were made using both structures. A second material, this time a predominantly hole-transporting polymer, was also investigated. This was deposited as an interlayer between the PEDOT:PSS anode and polycarbazole thin-film. Polymers **P3**, **P6** and **P7** were used in this study. The electroluminescent and spectroscopic properties of each device was evaluated and where possible, linked to various photophysical and electronic processes.

## 6.2 Butyl-PBD Heterojunction Devices

Given the low ionisation potential and electron affinity of many of the polycarbazoles studied in this work, it is likely that an imbalance in carrier injection and transport is limiting their performance in electroluminescent devices. As was demonstrated by the copolymers **P3** and **P7**, this can be overcome through the incorporation of electron accepting moieties into the polymer backbone. Alternatively, a heterojunction diode can be fabricated whereby the high electron affinity species is incorporated as a chemically distinct component.

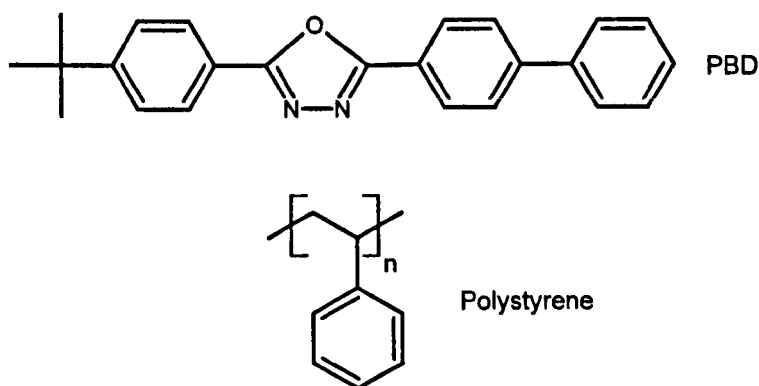


**Fig. 6.1:** The chemical structures of the electron transporting/hole blocking molecular material Bu-PBD and the inert polystyrene matrix.

The oxadiazole derivative 2-(4-*tert*-butylphenyl)-5-(4-biphenyl)-1,3,4-oxadiazole (Bu-PBD) (see figure 6.1 for the chemical structure) is often used in organic heterojunction LEDs. As a low molecular weight material, its deposition can be achieved through thermal evaporation,<sup>1-3</sup> or through solution-based processes when dispersed into a polymer matrix.<sup>4,5</sup> Adachi *et al.* were the first to demonstrate its use in a bilayer device.<sup>6</sup> They reported upon the fabrication of a series of LEDs that utilised a triphenylamine-based molecular material that functioned both as a hole transport layer and as the electroluminescent species. The study showed that through the incorporation Bu-PBD, thermally evaporated between

the luminescent layer and the cathode, a significant increase in the device's current efficiency, as much as four orders of magnitude, could be realised. As the emission spectrum showed no evidence of recombination occurring from within the Bu-PBD, they concluded that enhanced performance was afforded by the electron transporting capability of the interlayer.

Although beneficial to some device characteristics, the inclusion of a thermally evaporated Bu-PBD layer can result in reduced operational lifetimes. This molecular material is known to crystallise at room temperature, causing the formation of non-uniformities within the thin-film. Furthermore, the evolution of this process is enhanced by the heat that is produced during device operation. Stress, induced by these structural changes, will eventually lead to device failure.

In order to suppress crystallisation, several researchers have investigated the use of a polymer matrix. By blending Bu-PBD into an inert polymer such as polystyrene (PS) or poly(methyl methacrylate) (PMMA), significant improvements in device stability can be expected. This technique was initially applied using an insoluble PPV electroluminescent layer,<sup>4</sup> and later applied using soluble polymers.<sup>7-10</sup> To prevent the underlying electroluminescent layer from dissolving during the fabrication process, the polymer:PBD blend was deposited using solvents such as acetonitrile or cyclohexane.

Alternatively, Bu-PBD can be blended directly into the electroluminescent layer.<sup>5,11</sup> This strategy has the advantage of suppressing PBD crystallisation whilst precluding the use of an electronically inert material. It should be noted that phase separation is likely to occur in such a system. During the process of film formation, partial demixing of the two materials produces phases that are made up of differing blend compositions.<sup>12</sup> In effect, this results in an interface that extends throughout bulk of the film. The exact structure and composition of these phases can be influenced by the processing conditions, such as choice of solvent, spin speed and thermal treatments. In acknowledgement of these properties, blended polymer films are often referred to as bulk or distributed

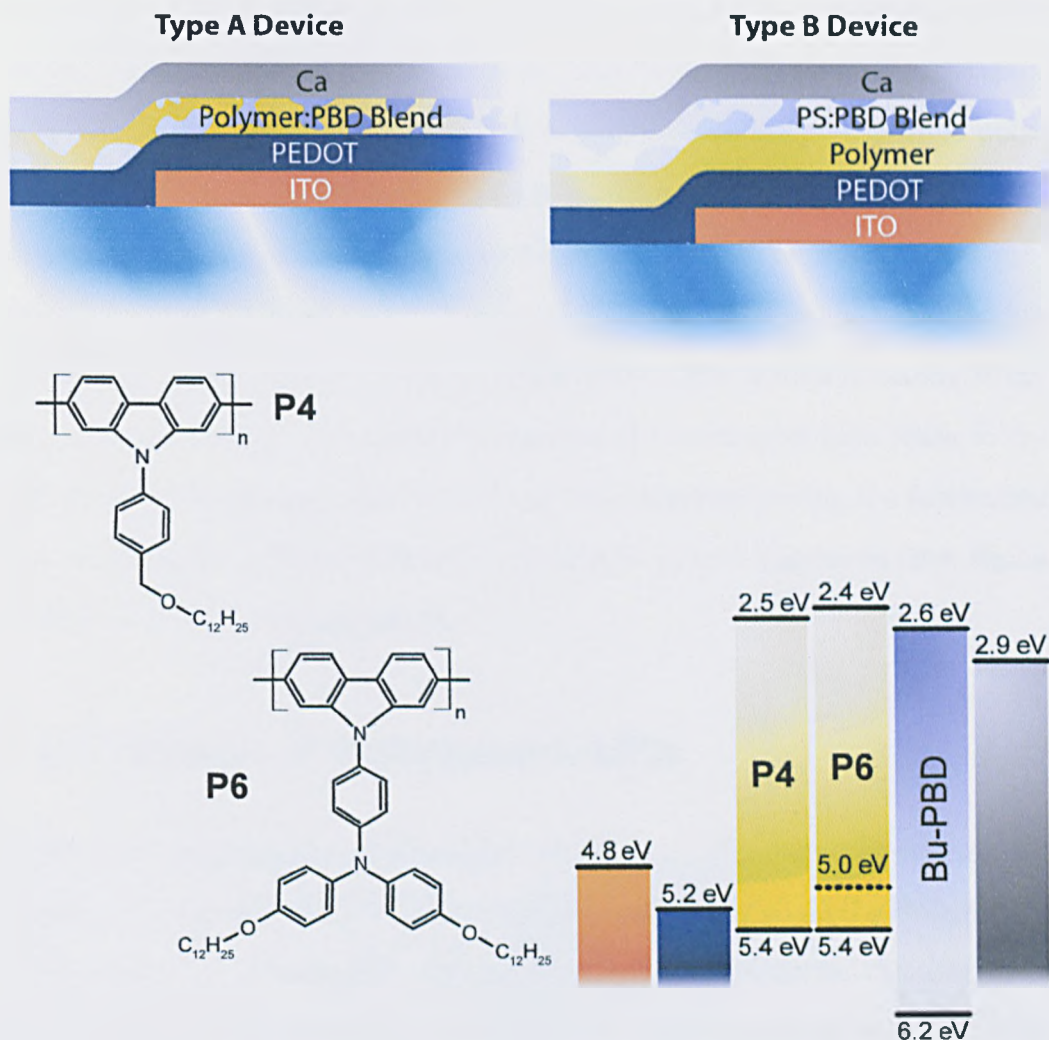


**Fig. 6.2:** The band diagram of the electron transporting/hole blocking molecular material Bu-PBD and the polycarbazoles P4 and P6.

heterojunctions. This is differentiated from the aforementioned planar heterojunction.

In this work, heterojunction LEDs were fabricated by using only solution based techniques. With respect to the polycarbazole:Bu-PBD heterostructures, two types of device were defined. Type A devices incorporated Bu-PBD into the active layer, forming a distributed heterojunction. This film was spin cast from solution from a 70:30 % w/w blend of polycarbazole and Bu-PBD. The solutions were prepared at a concentration of 15-20 mg/ml in toluene, depending upon which polymer was used. The type B device incorporated a bilayer in which

Bu-PBD was dispersed into an inert polystyrene matrix and deposited on top of the electroluminescent polycarbazole layer. The PS:Bu-PBD interlayer was spun from a cyclohexane solution that was incompatible with the predeposited polymer layer. Tak *et al.* reported upon this fabrication technique using a poly(phenyl phenylenevinylene) (PPPV) electroluminescent layer.<sup>13</sup> The solution was prepared with a blend ratio of 70:30 % w/w of PS to Bu-PBD and a concentration of 5 mg/ml. When spun at 3000 rpm for 1 minute, a film of approximately 30 nm thickness was formed. The absorption spectra of test samples were taken to ensure that the underlying polymer had not been dissolved during the fabrication process. Both Bu-PBD and PS ( $M_w = 97400$  g/mol) were purchased from Sigma Aldrich and were used as received.

### 6.2.1 Distributed Heterojunction LEDs

Figure 6.3 presents the I-V-L characteristics of type A, distributed heterojunction devices incorporating the aryl substituted polycarbazole **P4** and the triarylamine substituted polycarbazole **P6**. Also included in the figure are the characteristics of the homostructure devices (in which the Bu-PBD component is absent from an otherwise identical structure). The cathode of all 4 devices was formed from a Ca/Ag bilayer of 20 nm and 100 nm thickness respectively.

At a low applied bias, both of the type A LEDs sustained a smaller current density than their analogous homostructure devices. With polymer **P4**, a current density in excess of  $0.01$  mA/cm<sup>2</sup> flowed at a bias of 2.9 V in the single-component device. In the blend structure a bias of 5.1 V was necessary to drive an equivalent current. A similar trend was observed with polymer **P6**, with a bias of 3.3 V and 4.3 V being required in the non-blended and heterostructure devices respectively. As the bias was increased, the current flowing through the type-A devices increased rapidly and, in both polymers, surpassed that of the equivalent homostructure. The voltage at which this occurred was 7.1 V in the **P4** device and 4.9 V in the **P6** device.

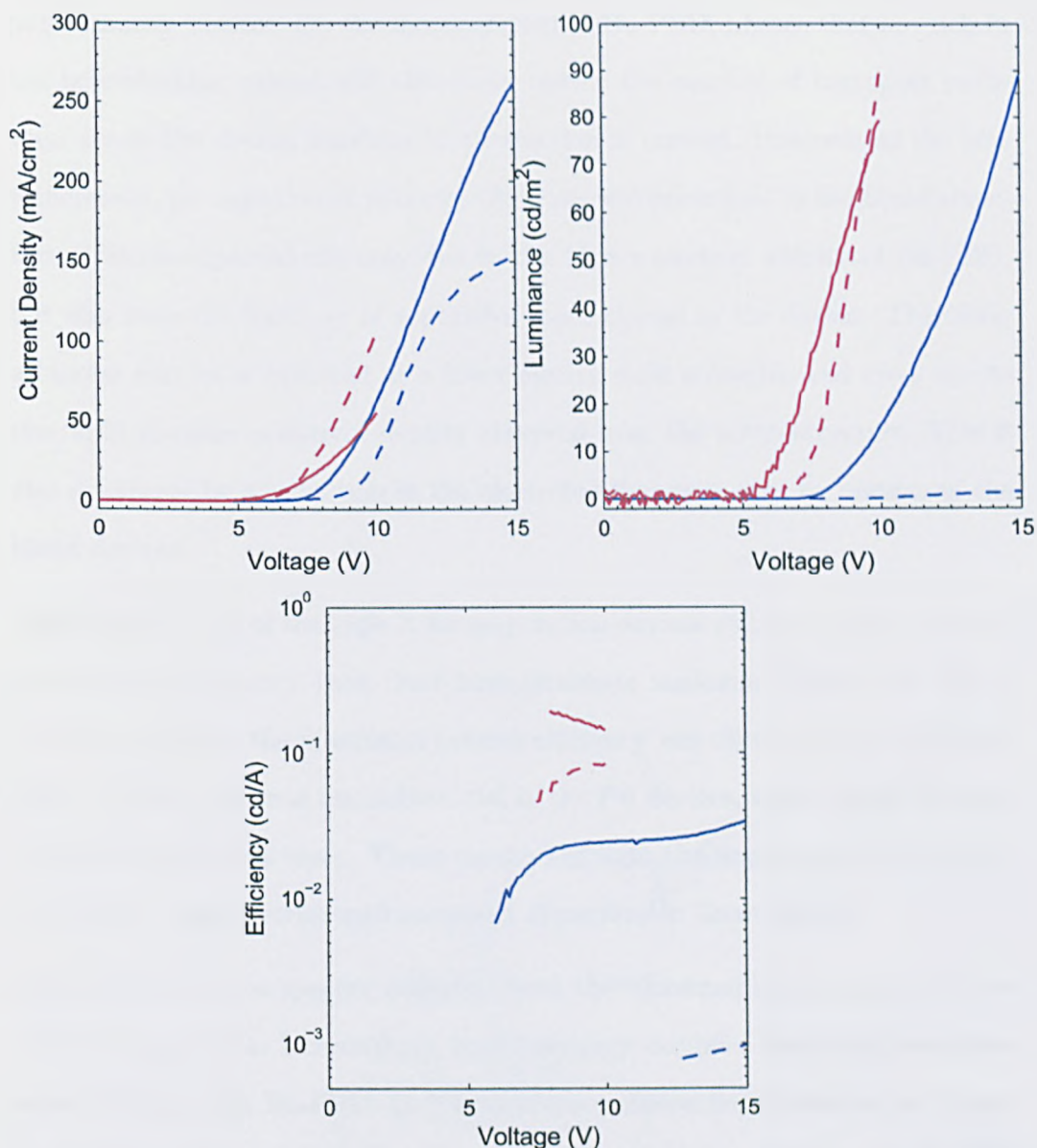


**Fig. 6.3:** The voltage dependence of current density, luminance and current efficiency of both type A heterojunction (solid line) and single-component (dashed line) LEDs. The polycarbazoles **P4** (blue) and **P6** (red) were used in this study.

The reduction in current density observed during the low voltage operation of type A heterojunction devices may reflect the hole-blocking character of Bu-PBD. At such biases, prior to the detection of electroluminescence, only a unipolar current flows. It is assumed that this is a p-type current, resulting from the injection and transport of hole-polarons through the low ionisation potential

polycarbazole matrix. On the incorporation of Bu-PBD, phases that are rich in the hole-blocking species will effectively reduce the number of transport pathways across the device, resulting in a reduction in current. However, as the bias is increased, the injection of minority electrons will occur first in the blend structure. This is expected not only due to the higher electron affinity of Bu-PBD, but also from the build up of a positive space charge in the device. Therefore, a bipolar current is initiated at a lower electric field strength, and gives rise to the rapid increase in current density observed from the heterostructure. This is also evidenced by a reduction in the electroluminescence turn on voltage of the blend devices.

Significantly, both of the type A heterojunction devices exhibit a higher electroluminescence efficiency than their homostructure analogue. In polymer **P4**, a 30-fold increase in the maximum current efficiency was observed from the blend device. The benefit was less substantial in the **P6** devices, with a 2-fold increase in the maximum efficiency. These results highlight the importance of achieving a balance in the injection and transport of carriers in these devices.

Electroluminescence spectra collected from the aforementioned devices are reported in figure 6.4. Interestingly, both polymers exhibit a broadened spectrum when blended with Bu-PBD. In **P4**, the blue emission band, peaking at 460 nm is predominant in both device structures. On the incorporation of Bu-PBD however, the intensity of the emission tail is enhanced between 500-600 nm. This results in an increase in the FWHM from 134 nm in the homostructure to 173 nm in the blend and a consequent shift in the CIE coordinates from  $x = 0.24$  and  $y = 0.29$  to  $x = 0.27$  and  $y = 0.33$ .

When Bu-PBD is blended with polymer **P6**, the change in the EL spectrum is much more significant. The emission maximum is shifted away from the intrinsic blue band at 428 nm due to the formation of a new peak at 485 nm. This new feature causes an undesirable broadening of the spectrum with an increase of the FWHM from 100 nm in the pristine device to 129 nm in the blend. Consequently,



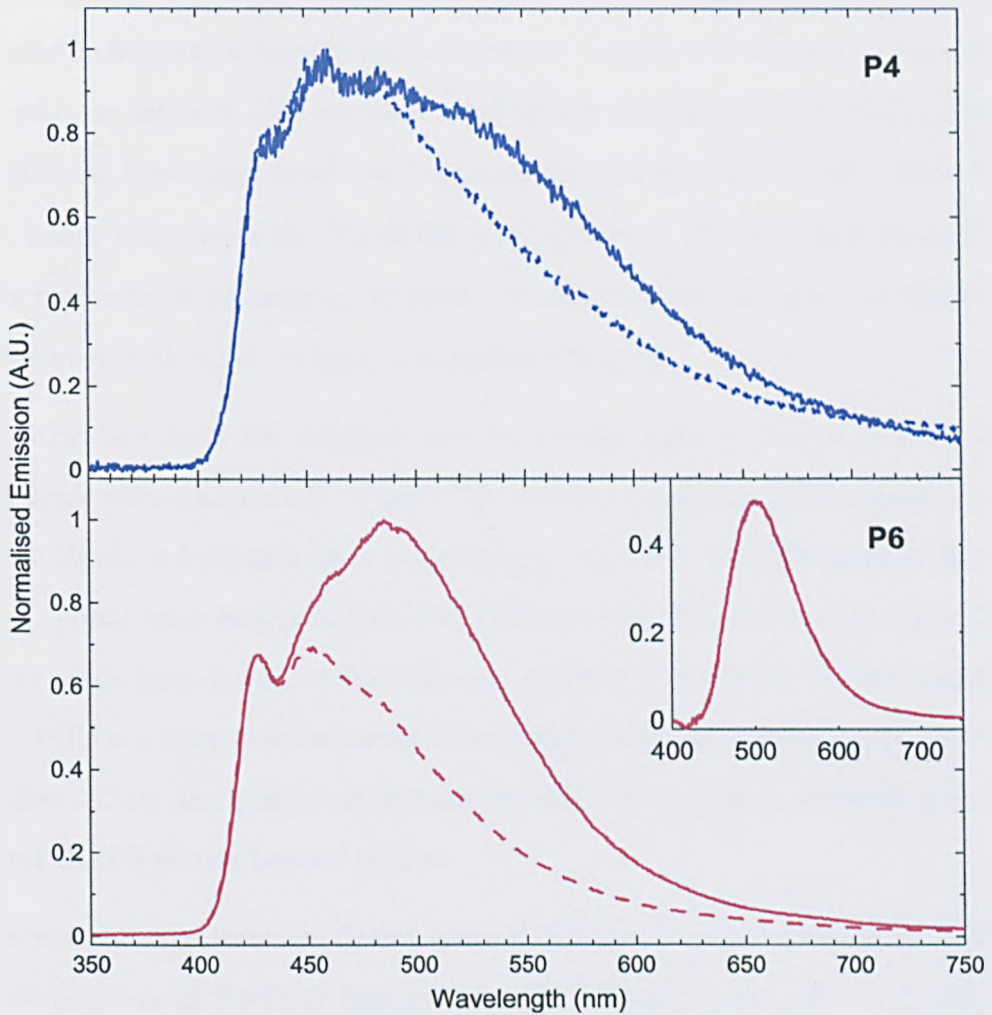


**Fig. 6.4:** Electroluminescence spectra collected from both heterojunction type A (solid line) and single-component (dashed line) LEDs. The inset shows the difference in the emission spectra of the **P6** devices when they are both normalised to the 428 nm peak.

emission from the heterostructure appears blue-green in colour with chromaticity coordinates of  $x = 0.21$  and  $y = 0.30$ .

Although the spectrum from the **P6**:Bu-PBD heterostructure is greatly modified, some of the features that were observed from the pristine device are still clearly discernable. For instance, the peak at 428 nm, assumed to be the 0-0 vibronic transition of singlet excitons that are localised to **P6**, is well resolved. The shoulder located between 450-460 nm in the blend device is also coincident with

a secondary peak in the intrinsic emission. It was therefore assumed that the spectrum from the heterostructure device was composed of two separate emission bands - an intrinsic blue emission band that is generated by **P6** alone, and an additional low-energy band resulting from the presence of Bu-PBD. The intrinsic band, taken from the EL of the pristine device, was then subtracted from the heterostructure emission to yield the additional green band. Its spectrum, presented in the inset of figure 6.4, peaks at 501 nm.

To elucidate upon the origin of this low-energy species, further spectroscopic analyses were undertaken. Figure 6.5, details photoluminescence spectra that were obtained from thin films comprising pristine **P6**, Bu-PBD blended into an inert polystyrene matrix and Bu-PBD blended with **P6**. Both of the blend films were made up to a ratio of 70:30 % w/w polymer to Bu-PBD. As demonstrated, Bu-PBD is a fluorescent material with a wide band gap. Emission was observed below 350 nm and peaked at 369 nm. Notably, there is little emission from the Bu-PBD:PS matrix beyond 450 nm.

As was observed from the device spectra, emission is significantly broadened on incorporation of Bu-PBD into polymer **P6**. These results show that the low energy species can be excited optically, as well as electronically. However, it should be noted that the relative intensity of the green band is greatly reduced when the emission is photogenerated. Significantly, the presence of the low energy band in the **P6**:Bu-PBD blend cannot be ascribed to emission from either of the two components. It is therefore likely that a new radiative species is formed through their interaction.

These observations are not uncommon in organic systems that incorporate a junction between electron-transporting (ET) and hole-transporting (HT) materials. By their very function, ET molecules typically have a high electron affinity to facilitate electronic injection from the cathode and subsequent carrier transport through the film. Likewise, HT molecules require a low ionisation potential. Thus, when these materials are brought into intimate contact, as would occur

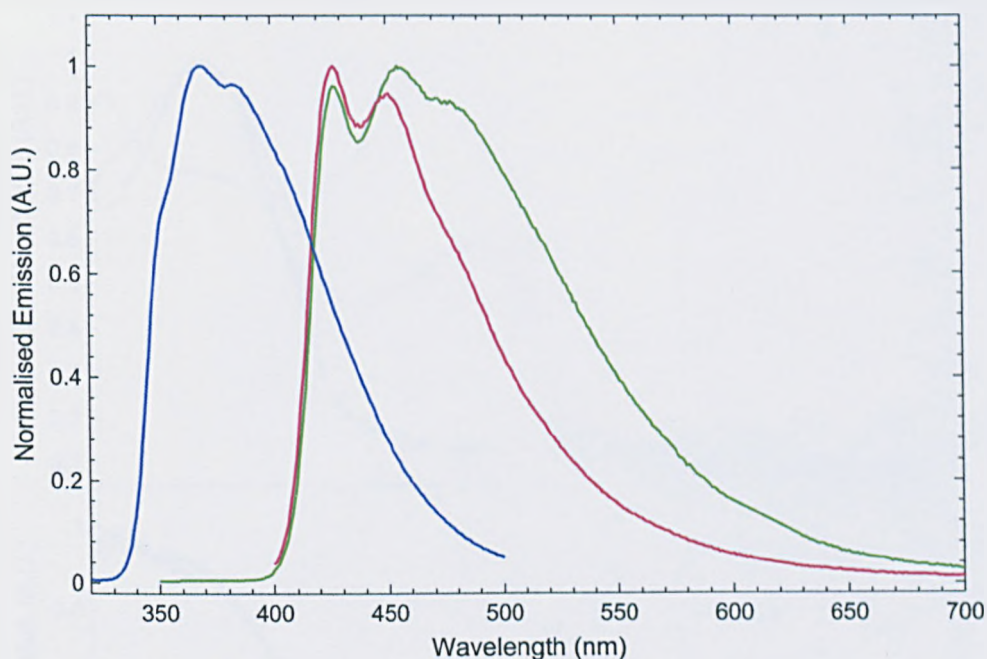


**Fig. 6.5:** Photoluminescence spectra collected from films of pristine **P6** (red), a 70:30 % w/w PS:PBD blend (blue) and a 70:30 % w/w **P6**:PBD blend (green).

in the **P6**:Bu-PBD blend, they are capable of forming electron donor-acceptor charge-transfer (CT) states. In particular, excited state complexes (exciplexes) have been identified as the source anomalous low-energy emission in such systems.<sup>14</sup>

The assignment of the 500 nm band in the **P6**:Bu-PBD blend to exciplex emission is further evidenced by the absorption and photoluminescence excitation spectra presented in figure 6.6. These measurements were carried out on the same samples that were used in the PL study, namely a film comprising pure **P6**, a 70:30 % w/w blend of polystyrene and Bu-PBD and a 70:30 % w/w **P6**:Bu-PBD blend. The triarylamine substituted polycarbazole exhibits a broad featureless absorption band, typical of a wide band gap conjugated polymer. The band peaks at 388 nm, with its edge located between 410 and 420 nm. The absorption of Bu-PBD is confined entirely to the UV, peaking at 308 nm. The polystyrene matrix, with an absorption edge below 300 nm,<sup>15</sup> should not influence the measurement

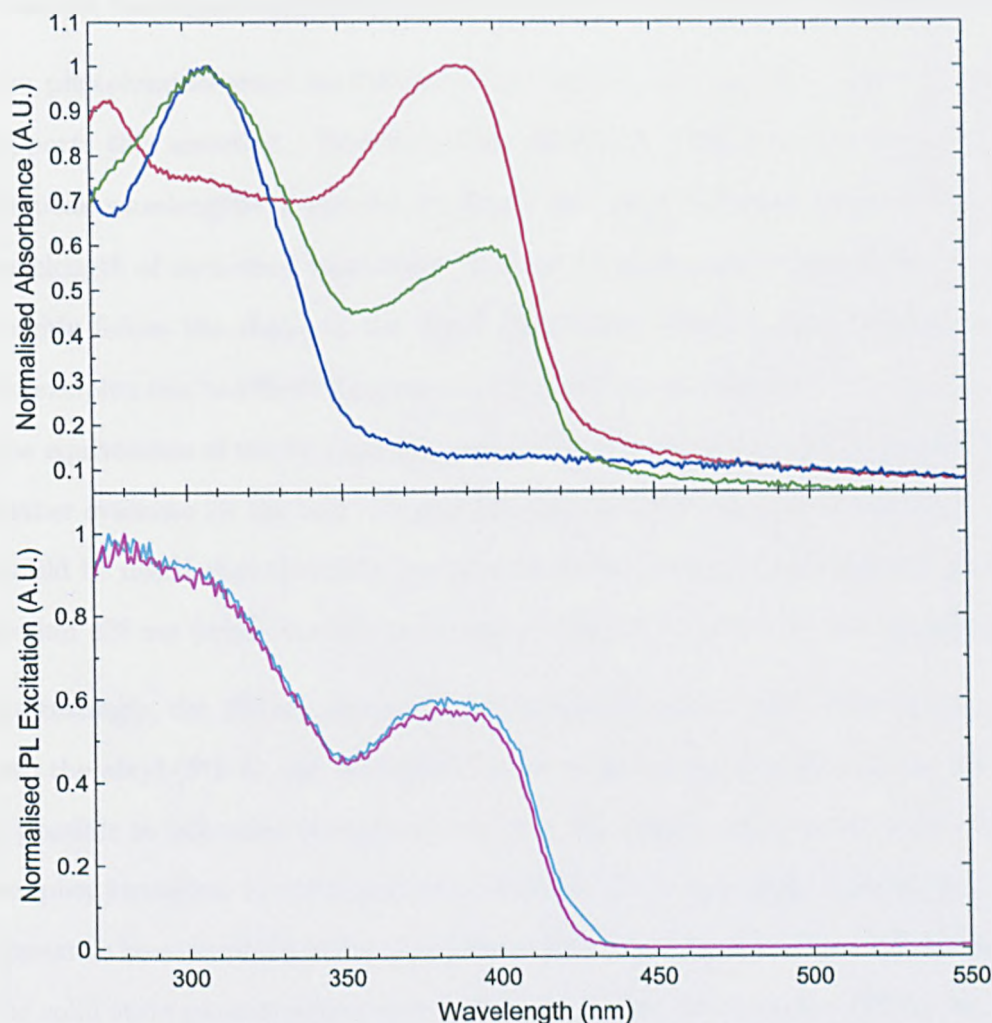


**Fig. 6.6:** **(Above)** Absorbance spectra collected from films of pristine **P6** (red), a 70:30 % w/w PS:PBD blend (blue) and a 70:30 % w/w **P6**:PBD blend (green). **(Below)** Photoluminescence excitation spectra of the **P6**:PBD blend, when detected at 428 nm (cyan) and 500 nm (magenta)

at these wavelengths.

Importantly, the absorption spectrum of the **P6**:Bu-PBD blend can be approximately constructed from a superposition of the two component spectra. There is no evidence of an additional long wavelength feature that would indicate the formation of a ground state charge-transfer complex. This observation is integral to the assignment of the 500 nm emission band to an exciplex. These species are photogenerated only after the monomolecular excitation of the donor or acceptor

molecule, leaving no signature in the absorption spectrum of the blend.

The photoluminescence excitation (PLE) spectra presented in figure 6.6 also supports this assertion. Emission from the P6:Bu-PBD film was detected at the peak wavelengths of the blue (428 nm) and green (500 nm) bands whilst the wavelength of excitation was varied. The two PLE spectra are well matched and roughly follow the shape of the blend absorption. These results suggests that the exciplex can be efficiently generated from the excitation of either component. The equivalence of the two spectra, particularly at the absorption edge, provides further evidence for the lack of a ground state associated with the green band. It should be noted that this data has been modified to remove an artifact centered around 428 nm (when the detection and excitation wavelengths are equivalent).

Interestingly, the 500 nm emission band is largely absent when PBD is blended into the alkyl-(P1-3) and aryl-(P4-5) substituted polycarbazoles. From this, it is possible to infer that the presence of the triarylamine group is fundamental to exciplex formation in these materials. Indeed, TAA and many of its derivatives appear to be susceptible to the generation of intermolecular species. For instance, the solid state photoluminescence spectrum of tris(*p*-tolyl)amine (TTA - see figure 6.7) was found to incorporate an additional low energy emission band that was absent from the solution spectrum.<sup>16</sup> This band, centered at 450 nm, was attributed to the formation of an excited state dimer (excimer). The efficiency of excimer formation in this material was believed to result from the planarity of the molecule, facilitating alignment and close packing. Such properties are also conducive to exciplex formation.

When combined with a suitable acceptor species, exciplex emission has also been observed from TTA. Owing to its low ionisation potential (5.3 eV),<sup>17</sup> TTA functions as an electron donor in such systems. One of the first observations of exciplex emission involving a conjugated polymer (poly-*p*-phenylene-2,6-benzobis(oxazole) or PBO) incorporated TTA as the donor molecule.<sup>18</sup> Since then, there have been numerous reports of exciplex emission from triarylamine

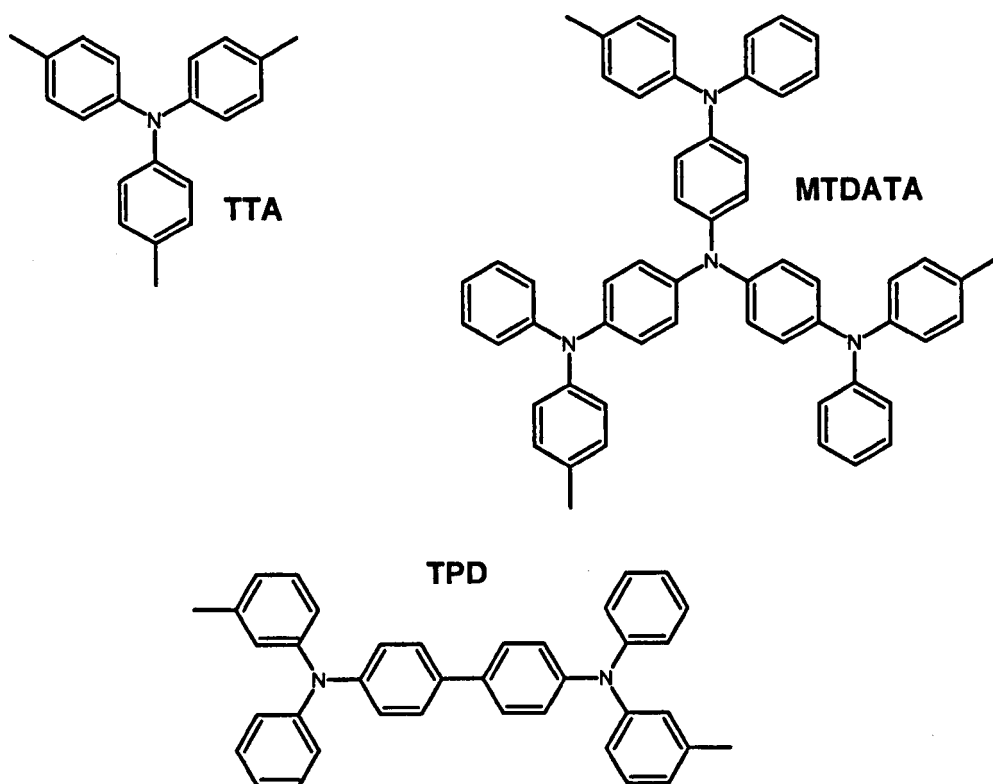


**Fig. 6.7:** The chemical structure of triarylamine derivatives from which exciplex emission has been observed.

derivatives.<sup>14,17,19-24</sup> Significantly, some of these studies have also used oxadiazole derivatives, such as Bu-PBD, as the acceptor species.<sup>20-24</sup>

Based upon the available evidence, it is possible to conjecture that the green emission band observed from EL and PL of the **P6** heterostructure may result from an excited state complex that is formed across the triarylamine pendant group and the Bu-PBD dopant. The feasibility of this statement is enhanced by the observation of electronic decoupling of the TAA side group, inferred from the electrochemical study of **P6**.<sup>25</sup> In such a process, the role of the polycarbazole backbone remains unclear. However, the residual presence of the structured blue band suggests that a fraction of the excited states remain localised to the polymer before radiatively decaying. When electronically generated, exciton formation at the heterojunction is enhanced, resulting in the predominance of the green band

during EL.<sup>26</sup>

## 6.2.2 Bilayer Heterojunction Devices

The I-V-L characteristics of the type B heterojunction devices, whereby the electron transporting component is dispersed into a polystyrene matrix and de-

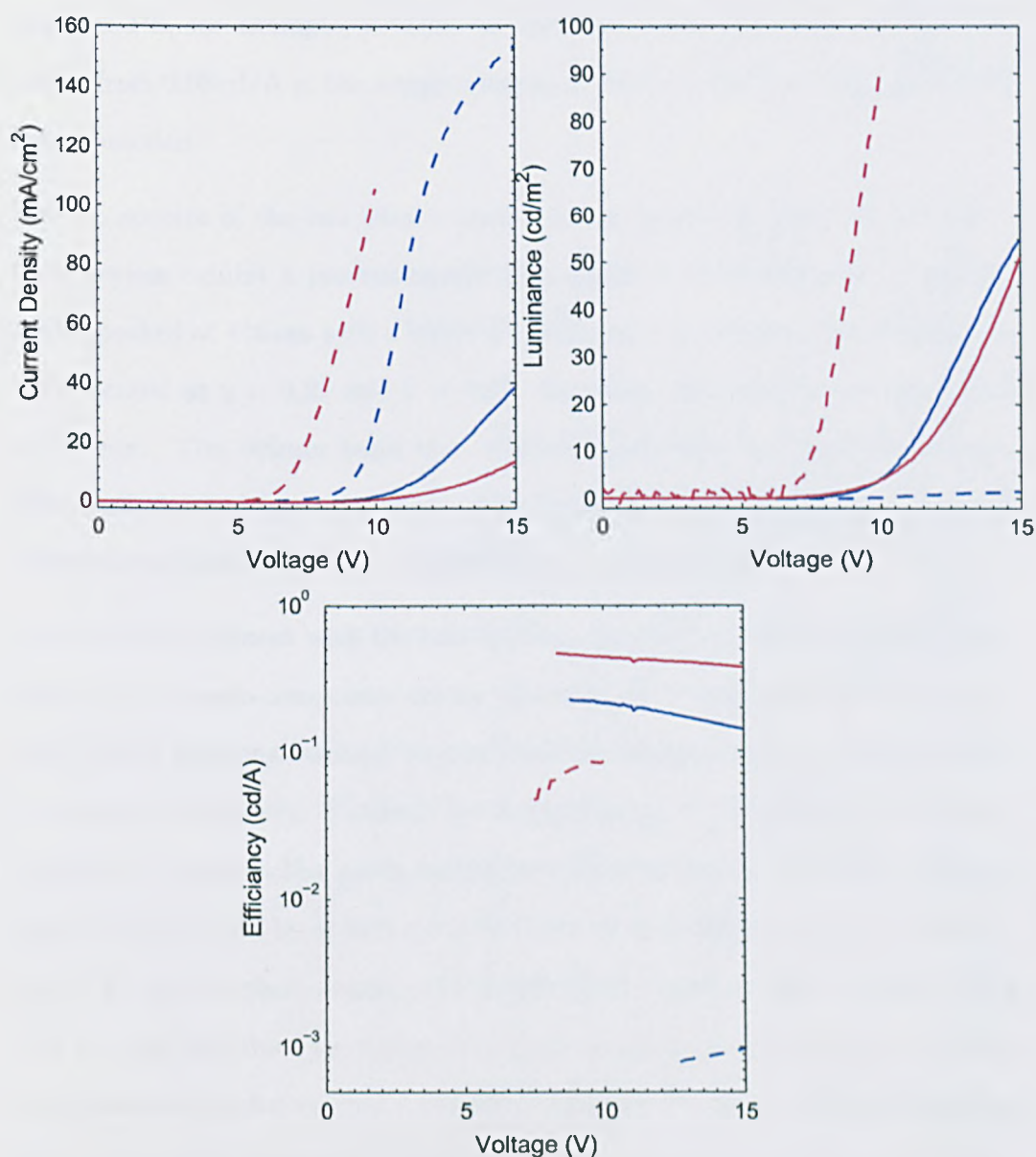


**Fig. 6.8:** The voltage dependence of current density, luminance and current efficiency of both type-B heterojunction (solid line) and single-component (dashed line) LEDs. The polycarbazoles P4 (Blue) and P6 (red) were used in this study.

posited as an interlayer, are shown in figure 6.8. For both polymers, the incorporation of the PBD:PS interlayer has resulted in a reduction in current density at a given bias. The voltage required to sustain a current density of  $0.01 \text{ mA/cm}^2$  was  $6.1 \text{ V}$  in the **P4** device and  $5.9 \text{ V}$  in the **P6** device. The turn on voltage for electroluminescence is also higher in these dual layer devices. The current efficiency however, shows a significant enhancement with the interlayer present. Polymer **P6**, for example, exhibits an increase in the maximum current efficiency from  $0.08 \text{ cd/A}$  in the single component device to  $0.47 \text{ cd/A}$  in the bilayer heterojunction.

The EL spectra of the two bilayer devices are presented in figure 6.9. Notably, both devices exhibit a predominantly blue emission. The spectrum of the **P4** device peaked at  $446 \text{ nm}$  with a FWHM of  $120 \text{ nm}$ . The chromaticity coordinates were located at  $x = 0.21$  and  $y = 0.25$ . Emission from the **P6** device peaked at  $426 \text{ nm}$ . The  $500 \text{ nm}$  band that was observed from the blend device was greatly diminished from the bilayer heterostructure. A FWHM of  $107 \text{ nm}$  and chromaticity coordinates of  $x = 0.20$  and  $y = 0.22$  reflect this.

This data is consistent with the hole blocking function of the Bu-PBD:PS interlayer.<sup>4</sup> In the single-component device structures, it was assumed that a majority flow of hole polarons resulted in a substantial leakage current and low electroluminescence efficiency. Through the incorporation of the interlayer, the direct transit of holes from the anode to the cathode is inhibited. The large injection barrier from the EL layer into the hole-blocking interlayer confines the hole polarons to the interface, causing the build up of a positive space charge. This acts not only to reduce the injection of more charge carriers from the anode, but also enhances the electric field across the interlayer, facilitating electron injection from the cathode. Although this results in an improvement in current efficiency, the concomitant decrease in the device's conductance necessitates the application of a higher operating bias. This in turn has a detrimental influence on the LED's bias-dependent power efficiency.



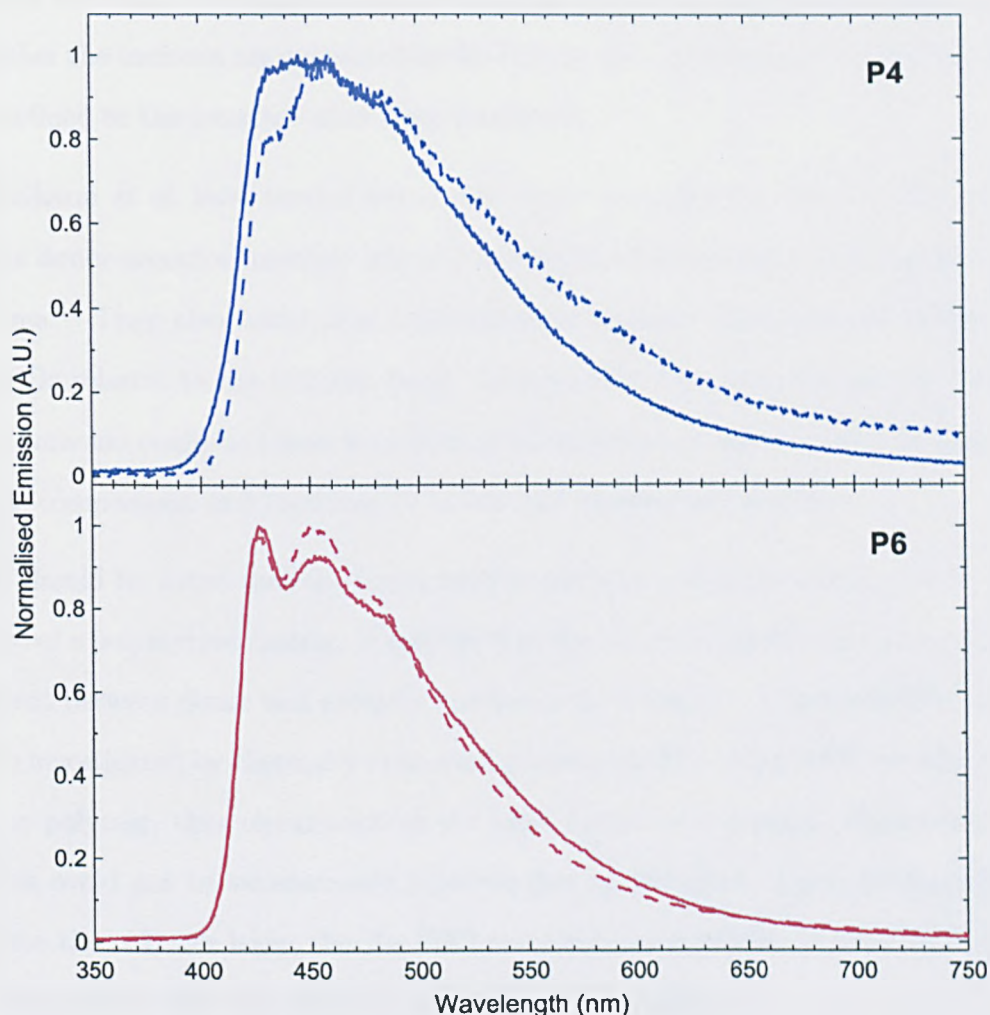


**Fig. 6.9:** Electroluminescence spectra collected from both heterojunction type B (solid line) and single-component (dashed line) LEDs.

From the electroluminescence spectra of the **P6** devices, it is apparent that the low-energy emission band which is present when Bu-PBD is blended into the polymer, can be suppressed by separating the two components into individual layers. This result is not surprising. In the **P6**:Bu-PBD blend, phase separation is likely to occur, resulting in the formation of donor-rich and acceptor-rich domains within the film. In effect, this will extend the interface between donor and acceptor species, increasing the number of sites at which the exciplex could form. From the EL of the bilayer device, it is apparent that intramolecular excitons can be efficiently generated on the polymer as a result of electronic injection

from Bu-PBD. The lack of exciplex emission from the bilayer would imply that either the excitons are generated in the bulk of the polymer, or that they are not confined to the interface after their formation.

Kulkarni *et al.* have carried out a systematic investigation into the affect that the donor-acceptor interface has on emission from exciplex-forming organic systems.<sup>17</sup> They also found that intramolecular emission was enhanced in bilayer LEDs relative to the exciplex band. Interestingly, they showed that the colour of emission could be tuned from blue-green to yellow-orange to white by varying the composition and thickness of blends and bilayers respectively.

It should be noted that the interpretation of these results is complicated by the use of a polystyrene matrix. It may be that the matrix is inhibiting cofacial alignment between donor and acceptor species at the interface. This possibility could be investigated by thermally evaporating a pristine film of Bu-PBD directly onto the polymer, thus circumventing the requirement of a matrix. Unfortunately, this could not be satisfactorily achieved during this work. Upon its deposition onto the polymer layer, the Bu-PBD appeared to crystallise. Devices that were fabricated in this way failed to exhibit electroluminescence.

### 6.2.3 Spectral Stabilisation in Heterojunction Devices

For the practical application of new electroluminescent organic compounds, the purity and stability of emission colour are greatly important. Of the single-component devices reported in Chapter 6, the 3,6-methyl-protected polyalkyl-carbazoles **P1** and **P2** in particular suffered from broad spectra and unsaturated emission. Indeed, both devices exhibited multiple emission bands that were distributed across the visible spectrum. This resulted in a change in the colour of emission from the intrinsic blue that was observed during photoluminescence to a tinted white colour during EL. The relative intensity of these bands would change as the device was operated, resulting in a further shift in colour. Figure

6.10 shows how the spectrum of the **P2** single-component device evolved during the first 20 s of its operation. The LED was driven with a constant-current of 0.5 mA (11.1 mA/cm<sup>2</sup>). During this time the applied bias increased from approximately 7.5 V to 8.5 V.

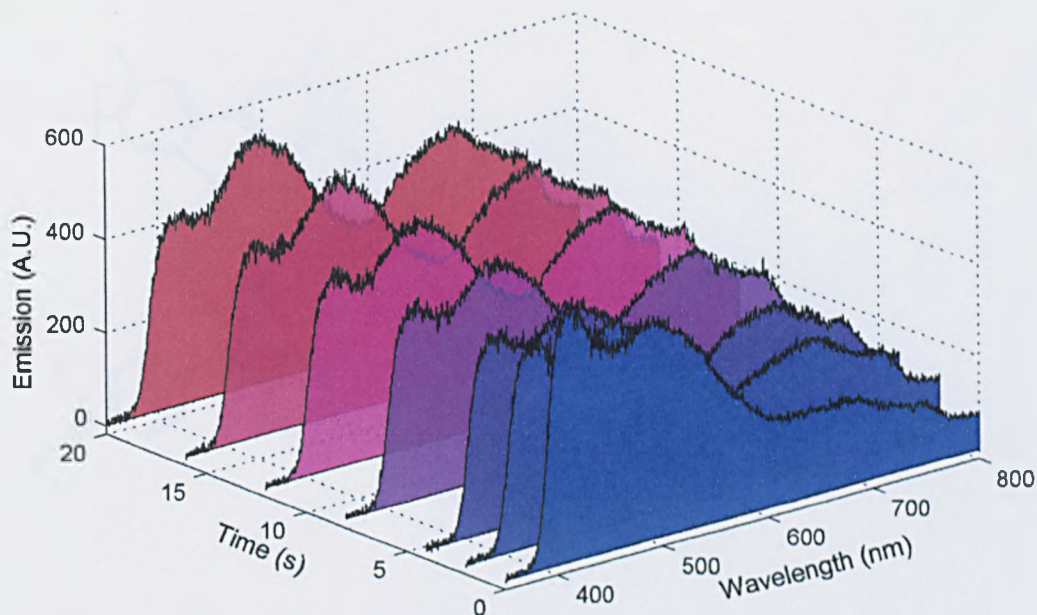


**Fig. 6.10:** The spectral evolution of a 'single-component' device fabricated from polymer **P2**. The data was collected during the initial 20 s of operation at a constant current of 0.5 mA.

On its initial operation, emission from the device peaked at 414 nm, similar in position to the maximum of the PL spectrum. However, an additional band, peaking at 490 nm, can also be resolved. The emission tail extends beyond 800 nm. As the device was run, the intensity of the blue band diminished, whilst the 490 nm peak was enhanced. After 20 s of operation, the emergence of a third emission band, peaking at around 680 nm, can be clearly seen.

Interestingly, a similar red emission band (seen only during electroluminescence) has been observed from a variety of methyl-protected polycarbazoles (see figure 6.11 for their chemical structures). Indeed, throughout this study the only methyl-protected polymer that did not exhibit a red band during device opera-

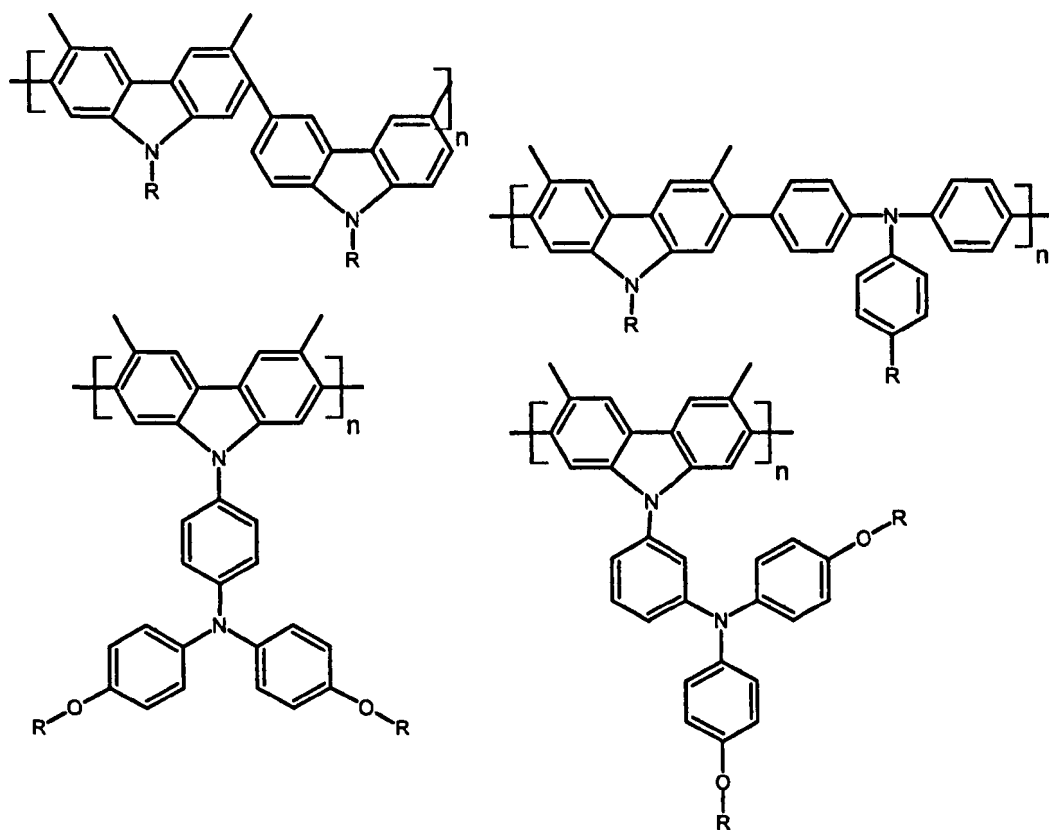


**Fig. 6.11:** The chemical structure of 3,6-methyl-substituted polycarbazoles that exhibit anomalous low-energy emission bands during electroluminescence.

tion was the oxadiazole-containing copolymer **P3**. It should also be noted that, of the two other alkyl-substituted polymers (**P1** and **P2**), it was the partially protected copolymer **P2** that exhibited the least intense red band, which grew in intensity as the device was operated. In contrast, the EL spectrum of the homopolymer consisted predominantly of the red band, even during the device's initial operation.

A significant change in the electroluminescence spectrum of **P2** is observed when Bu-PBD is blended into the active layer. The type A heterojunction device was fabricated with a blend ratio of 70:30 % w/w of **P2** to Bu-PBD. The evolution of its emission spectrum during an initial 60s period of operation is presented in figure 6.12. Again, a constant current of 0.5 mA was used. The applied bias increased from 7.5 V to 13 V during the measurement period.

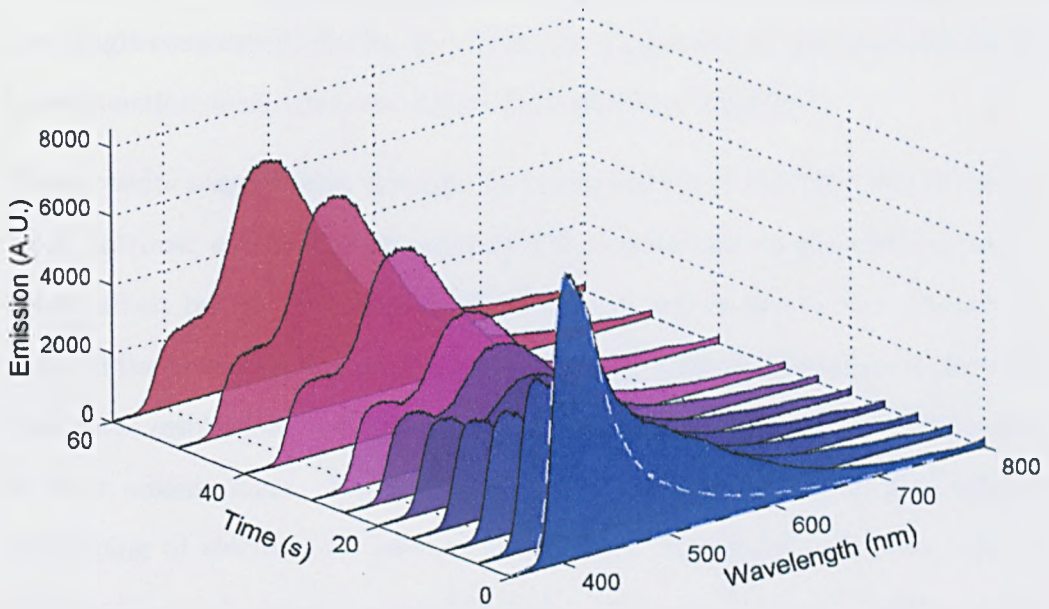


**Fig. 6.12:** The spectral evolution of a **P2:Bu-PBD** distributed heterojunction device. The data was collected during the initial 60 s of operation at a constant current of 0.5 mA. The PL spectrum of **P2** is also presented (dashed line)

In contrast to the single-component spectra presented in figure 6.10, the blend device exhibits blue electroluminescence on its initial operation. This data closely matches the intrinsic PL spectrum (highlighted by the dashed line) between 400-500 nm, although there is still greater emission from the tail. Based upon the initial emission spectra obtained from each device, the incorporation of Bu-PBD into the active layer results in a shift of the chromaticity coordinates from  $x = 0.26$  and  $y = 0.30$  to  $x = 0.23$  and  $y = 0.23$ .

Over the full 60 s measurement period, the emission spectrum of the heterojunction device changes dramatically. Within the first 20 seconds of operation, a new peak at 490 nm has emerged and become the predominant emission band. Its intensity continues to increase until the spectrum stabilises after about 50 s. As the new band grows in, the intrinsic blue peak diminishes. At the end of the measurement, the chromaticity coordinates have shifted to  $x = 0.24$  and

$y = 0.37$ . Notably, emission from the 680 nm band that was observed from the 'single-component' device is completely suppressed in the spectrum of the heterojunction, even when the device had otherwise degraded.

These results suggest that, through the incorporation of Bu-PBD into the active layer, intrinsic emission from polymer **P2** is stabilised during electroluminescence, albeit briefly. The underlying process by which this occurs remains unclear. If the molecular dopant is acting as a conduit for the transport of electrons, then these results may indicate an instability of methyl-protected polycarbazoles in their anionic state. Equally however, dopant molecules may facilitate the detrapping of electrons at intrinsic defect sites that would otherwise undergo hole-capture and radiative recombination. Alternatively, these results may reflect a shift in the recombination zone away from cathode induced defects. This mechanism was proposed by Mauthner and coworkers when investigating colour stabilisation in PPP based devices.<sup>27</sup> Further work is required to elucidate the processes involved. Some insight into the properties of these methyl-protected polymers may be gained through the electrochemical study of their reduced state, and degradation studies on single carrier devices.

### 6.3 TFB Interlayer

The interface between the anode and emissive layer has been identified as a common site of degradation in organic LEDs. Early studies showed that an ITO anode could act as a source of oxygen for defect formation when the light-emitting polymer (LEP) was deposited directly on top of it.<sup>28</sup> This degradation route however, could be successfully inhibited through the incorporation of an orthogonally soluble polymeric conductor between the anode and LEP.<sup>29</sup> Subsequently, the use of PEDOT:PSS as an anode modification has been widely adopted.

Recent work however, has revealed that the PEDOT:PSS layer may itself be a

source of device instability. For instance, de Jong and co-workers discovered that indium, liberated from the underlying ITO anode by the acidic PSS component, can migrate throughout the PEDOT layer and penetrate the PEDOT/LEP interface.<sup>30</sup> Kim *et al.* have also shown that the incorporation of PEDOT can have a detrimental influence on the electroluminescent polymer.<sup>31</sup> They suggested that the EL layer could become irreversibly oxidised at the PEDOT/polymer interface, creating luminescence-quenching defects. The process was counterbalanced by the presence of anions from PSS. Studies on the electrical degradation of PEDOT:PSS have also shown that oxygen and sulphur-containing species could be released during device operation.<sup>32</sup> These would be free to migrate through the LEP causing further degradation and influencing charge transport.

The incorporation of an anodic interlayer, deposited between the PEDOT:PSS anode and the electroluminescent layer, can therefore serve many functions. Firstly, if an appropriate material is used, the interlayer can enhance hole injection through the gradation of the energy barriers. Similarly, the extraction of a surplus electron current can be inhibited if the electron affinity of the interlayer is sufficiently low enough to block electronic injection.<sup>33</sup> Both of these mechanisms are of relevance when electrons are the majority carrier in the emissive layer. As such, the incorporation of an anodic interlayer should be advantageous in

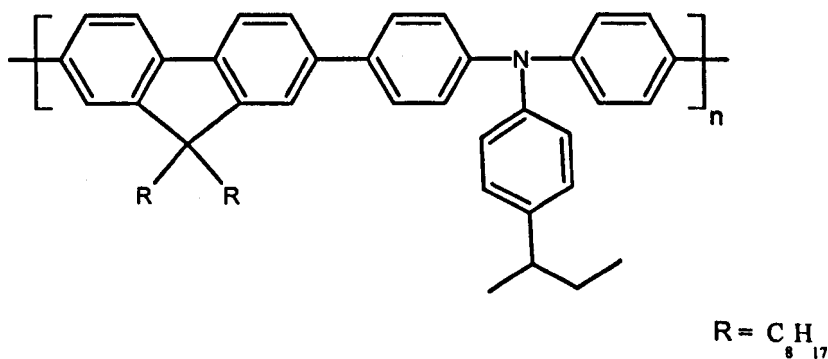


**Fig. 6.13:** The chemical structure of the fluorene-triarylamine copolymer TFB.

the primarily n-type oxadiazole-containing polymers **P3** and **P7**. Furthermore, non-radiative decay channels resulting from quenching at the PEDOT/polymer interface should be inhibited if the interlayer confines excitons to the LEP.<sup>34</sup>

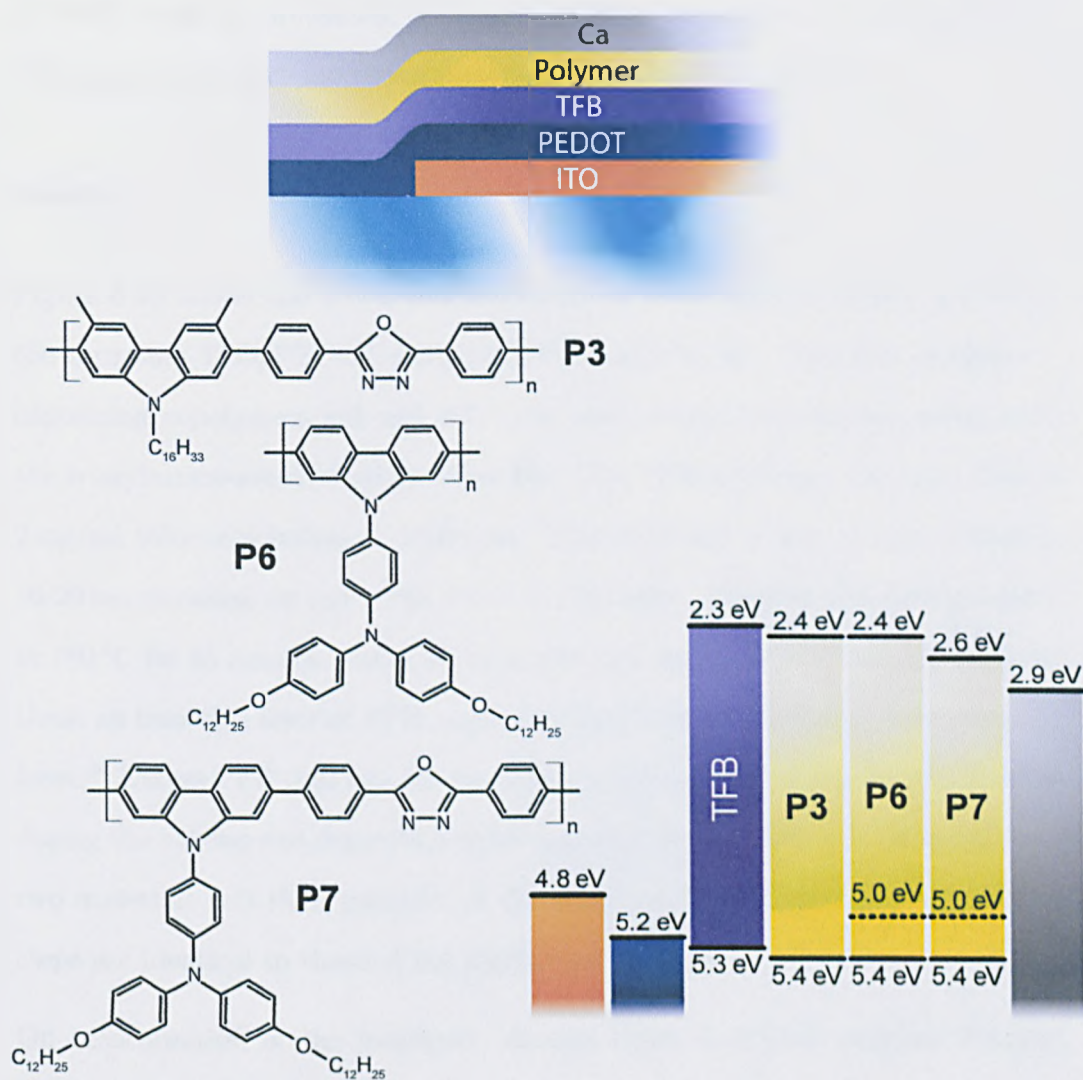


**Fig. 6.14:** The device structure and band diagram of devices containing a TFB interlayer.

The influence of a hole-injection interlayer on polycarbazole device characteristics is discussed herein. The fluorene-triarylamine copolymer poly(9,9'-dioctylfluorene-*co-N*-(4-butylphenyl)diphenylamine) (TFB) was used in this study (see figure 6.14). TFB, has been identified as a promising hole injection and transport material owing to its low ionisation potential (5.3 eV) and high hole mobility (reported values ranging from  $3 \times 10^{-3} \text{ cm}^2/\text{Vs}$  at 0.25 MV/cm to  $1 \times 10^{-2} \text{ cm}^2/\text{Vs}$



at 0.16 MV/cm).<sup>35,36</sup> Its use as an interlayer, in combination with an emissive F8BT film has been previously documented by Kim *et al.*<sup>34</sup> They found that by annealing the TFB interlayer, its dissolution on the subsequent deposition of F8BT could be prevented. Lee and coworkers have also reported upon this technique using other interlayer materials (namely PVK and PFB).<sup>37</sup>

## Results

Figure 6.15 shows the I-V-L characteristics of three heterojunction devices of the structure ITO/PEDOT:PSS/TFB/Polymer/Ca/Ag. The two oxadiazole-containing copolymers **P3** and **P7** were used in this investigation along with the triarylamine-substituted polymer **P6**. The TFB interlayer was spun from a 2 mg/ml toluene solution at 1000 rpm. This produced a film of approximately 10-20 nm thickness on top of the PEDOT:PSS layer. The film was then annealed at 180 °C for 15 minutes under an inert nitrogen atmosphere. Under such conditions, an insoluble layer of TFB, approximately 10 nm in thickness, is expected to form.<sup>34</sup> Excess TFB that has not hardened as a result of this process will dissolve during the subsequent deposition of the polycarbazole layer. It is likely that the two materials will then intermix at the interface.<sup>37</sup> The remaining fabrication steps are identical to those of the single layer devices.

On incorporation of the interlayer, devices containing both polymer **P3** and **P6** sustain smaller current densities at low applied bias than their single layer analogs. For example, the **P3** device reaches a current density of 0.01 mA/cm<sup>2</sup> at 4.2 V when the interlayer is included, and 3.9 V when it is absent. In the **P6** device, the difference is more significant with a bias of 4.4 V being required for the interlayer device and only 3.3 V for the single layer device.

In the case of the **P3** device, this may simply be a consequence of the reduction in average field strength across the organic films. Energetic considerations suggest that the barrier to the injection of holes should be similar in both **P3** and TFB. A significant enhancement in hole injection on incorporation of the

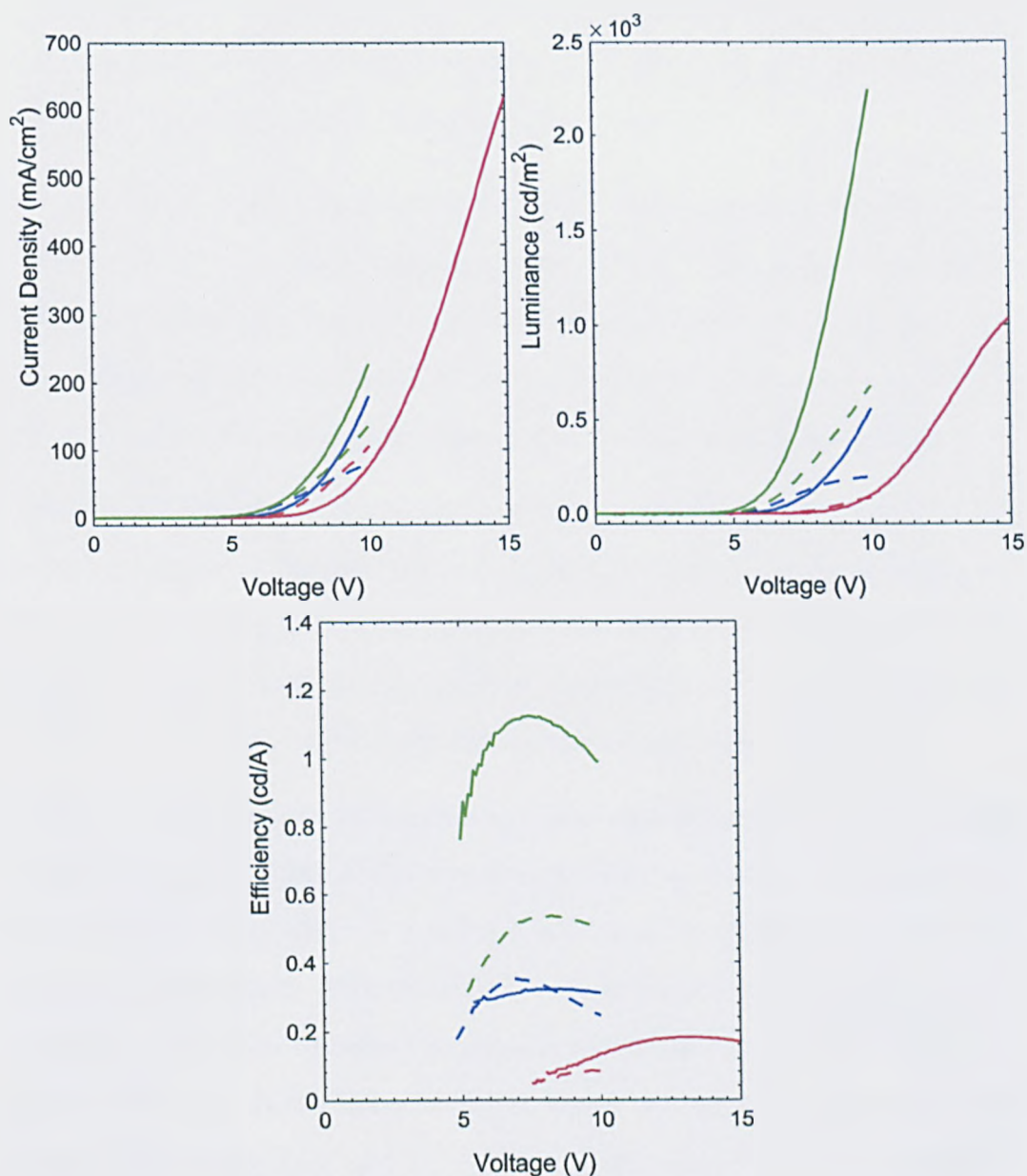


**Fig. 6.15:** The voltage dependence of current density, luminance and current efficiency of devices incorporating a TFB interlayer (solid lines). The polycarbazoles **P3** (blue), **P6** (red) and **P7** (green) were used in this investigation. The characteristics of single-layer devices are also presented (dashed lines)

interlayer is therefore unlikely. In the **P6** device however, it is plausible that the injection of holes is actually inhibited by the TFB interlayer. As discussed in Chapter 5, polymer **P6** exhibits two oxidation potentials, corresponding to an ionisation potential of 5.0 eV and 5.4 eV. With an ionisation potential between

5.33-5.45 eV,<sup>35,38</sup> the TFB layer should inhibit hole injection into the lower energy manifold of states. This may be the reason for the significant reduction in current density at low bias in the **P6** interlayer device.

At low bias, the **P7** interlayer device shows almost identical current-voltage characteristics to its single-layer equivalent. Both LEDs sustained a current density of 0.01 mA/cm<sup>2</sup> at 2.8 V. These results are perhaps indicative of the fact that charge transport, and not injection, is limiting the hole current through the **P7** active layer. This postulate supports the findings reported in Chapter 4.

Interestingly, all three interlayer devices sustained larger current densities in the high bias regime. The **P6** device exemplified this with a current density of 617 mA/cm<sup>2</sup> flowing at 15 V. In the single layer device, the J-V curve plateaued at a much lower current density and bias. This suggests that the presence of the interlayer may indeed stabilise the device against electronic degradation.

Similar trends are seen in the luminance-voltage characteristics of the **P3** and **P6** interlayer devices. These LEDs exhibit a smaller luminance at low biases when the interlayer is included. A luminance of 1 cd/m<sup>2</sup> is attained at 4.8 V in the single-layer **P3** device. With the addition of the interlayer, a voltage of 5.1 V is necessary to reach an equivalent brightness. When the device is fabricated using polymer **P6**, the incorporation of the interlayer necessitates an increase in the operating bias from 7.6 V to 8.2 V to attain a luminance in excess of 10 cd/m<sup>2</sup>.

As was the trend in the J-V characteristics of these devices, incorporation of the interlayer also results in enhanced brightness at high bias. At 10 V, the luminance obtained from the **P3** LED increases from 198 cd/m<sup>2</sup> to 557 cd/m<sup>2</sup> on the inclusion of the interlayer. At the same bias, the brightness of the **P6** device increases from 90 cd/m<sup>2</sup> to 103 cd/m<sup>2</sup>. However, when a bias of 15 V is applied to the TFB/**P6** device, a luminance of 1,032 cd/m<sup>2</sup> is attained. In contrast, the **P6** single-layer device only achieves a luminance of 147 cd/m<sup>2</sup> at 15 V.

The TFB/**P7** device displayed the most promising luminance-voltage character-

istics of all of the LEDs fabricated during this work. Electroluminescence from this device could be detected at a bias 2.8 V. A luminance of  $10 \text{ cd/m}^2$  was attained at 4.7 V and a maximum luminance of  $2240 \text{ cd/m}^2$  was recorded at 10 V. This represents a decrease in the operating voltage at  $10 \text{ cd/m}^2$  of 0.5 V, and a 3-fold increase in the maximum luminance at 10 V on incorporation of the TFB interlayer. The current efficiency of this device also showed a marked improvement, its maximum increasing from  $0.54 \text{ cd/A}$  to  $1.12 \text{ cd/A}$ . Interestingly, the current efficiency of the **P3** device showed little dependence upon the presence of the interlayer.

Electroluminescence spectra of the three devices are presented in figure 6.16. The EL spectra of **P6** and **P7** show little change on the introduction of the TFB interlayer, suggesting that emission is generated by intramolecular charge recombination from within the polycarbazole bulk. However, emission from the TFB/**P3** device is notably different to that of the single-layer spectrum. The emission peak is shifted from 442 nm to 436 nm and the FWHM is narrowed from 74 nm to 60 nm by incorporating the interlayer. Significantly, vibronic replica can also be resolved in the bilayer spectrum, whereas emission from the single layer device is featureless. The first of these replica is located at 459 nm and a shoulder is discernable between 480-500 nm.

The photoluminescence spectrum obtained from a thin film of TFB, excited by the 325 nm line of a HeCd laser, is shown alongside the EL spectra of the two **P3** devices. Many of the features observed from the emission spectrum of TFB are replicated in the bilayer spectrum. This is a clear indication that radiative decay is occurring predominantly from within the TFB interlayer. Emission from the bilayer is broader than the TFB spectrum, suggesting that there is also a contribution from excitons that recombine within the polycarbazole film. Significantly however, there is no indication of a low energy emission band that would signify the formation of intermolecular states.

This result demonstrates an alternative approach to generating blue electrolu-

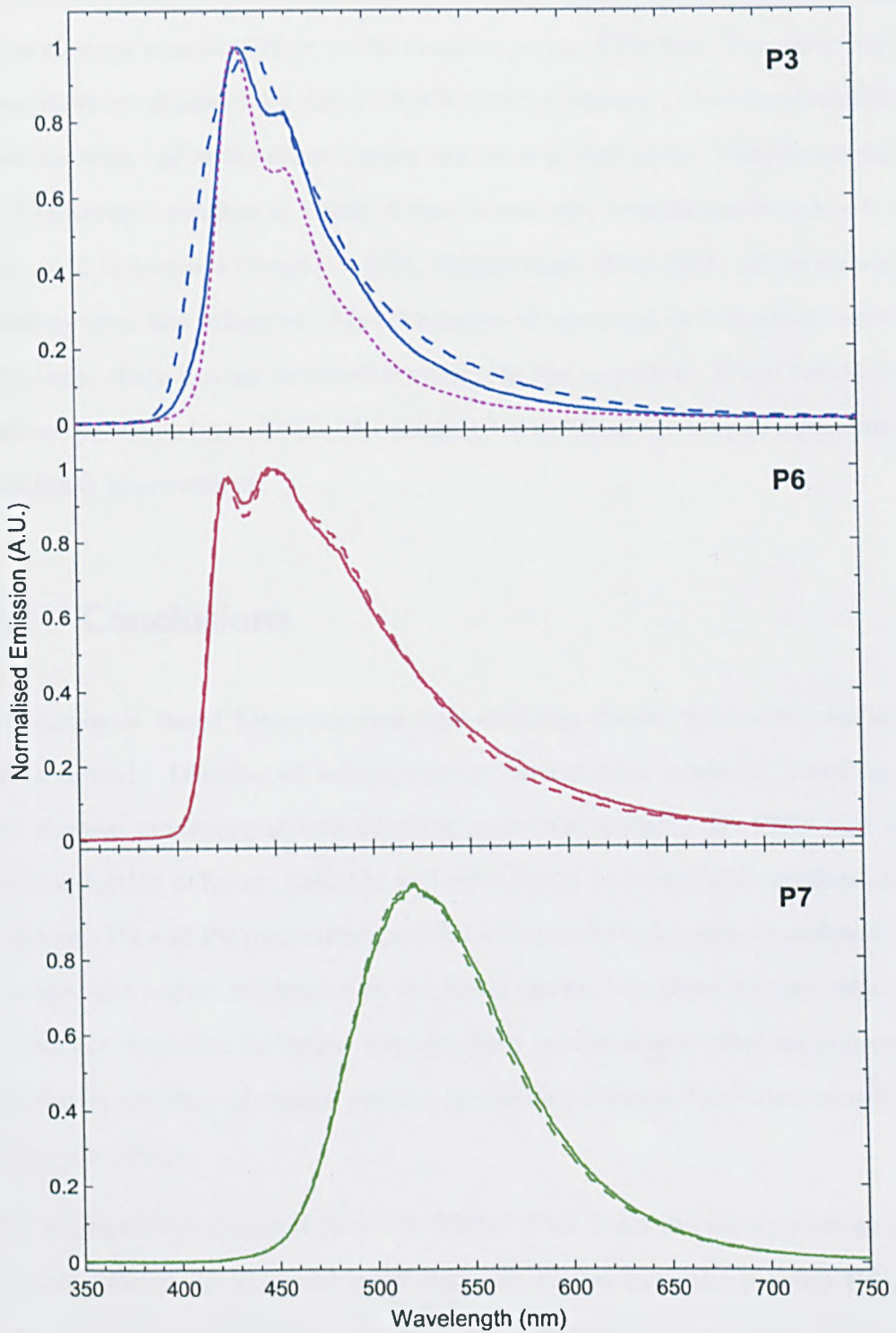


**Fig. 6.16:** Electroluminescence spectra collected from ‘single-component’ devices (dashed line) and devices incorporating a TFB interlayer (solid line). The polycarbazoles **P3** (blue), **P6** (red) and **P7** (green) were used in this investigation. The photoluminescence spectrum of TFB is also presented (magenta dotted line)

minescence from these materials. Here, the polycarbazole film functions more as an electron transport layer to the emissive p-type TFB film. Focussing solely upon its spectral properties, the TFB/P3 device produced a more saturated blue emission than any of the other devices discussed in this thesis. The introduction of the interlayer resulted in a shift of the chromaticity coordinates from  $x = 0.18$  and  $y = 0.15$  to  $x = 0.17$  and  $y = 0.13$ . Furthermore, the stability of the emission spectrum was also enhanced. After 2 minutes of operation at a constant current of 0.5 mA, there was no discernable change in the spectrum. When contrasted against the single layer device, the enhanced stability of the bilayer represents a significant improvement.

## 6.4 Conclusions

Polycarbazole based heterojunction light-emitting diodes were fabricated and characterised. Distributed heterojunction devices were made by blending in the electron transporting/hole blocking molecular material Bu-PBD into the semiconducting polymer. Both the aryl-substituted and triarylamine-substituted polymers, P4 and P6 respectively, exhibited lower electroluminescence threshold voltages and higher efficiencies in the blend device. As there was no evidence of emission from the molecular dopant, these results suggest that an improved balance in the flow of charge carriers is attained through the enhancement of electron injection.

The EL spectrum obtained from the P6:Bu-PBD blend did incorporate an additional, low-energy emission band that was absent from the pristine P6 device. Data from absorption, photoluminescence and PL excitation measurements suggested that this new species was an excited state complex, formed between the polymer and dopant. Its absence from the emission spectrum of other polycarbazole:Bu-PBD blends led to the conclusion that the presence of the triarylamine group was fundamental to exciplex formation. By separating

the donor and acceptor units into individual layers, exciplex generation could be largely suppressed. As a result, the **P6** planar heterojunction device exhibited blue emission with improved efficiency. However, device resistance was increased by the presence of the electronically insulating polystyrene matrix. This was manifest by a higher operating voltage.

A Bu-PBD heterojunction device fabricated using the 3,6-methyl-protected polymer **P2** displayed an enhancement of intrinsic emission on its initial operation. This was attributed to the electron transporting function of the dopant molecules. From these observations, it was inferred that the methyl-protected polymer may contain emissive electron traps that are either intrinsic to the material or that are generated under device operation.

Three devices, fabricated from polymers **P3**, **P6** and **P7**, showed enhanced EL operation on the incorporation of a TFB interlayer. This was particularly true for the n-type oxadiazole-containing polymers, in which the interlayer is expected to improve the balance of charge carriers flowing through the device. The triarylamine-substituted homopolymer **P6** also benefited from the presence of the interlayer. This was attributed to the removal of the anode/emitter interface, a known site for the occurrence of degradation. Saturated blue emission was observed from the **P3** device as a result of recombination from within the TFB interlayer. This stabilised the device against an operationally induced colour shift.

## References

- [1] Granstrom, M. and Ingnas, O. *Appl. Phys. Lett.* **68**(2), 147–149 January (1996).
- [2] Andersson, M. R., Thomas, O., Mammo, W., Svensson, M., Theander, M., and Ingnas, O. *J. Mater. Chem.* **9**(9), 1933–1940 (1999).
- [3] Su, Z. S., Che, G. B., Li, W. L., Su, W. M., Li, M. T., Chu, B., Li, B., Zhang, Z. Q., and Hu, Z. Z. *Appl. Phys. Lett.* **88**(21), 213508 May (2006).
- [4] Brown, A. R., Bradley, D. D. C., Burroughes, J. H., Friend, R. H., Greenham, N. C., Burn, P. L., Holmes, A. B., and Kraft, A. *Appl. Phys. Lett.* **61**(23), 2793–2795 December (1992).
- [5] Fujii, A., Kawahara, H., Yoshida, M., Ohmori, Y., and Yoshino, K. *J. Phys. D: Appl. Phys.* **28**(10), 2135–2138 (1995).
- [6] Adachi, C., Tsutsui, T., and Saito, S. *Appl. Phys. Lett.* **55**(15), 1489–1491 (1989).
- [7] Parker, I. D., Pei, Q., and Marrocco, M. *Appl. Phys. Lett.* **65**(10), 1272–1274 (1994).
- [8] Edwards, A., Blumstengel, S., Sokolik, I., Yun, H., Okamoto, Y., and Dorsinville, R. *Synth. Met.* **84**(1-3), 639–640 (1997).
- [9] Hong, Z. Y., Wang, D. K., Ma, D. G., Zhao, X. J., Jing, X. B., and Wang, F. S. *Synth. Met.* **91**(1-3), 321–322 (1997).
- [10] Ma, D. G., Wang, D. K., Hong, Z. Y., Zhao, X. J., Jing, X. B., and Wang, F. S. *Synth. Met.* **91**(1-3), 331–332 (1997).
- [11] Zhang, C., Vonseggern, H., Kraabel, B., Schmidt, H. W., and Heeger, A. J. *Synth. Met.* **72**(2), 185–188 (1995).
- [12] Moons, E. *J. Phys.: Condens. Matter* **14**(47), 12235–12260 December (2002).
- [13] Tak, Y. H., Bassler, H., Leuninger, J., and Mullen, K. *J. Phys. Chem. B* **102**(25), 4887–4891 (1998).
- [14] Jenekhe, S. A. and Osaheni, J. A. *Science* **265**(5173), 765–768 August (1994).
- [15] Li, T., Zhou, C. L., and Jiang, M. *Polym. Bull.* **25**(2), 211–216 February (1991).
- [16] Kalinowski, J., Giro, G., Cocchi, M., Fattori, V., and Di Marco, P. *Appl. Phys. Lett.* **76**(17), 2352–2354 April (2000).
- [17] Kulkarni, A. P. and Jenekhe, S. A. *J. Phys. Chem. C* **112**(13), 5174–5184 April (2008).



- [18] Osaheni, J. A. and Jenekhe, S. A. *Macromolecules* **27**(3), 739–742 January (1994).
- [19] Wang, J. F., Kawabe, Y., Shaheen, S. E., Morrell, M. M., Jabbour, G. E., Lee, P. A., Anderson, J., Armstrong, N. R., Kippelen, B., Mash, E. A., and Peyghambarian, N. *Adv. Mater.* **10**(3), 230 February (1998).
- [20] Kalinowski, J., Cocchi, M., Di Marco, P., Stampor, W., Giro, G., and Fattori, V. *J. Phys. D: Appl. Phys.* **33**(19), 2379–2387 October (2000).
- [21] Cocchi, M., Virgili, D., Giro, G., Fattori, V., Di Marco, P., Kalinowski, J., and Shirota, Y. *Appl. Phys. Lett.* **80**(13), 2401–2403 April (2002).
- [22] Su, W. M., Li, W. L., Xin, Q., Su, Z. S., Chu, B., Bi, D. F., He, H., and Niu, J. H. *Appl. Phys. Lett.* **91**(4), 043508 July (2007).
- [23] Yang, S. Y., Zhang, X. L., Lou, Z. D., and Hou, Y. B. *Eur. Phys. J. B* **59**(2), 151–154 September (2007).
- [24] Yap, C. C., Yahaya, M., and Salleh, M. M. *Curr. Appl. Phys.* . Article in press. Available online 27/11/2008.
- [25] Yi, H. N., Iraqi, A., Stevenson, M., Elliott, C. J., and Lidzey, D. G. *Macromol. Rapid Commun.* **28**(10), 1155–1160 May (2007).
- [26] Gebler, D. D., Wang, Y. Z., Blatchford, J. W., Jessen, S. W., Fu, D. K., Swager, T. M., MacDiarmid, A. G., and Epstein, A. J. *Appl. Phys. Lett.* **70**(13), 1644–1646 March (1997).
- [27] Mauthner, G., Collon, M., List, E. J. W., Wenzl, F. P., Bouguettaya, M., and Reynolds, J. R. *J. Appl. Phys.* **97**(6), 063508 (2005).
- [28] Scott, J. C., Kaufman, J. H., Brock, P. J., DiPietro, R., Salem, J., and Goitia, J. A. *J. Appl. Phys.* **79**(5), 2745–2751 March (1996).
- [29] Scott, J. C., Carter, S. A., Karg, S., and Angelopoulos, M. *Synth. Met.* **85**(1-3), 1197–1200 February (1997).
- [30] de Jong, M. P., van IJzendoorn, L. J., and de Voigt, M. J. A. *Appl. Phys. Lett.* **77**(14), 2255–2257 October (2000).
- [31] Kim, J. S., Ho, P. K. H., Murphy, C. E., Seeley, A. J. A. B., Grizzi, I., Burroughes, J. H., and Friend, R. H. *Chem. Phys. Lett.* **386**(1-3), 2–7 March (2004).
- [32] Crispin, X., Marciniak, S., Osikowicz, W., Zotti, G., Van der Gon, A. W. D., Louwet, F., Fahlman, M., Groenendaal, L., De Schryver, F., and Salaneck, W. R. *J. Polym. Sci., Part B: Polym. Phys.* **41**(21), 2561–2583 November (2003).
- [33] Yan, H., Scott, B. J., Huang, Q. L., and Marks, T. J. *Adv. Mater.* **16**(21), 1948 November (2004).
- [34] Kim, J. S., Friend, R. H., Grizzi, I., and Burroughes, J. H. *Appl. Phys. Lett.* **87**(2), 023506 July (2005).

- 
- [35] Redecker, M., Bradley, D. D. C., Inbasekaran, M., Wu, W. W., and Woo, E. P. *Adv. Mater.* **11**(3), 241 February (1999).
- [36] Fong, H. H., Papadimitratos, A., and Malliaras, G. G. *Appl. Phys. Lett.* **89**(17), 172116 October (2006).
- [37] Lee, T. W., Kim, M. G., Kim, S. Y., Park, S. H., Kwon, O., Noh, T., and Oh, T. S. *Appl. Phys. Lett.* **89**(12), 123505 September (2006).
- [38] Duan, L., Chin, B. D., Yang, N. C., Kim, M. H., Kim, H. D., Lee, S. T., and Chung, H. K. *Synth. Met.* **157**(8-9), 343-346 May (2007).

## Chapter 7

# Solvatochromism in Triarylamine-Substituted Polycarbazoles

### 7.1 Introduction

Photoluminescence measurements that were carried out on solutions of the triarylamine-substituted homopolymer **P6** revealed a strong solvent dependence. This chapter details an investigation into the origin of this phenomenon. The influence of solution concentration and solvent polarity upon the emission spectrum of the polymer has been studied. Photoluminescence lifetimes have also been obtained using the time-correlated single photon counting technique. The data collected was used to evaluate possible theories pertaining to the origin of this solvatochromic behaviour.

## 7.2 Results

### 7.2.1 Solvent Dependant Spectra

Figure 7.1 presents the solution photoluminescence spectra obtained from the triarylamine substituted homopolymer **P6** when dissolved in *para*-xylene, toluene, chlorobenzene, chloroform and dichloromethane (DCM). All solutions were prepared at a concentration of  $0.1 \text{ gL}^{-1}$  (less than  $10^{-5} \text{ M}$ ), and were excited using the 325 nm line of a HeCd laser.

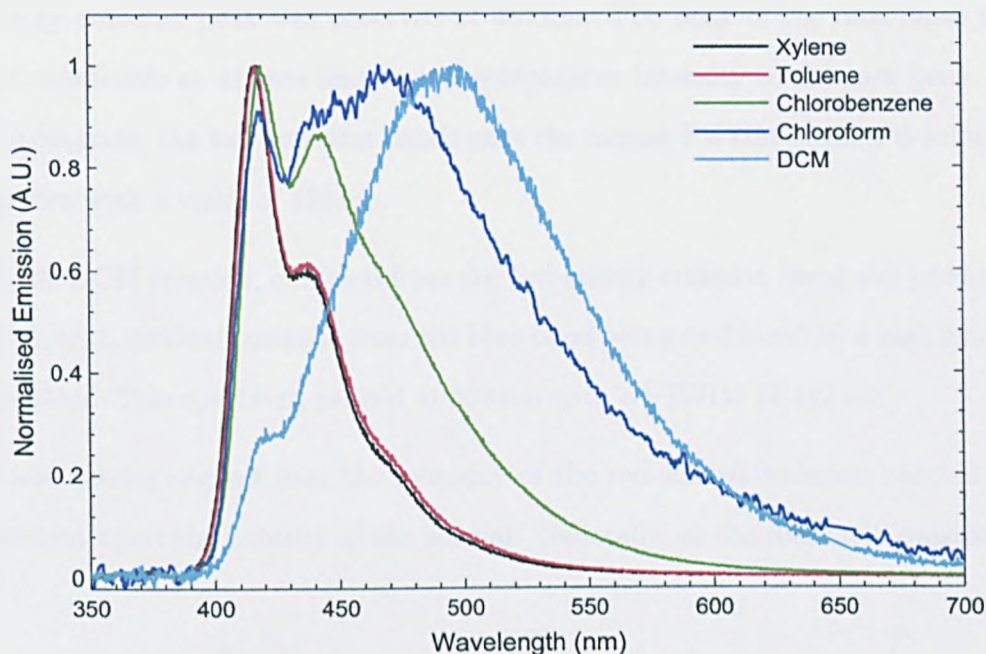


**Fig. 7.1:** The photoluminescence spectra of polymer **P6** dissolved in various solvents.

These results are a clear demonstration of solvatochromic behaviour. By changing the nature of the solvent, the structure of the emission spectrum has been dramatically altered. When dissolved in the dimethyl-substituted aromatic solvent *p*-xylene, **P6** exhibited a narrow emission band with a FWHM of 40 nm, peaking at 418 nm. This spectrum also featured multiple shoulders, similar to the vibronic structures that are commonly observed in conjugated organic molecules.

The first of these, presumed to result from the 0-1 transition, was located at 438 nm. The emission spectrum from **P6** when dissolved in toluene was largely the same, but with a marginal red-shift.

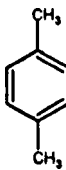
When chlorobenzene was used as the solvent, the PL spectrum of polymer **P6** was significantly broadened. The emission peak underwent a small redshift to 420 nm and the 0-1 transition increased in intensity, becoming more easily defined. This secondary peak was now located at 444 nm. The FWHM of the spectrum increased to 69 nm.

In the spectrum that was obtained from the chloroform solution, a new lower-energy emission peak was observed at 467 nm. The peak of the blue band was still resolvable at 418 nm and was of comparable intensity to the new peak. In combination, the two emission bands gave the largest FWHM of the **P6** solution spectra with a value of 123 nm.

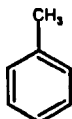
In the DCM solution, emission from the low-energy emission band was predominant, with residual emission from the blue band being evidenced by a high energy shoulder. This spectrum peaked at 498 nm with a FWHM of 112 nm.

These results suggest that the intensity of the red-shifted emission band is dependent upon the polarity of the solvent. Generally, as the dielectric constant

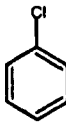
Solvent	$\epsilon_r$	$\lambda_{\max}(\text{nm})$
<i>p</i> -Xylene	2.27	418
Toluene	2.41	417
Chloroform	4.63	467
Chlorobenzene	5.54	420
DCM	8.51	498



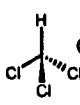
*p*-Xylene



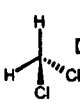
Toluene



Chlorobenzene



Chloroform



DCM

**Fig. 7.2:** A list of the static dielectric constants of each of the solvents that were used in this study (values were obtained from reference 1). The molecular structure of each solvent is shown for reference.

of the solvent was increased, emission from the low-energy band was enhanced and its peak was shifted to longer wavelengths. In going from *p*-xylene, with a dielectric constant of  $\epsilon_r = 2.27$ , to DCM, with a dielectric constant of  $\epsilon_r = 8.51$ , the emission maximum was red-shifted by 80 nm. These results are summarised in figure 7.2.

Figure 7.3 presents the absorption spectra of polymer **P6** when dissolved in toluene and DCM. Again, both solutions were prepared at a concentration of  $0.1 \text{ gL}^{-1}$ . In toluene, the spectrum peaks at 385 nm. In DCM however the peak is red-shifted to 394 nm, indicating a change in the conformation of the polymer chains.

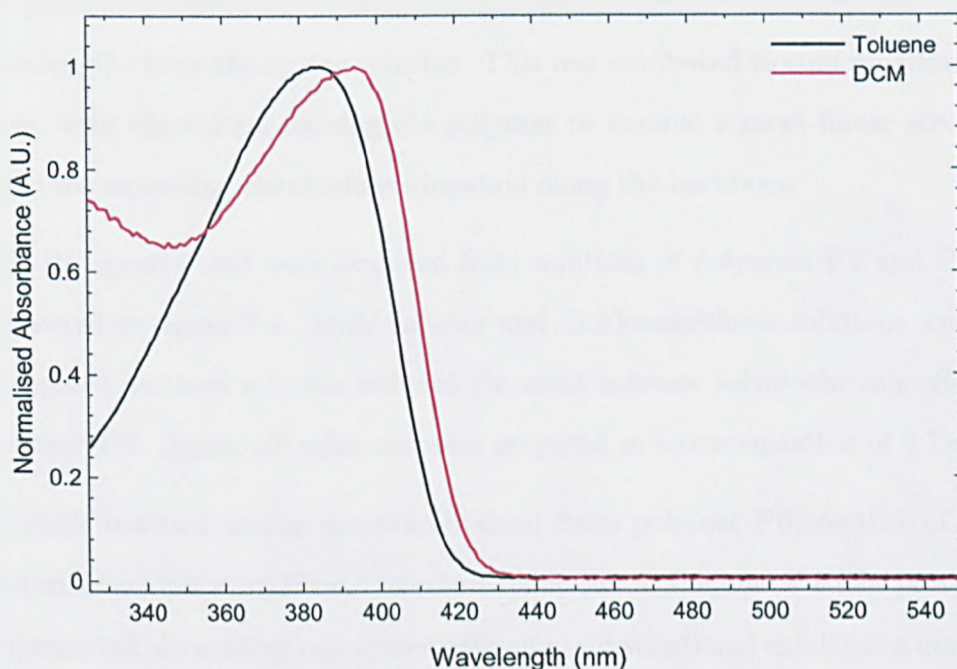


**Fig. 7.3:** The absorption spectra of polymer **P6** when dissolved in toluene and dichloromethane.

Similar observations have been made from one of the most widely investigated conjugated polymers, MEH-PPV. In their study of this material, Schwartz *et al.* have demonstrated the importance of solute-solvent interactions in controlling molecular geometry and ultimately determining the polymer's electronic properties.<sup>2,3</sup> Dynamic light scattering measurements showed that a good solvent (in

this case chlorobenzene) would favour polymer-solvent interactions, causing the polymer chains to adopt a relatively linear conformation. Conversely, in a poor solvent (THF) the molecules would collapse into a more coiled structure, minimising interactions with the solvent. The resulting increase in the number of conformational defects would, on average, shorten the conjugation length of the chromophores, causing a blue-shift in the polymer's absorption spectrum. The authors stressed that this was only true for dilute solutions, where interactions between neighbouring polymer chains were negligible.

This effect has also been reported using other solvents. For instance, Aharon *et al.* noted differences in the absorption spectrum of MEH-PPV when it was dissolved in xylene and chloroform.<sup>4</sup> They observed an enhancement in absorption at short wavelengths from the xylene solution. This was attributed to conformational effects, with chloroform causing the polymer to assume a more linear structure and thus extending electronic conjugation along the backbone.

The PL spectra that were obtained from solutions of polymers **P2** and **P4** are presented in figure 7.4. Only toluene and dichloromethane solutions were investigated as these solvents induced the most extreme solvatochromic effect in polymer **P6**. Again, all solutions were prepared at a concentration of  $0.1 \text{ gL}^{-1}$ .

In stark contrast to the spectra obtained from polymer **P6**, neither of these materials exhibit a significant solvatochromic effect. Polymer **P2** (the protected-unprotected alternating copolymer with alkyl substitutions) exhibited a marginal red-shift in the emission peak ( $\lambda_{\text{max}}$ ) from 391 nm in toluene to 396 nm in DCM. This material also displayed a slight enhancement in emission at longer wavelengths. In the poly(aryl carbazole) (**P4**), the influence of the solvent was even smaller. Although a marginal red-shift can be resolved in going from toluene to DCM, both of the spectra peaked at 416 nm. The implication of these results is that the full triarylamine substitution of polymer **P6** is key to the solvatochromic behaviour exhibited by this material.

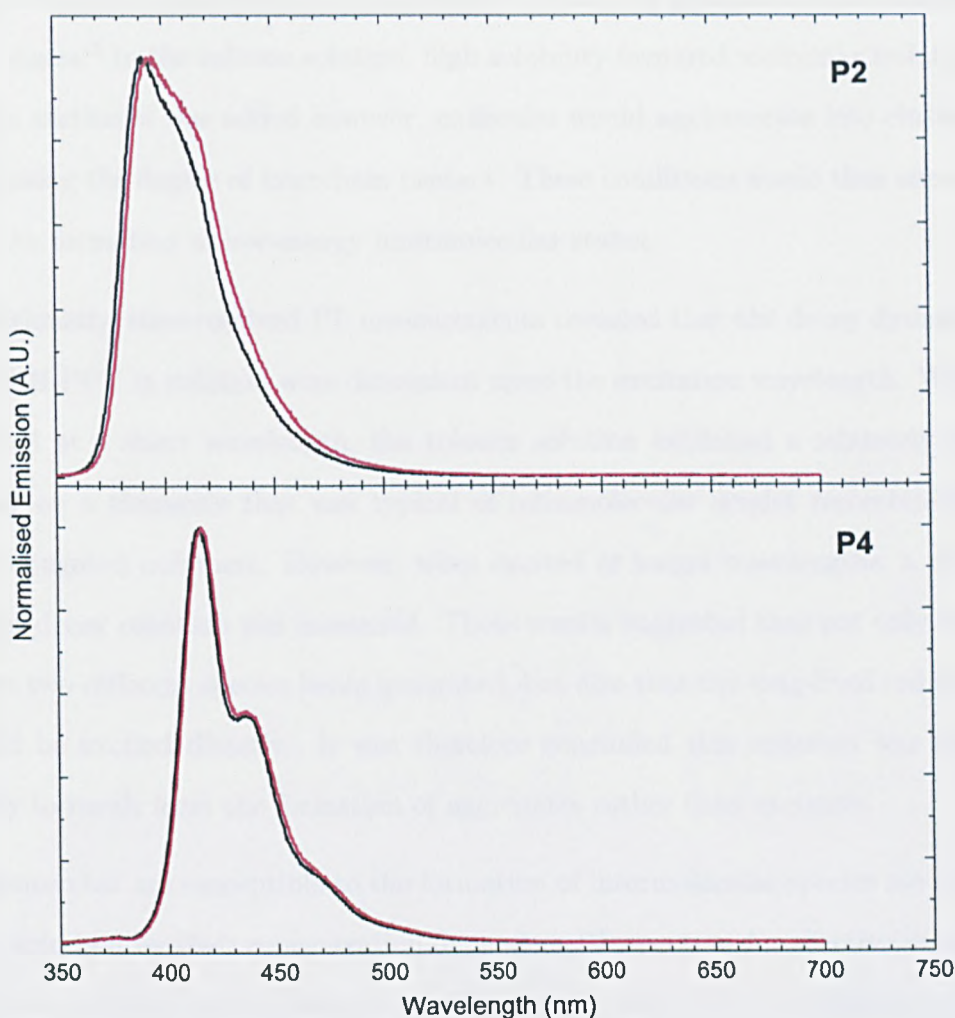


**Fig. 7.4:** The photoluminescence spectra of polymers **P2** and **P4** when dissolved in toluene (black) and dichloromethane (red).

## 7.2.2 Solution Concentration

Solvatochromism in conjugated materials can be attributed to a variety of photophysical processes. In the cyano-substituted PPV-based polymer CN-PPV, Samuel and coworkers found that the nature of photoluminescence was dependent upon the quality of the solvent used.<sup>5</sup> In a good solvent (toluene was used in their investigation), the PL spectrum of CN-PPV was characterised by a narrow and structured emission band. However, on the addition of a poor solvent such as methanol, the spectrum red-shifted whilst becoming broad and featureless.



The authors proposed that this new emission band was generated by intermolecular states.<sup>5</sup> In the toluene solution, high solubility favoured molecular isolation. When methanol was added however, molecules would agglomerate into clusters, increasing the degree of interchain contact. These conditions would thus encourage the formation of low-energy intermolecular states.

Additionally, time-resolved PL measurements revealed that the decay dynamics of MEH-PPV in solution were dependent upon the excitation wavelength. When excited at a short wavelength, the toluene solution exhibited a relatively fast decay on a timescale that was typical of intramolecular singlet recombination in conjugated polymers. However, when excited at longer wavelengths, a much larger decay constant was measured. These results suggested that not only were there two different species being generated, but also that the long-lived red state could be excited directly. It was therefore concluded this emission was more likely to result from the formation of aggregates rather than excimers.

Systems that are susceptible to the formation of intermolecular species are often characterised by their concentration dependent PL spectra. An effective demonstration of this behaviour was provided by Birks *et al.* whilst investigating pyrene and several of its derivatives.<sup>6</sup> When dissolved in a dilute solution of cyclohexane ( $10^{-4}$  M), the PL spectrum of pyrene was highly structured, peaking between 350 nm and 400 nm. However, as the concentration of the solution was increased a new structureless emission band emerged, approximately centered at 480 nm. The relative intensity of this band increased with concentration, signifying the enhancement of intermolecular interactions. At a concentration of  $10^{-2}$  M, the new emissive species was predominant.

Figure 7.5 shows the PL spectrum of polymer **P6** in dichloromethane at a variety of concentrations. It should be noted that the spectrum from a  $0.01 \text{ gL}^{-1}$  solution was also obtained. This data was not presented owing to a high level of noise. However, the general form of this spectrum was similar to those shown in figure 7.5 and there was no indication of any additional features.

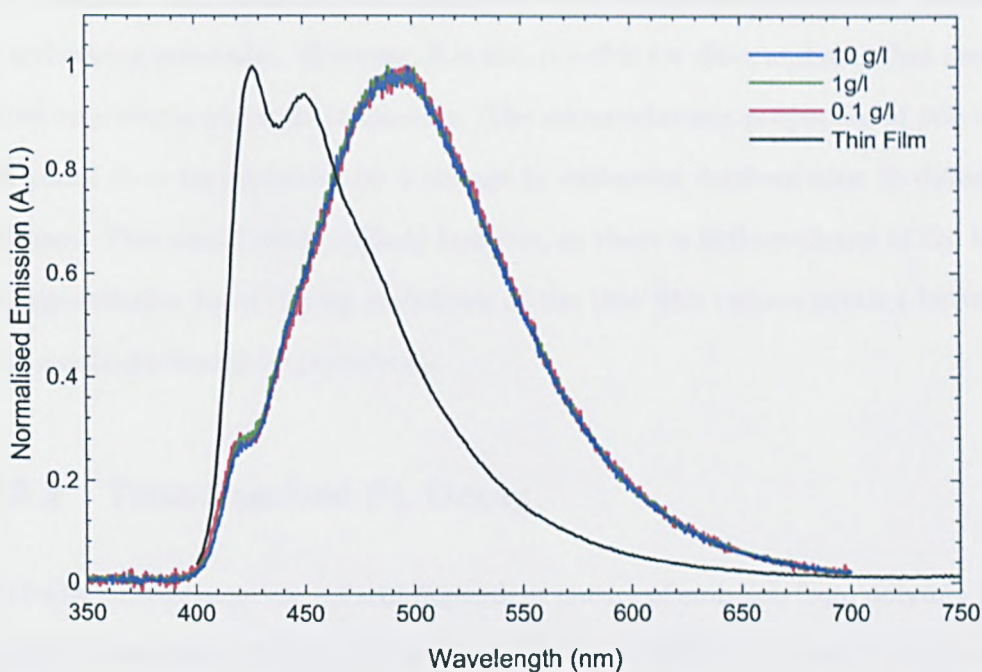


**Fig. 7.5:** The photoluminescence spectra of polymer **P6** dissolved in dichloromethane at different concentrations. The thin film spectrum is also presented.

Significantly, the PL spectrum of polymer **P6** appears to be independent of the solution concentration. These results suggest that intermolecular interactions may not be responsible for the low-energy emission band observed from **P6** in dichloromethane. This interpretation is however complicated by the fact that a single polymer chain can accommodate multiple chromophores. It is therefore more appropriate to express the solution concentration in terms of the molarity of chromophoric units.

In their study of fluorene oligomers (with a similar bridged biphenyl structure to polycarbazole), Klaerner *et al.* showed that the conjugation length of these materials was limited to around 12 repeat units.<sup>7</sup> If it is assumed that the **P6** chromophore is similar in size, then the lowest concentration solution ( $0.01 \text{ gL}^{-1}$ ) would have a molarity of  $2.0 \times 10^{-7} \text{ M}$ . In comparison, the pyrene-cyclohexane solutions that were studied by Birks *et al.* showed no evidence of intermolecular emission below a concentration of  $10^{-4} \text{ M}$ .<sup>6</sup>

This analysis only considers the possibility of chromophore interactions between neighbouring molecules. However, it is also possible for chromophores that are located on a single molecule to interact. The solvatochromic properties of polymer P6 could then be explained by a change in molecular conformation in different solvents. This would seem unlikely however, as there is little evidence of the low-energy emission band during excitation of the thin film (where contact between chromophores would be prevalent).

### 7.2.3 Time-Resolved PL Decay

To further investigate the solvent dependent nature of emission from polymer P6, photoluminescence lifetime measurements were undertaken. Figure 7.6 shows the PL decay curves that were obtained from toluene and dichloromethane solutions. These were chosen to represent the extreme states of solvatochromism.

Each curve shows the temporal evolution of photoluminescence following excitation of the solution. For each of the solutions, two decay curves are presented: one represents the lifetime at short wavelengths (where emission is predominant in the low-dielectric constant solvents) and the other represents the PL decay at long wavelengths (where emission peaked when high-dielectric constant solvents were used). For the toluene solution, detection wavelengths of  $\lambda_s = 440$  nm and  $\lambda_l = 500$  nm were chosen. Emission from the DCM solution was detected at slightly longer wavelengths in order to maintain an acceptable signal-to-noise ratio, with  $\lambda_s = 460$  nm and  $\lambda_l = 520$  nm. As described in chapter 2, both solutions were excited at 380 nm.

To avoid damaging the polymer, a relatively low excitation density was used. Consequently, all four data sets suffer from a high level of noise. Nevertheless, these results demonstrate some key features. The most notable of these is the difference in the PL lifetime observed from the two solutions. When fitted to a single exponential decay, the data obtained from the toluene solution yielded a

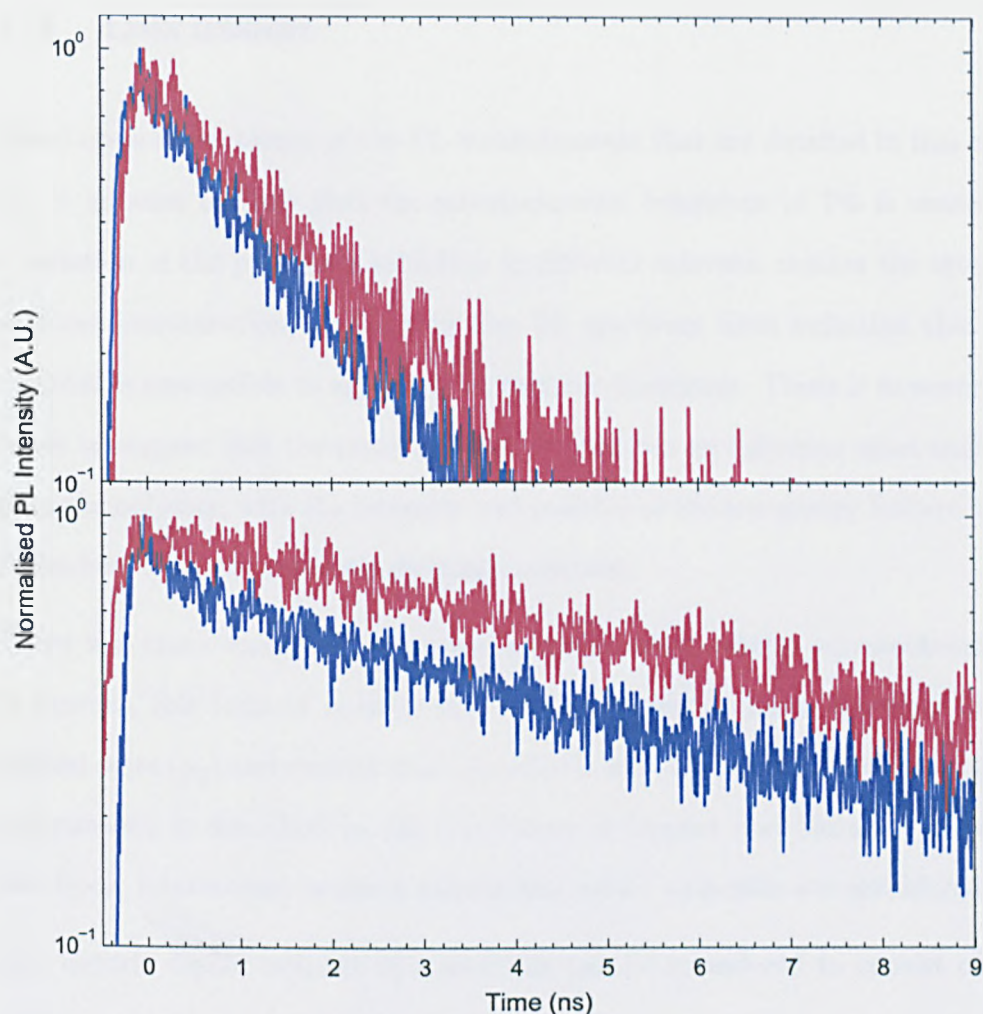


**Fig. 7.6:** The time-resolved photoluminescence of polymer **P6** during pulsed excitation. **(Above)** Emission from the toluene solution detected at 440 nm (blue) and 500 nm (red). **(Below)** Emission from the dichloromethane solution detected at 460 nm (blue) and 520 nm (red).

time-constant of  $\tau_s = 1.6$  ns (for 440 nm detection), and  $\tau_l = 2.0$  ns (for 500 nm detection). In contrast, the decay curves of the DCM solution had a much longer lifetime. The long wavelength decay at 520 nm could be fitted to a single exponential, yielding a time-constant of  $\tau_l = 10$  ns. The short wavelength data appeared to exhibit a bi-exponential decay. However, owing to the level of noise, this cannot be accurately verified. When fitted to a bi-exponential function, the long lifetime component had a time-constant of  $\tau_s = 5.2$  ns.

## 7.3 Discussion

Based upon the evidence of the PL measurements that are detailed in this chapter, it appears unlikely that the solvatochromic behaviour of **P6** is caused by a variation of the polymer's solubility in different solvents; neither the study of solution concentration, or the thin film PL spectrum have indicated that this material is susceptible to aggregate or excimer formation. There is however evidence to suggest that the polarity of the solvent has an influence upon emission from the polymer, with the intensity and position of the low-energy feature being dependent upon the solvent's dielectric constant.

There are many examples of organic materials that exhibit solvatochromism. In general, this form of polarity dependence suggests a large difference in the ground state ( $\mu_g$ ) and excited state ( $\mu_e$ ) dipole moments of the fluorophore. This phenomenon is described by the theory of Lippert and Mataga,<sup>8</sup> in which the dipole interactions between solvent and solute molecules are considered.<sup>9</sup>

The electric dipole moment of a molecule can be considered to consist of two components; a permanent dipole that results from a variation in the electronegativity of constituent atoms, and an induced dipole that is caused by the spatial redistribution of charge under the influence of an electric field. The polarisability of a medium is defined by the interactions of these dipoles. Orientation polarisation describes the rotation of a molecule such that its permanent dipole moment becomes aligned with an external field. Electronic polarisation describes the formation of an induced dipole.<sup>10</sup> Significantly, the time-scale over which the two processes occur differs by several orders of magnitude in common organic solvents.

The theory of solvent effects considers the interaction between a conjugated solute molecule and its surrounding solvation shell as it undergoes an electronic transition. The ground state dipole moment of the solute  $\mu_g$  will induce both orientational and electronic polarisation in the surrounding solvent molecules.

The strength of this interaction will depend upon the dipole moments of the solute and solvent, as well as the temperature (thermal agitation of the molecules will disrupt dipole alignment). In turn, the reaction field that is generated by the polarised solvation shell stabilises the ground state of the molecule such that  $E_s < E_v$  where  $E_s$  is the energy of the ground state in solution and  $E_v$  is the energy of the ground state in the vapour phase (or of an isolated molecule).

When the solute molecule is excited to a state with an increased dipole moment  $\mu_e$ , the polarisation of the solvation shell will also increase. As mentioned however, the relaxation time for electronic and orientational polarisations is markedly different. Whereas electronic relaxation effectively occurs instantaneously, orientational relaxation occurs *circa* 10-100 ps. It follows that, during the process of absorption the excited state is stabilised only by the increase in electronic polarisation of the solvation shell. However, orientational polarisation will occur over the typical lifetime of a fluorophore. Thus, prior to emission, the excited state will be stabilised by both electronic and orientational polarisations. The difference in energy between the two transitions (i.e. the solvent induced Stoke's shift) is therefore dependent only upon the orientation polarisation of the solvent ( $\Delta f$ ) and the change in dipole moment of the solute upon excitation ( $\mu_e - \mu_g$ ). The Lippert-Mataga equation is used to describe the orientational polarisation of a solvent

$$\Delta f = \frac{\epsilon - 1}{2\epsilon + 1} - \frac{n^2 - 1}{2n^2 + 1} \quad (7.1)$$

where  $\epsilon$  is the static dielectric constant and  $n$  is the refractive index.

Interestingly, when the solvents that are listed in figure 7.2 are reorganised based upon their orientation polarisabilities (as apposed to just their static dielectric constant) then their ordering is better correlated with the intensity of the red band emission.

By analysing the dependence of the Stoke's shift,  $\nu_a - \nu_f$  (where the position

Solvent	$\epsilon_r$	$n$	$\Delta f$	$\lambda_{\max}(\text{nm})$
<i>p</i> -Xylene	2.27	1.49	0.005	418
Toluene	2.41	1.49	0.018	417
Chlorobenzene	5.54	1.52	0.143	420
Chloroform	4.63	1.44	0.145	467
DCM	8.51	1.42	0.215	498

**Table 7.1:** The revised list of solvents in which they have been ordered by their orientation polarisabilities. The static dielectric constant and refractive index of each solvent was obtained from references 1 and 11 respectively.

of absorption and fluorescence peaks are expressed as wavenumbers), upon the polarisability of the solvent ( $\Delta f$ ), the theory of Lippert and Mataga can be used to determine the change in dipole moment that is induced by an electronic transition.<sup>8</sup> However, the emission spectra that were obtained from polymer **P6** suggest the occurrence of more than one transition. Similar results, in which two distinct emission bands are observed (the relative intensities of which are dependent upon the polarity of the solvent), have been previously termed 'dual fluorescence'.<sup>12</sup>

This phenomenon can be explained by the existence of two different excited electronic states that are closely spaced in energy.<sup>13</sup> Relating to the measurements presented here, the 'locally-excited' (LE) state decays with the structured blue emission that was observed from the non-polar solvents (xylene and toluene). The transition from the ground state to the LE state is characterised by a relatively small change in dipole moment. This is evidenced by the slight red-shift of vibronic features with solvent polarisability (in going from xylene to toluene to chlorobenzene). The featureless low-energy emission band that was predominant in the spectrum of the DCM solution originates from a charge-transfer (CT) state. Here, electronic excitation results in a relatively large increase in the dipole moment of the chromophore. It is therefore possible for the CT state to be preferentially stabilised by the relaxation of polar solvent molecules. Hence, by varying

the polarisability of the solvent, an inversion of the lowest lying excited state can be induced. Such a mechanism has been proposed to explain the observation of dual fluorescence from a fluorene-based copolymer<sup>14</sup> and oligomer.<sup>15</sup>

PL measurements also revealed that neither the alkyl-substituted polycarbazole (P2), or the alkoxy-substituted poly(aryl carbazole) (P4) exhibited emission from the charge-transfer state. Indeed, the spectra obtained from polymer P4 in both toluene and DCM strongly resembled that of the LE emission from polymer P6 with a difference of only 2 nm in their PL maxima. As these polymers incorporate an identical aryl-substituted carbazole backbone, this may suggest that the LE state of P6 is localised to the main-chain. It therefore follows that the formation of the CT state must be dependent upon the nature of the substitution.

Many of the materials that exhibit dual fluorescence incorporate a single bond that links between the donor and acceptor species. This may facilitate a twisting motion between the two components. In the theory of 'twisted intramolecular charge transfer' (TICT) the donor and acceptor moieties will rotate relative to each other upon excitation.<sup>16</sup> The transition from a more planar ground state to an orthogonal excited state causes electronic decoupling, thus increasing the degree of charge separation.

The aromatic molecule *p*-N,N-dimethylamino-benzonitrile (DMABN) has been the primary focus of investigations into the TICT process (see figure 7.7 for chemical structures). Here, the formation of an ICT state is believed to be accompanied by a rotation of the dimethylamino substituent into orthogonality with the plane of the phenyl ring.<sup>16,17</sup> Studies into derivative compounds whereby the twist angle of the DMA group is fixed relative to the phenyl ring have demonstrated the requirement of the twisting mechanism. When the DMA group was bridged such that the molecule was fixed into a planar conformation, only LE-type emission was observed. Conversely, the orthogonal conformation only exhibited the ICT band.



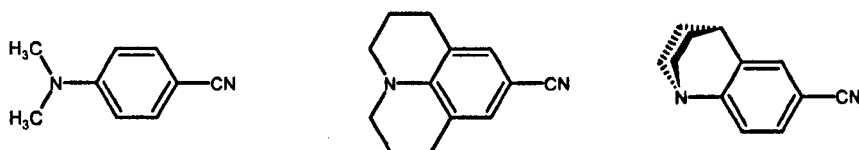


**Fig. 7.7:** The chemical structures of DMABN (left) and derivatives within which the DMA group has been constrained into planarity (center) and orthogonality (right).<sup>17</sup>

Such conformational changes may be responsible for the observation of dual fluorescence and solvatochromism in polymer **P6**. During this work, similar behaviour was also observed from a dialkylamino-substituted poly(aryl carbazole).<sup>18</sup> If a twisting mechanism does occur, this observation may locate it at the  $\sigma$ -bond that links the dialkylamine/diarylamino substituents to the aryl carbazole backbone as this feature is common to both materials. Currently however, the data available is insufficient to substantiate this theory.

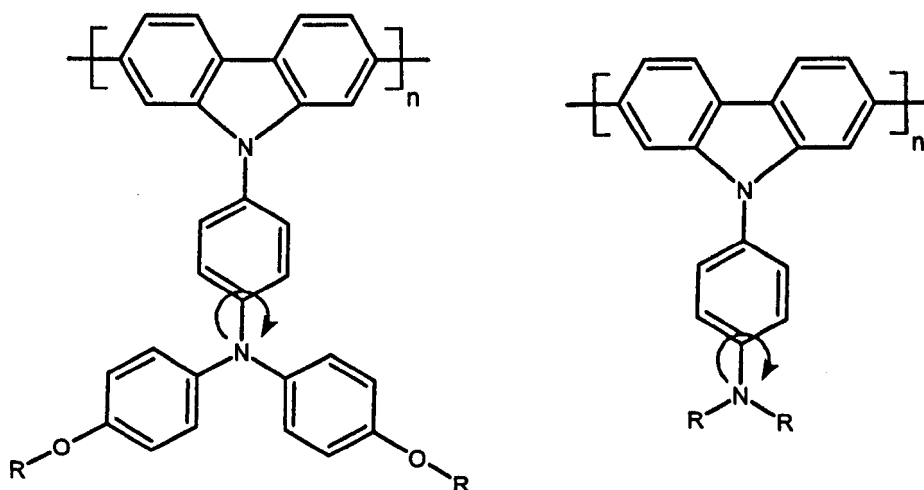


**Fig. 7.8:** Diagram highlighting the possible location of a bond twist in polymer **P6** and a related dialkylamino-substituted poly(aryl carbazole).

It should be noted that the synthesis of an analogous polymer to **P6** was reported by Kobayashi and coworkers.<sup>19</sup> They also observed the low energy emission band

from a chloroform solution (although the full solvatochromic behaviour was not reported upon). Interestingly, they noted that when the diarylamine substitution was made in the *para* or *ortho* positions, this feature was largely suppressed.

## 7.4 Conclusions

The triarylamine-substituted homopolymer **P6** has exhibited strong solvatochromic characteristics. In non-polar solvents such as xylene and toluene, the photoluminescence spectrum features a narrow emission band with vibronic structure, peaking at 418 nm. However in dichloromethane (a polar solvent) the spectrum was dominated by a low-energy emission band that was broad and featureless. A small amount of residual emission from the high-energy band could also be resolved.

Neither the intensity or position of the low-energy emission band exhibited a dependence upon solution concentration. It was also absent from the thin-film photoluminescence spectrum of **P6**. These results suggested that the low-energy emission band was unlikely to be generated by intermolecular species such as aggregates or excimers.

An alternative explanation as to the origin of dual fluorescence from polymer **P6** has been proposed. This involves the presence of a charge-transfer state between the polymer backbone and the triarylamine pendant group. Due to its high dipole moment, this CT state is preferentially stabilised by polar solvents. In a non-polar medium (such as xylene), emission from the intrinsic locally excited state (which has a smaller dipole moment) was predominant. However, as the polarity of the solvent was increased, an inversion of the energy levels was induced. Emission from the locally excited state became less favourable and the intensity of the CT state increased. The possibility of a simultaneous conformational change that further stabilises the CT state has also been discussed.

---

## References

- [1] Wohlfarth, C. *Landolt-Börnstein - Numerical Data and Functional Relationships in Science and Technology: Group IV Physical Chemistry*, volume 17. Springer, (2008).
- [2] Schwartz, B. J. *Annu. Rev. Phys. Chem.* **54**, 141–172 (2003).
- [3] Nguyen, T. Q., Doan, V., and Schwartz, B. J. *J. Chem. Phys.* **110**(8), 4068–4078 (1999).
- [4] Aharon, E., Breuer, S., Jaiser, F., Kohler, A., and Frey, G. L. *Chem. Phys. Chem.* **9**(10), 1430–1436 July (2008).
- [5] Samuel, I. D. W., Rumbles, G., Collison, C. J., Moratti, S. C., and Holmes, A. B. *Chem. Phys.* **227**(1-2), 75–82 February (1998).
- [6] Birks, J. B. and Christophorou, L. G. *Spectrochim. Acta* **19**(2), 401–410 (1963).
- [7] Klaerner, G. and Miller, R. D. *Macromolecules* **31**(6), 2007–2009 March (1998).
- [8] Mataga, N., Kaifu, Y., and Koizumi, M. *Bull. Chem. Soc. Jpn.* **29**(4), 465–470 (1956).
- [9] Lakowicz, J. R. *Principles of Fluorescence Spectroscopy*. New York: Springer, 3<sup>rd</sup> edition, (2006).
- [10] Hecht, E. *Optics*. Addison Wesley, 4th edition, (2002).
- [11] Wohlfarth, C. *Landolt-Börnstein - Numerical Data and Functional Relationships in Science and Technology: Group III Condensed Matter*, volume 47. Springer, (2008).
- [12] Rettig, W. *Angew. Chem., Int. Ed.* **25**(11), 971–988 November (1986).
- [13] Singh, M. K., Pal, H., Bhasikuttan, A. C., and Sapre, A. V. *Photochem. Photobiol.* **68**(1), 32–38 July (1998).
- [14] Redecker, M., Bradley, D. D. C., Baldwin, K. J., Smith, D. A., Inbasekaran, M., Wu, W. W., and Woo, E. P. *J. Mater. Chem.* **9**(9), 2151–2154 September (1999).
- [15] Dias, F. B., Pollock, S., Hedley, G., Palsson, L. O., Monkman, A., Perepichka, I. I., Perepichka, I. F., Tavasli, M., and Bryce, M. R. *J. Phys. Chem. B* **110**(39), 19329–19339 October (2006).
- [16] Grabowski, Z. R., Rotkiewicz, K., and Rettig, W. *Chem. Rev.* **103**(10), 3899–4031 October (2003).
- [17] Valeur, B. *Molecular Fluorescence*. Wiley-VCH, 1<sup>st</sup> edition, (2002).

- [18] Iraqi, A., Simmance, T. G., Yi, H. N., Stevenson, M., and Lidzey, D. G. *Chem Mater* **18**(24), 5789–5797 (2006).
- [19] Kobayashi, N., Koguchi, R., and Kijima, M. *Macromolecules* **39**(26), 9102–9111 (2006).

## Chapter 8

# Conclusions and Suggestions for Further Work

### 8.1 Conclusions

This work has focussed upon the optical and electronic characterisation of a series of main-chain polycarbazoles. Initial electrochemical studies into this new class of intrinsically blue-emitting conjugated polymer had revealed a low-lying HOMO level, a requisite for the efficient injection and transport of holes in LEDs. These materials however are known to be prone to degradation due to the reactivity of the 3- and 6-positions. In an effort to improve their stability, polymers in which the susceptible positions have been protected via methyl and fluorine substitutions were synthesised.

In a study of their thermal stability, four of the polymers were spin-cast on to quartz substrates and exposed to a variety of heat treatments. After being annealed in air at 150 °C for up to two hours, all four materials exhibited significant signs of degradation. The photoluminescence spectra of the three alkyl-substituted polymers (each carrying methyl substitutions at the 3- and 6-positions) were red-shifted and broadened by this treatment. Although  $\lambda_{\text{max}}$  was shifted toward lower energies, this resulted from the preferential quenching of short wavelength emission and not the formation of a new emissive species (as has been observed from polyfluorene and some of its derivatives).

The triarylamine-substituted homopolymer **P6** displayed a notably different behaviour. Although this polymer also suffered from quenching as a result of the heat treatment, emission was reduced equally across the full width of its spectrum. Consequently, this material has shown an extreme stability against colour degradation.

These results demonstrated that the process of degradation was dependent upon the presence of oxygen. When annealed under an inert nitrogen atmosphere (but otherwise identical conditions), none of the polymers exhibited significant changes to their spectra. It was speculated that the differences in the behaviour of polymers **P1-P3**, and polymer **P6** may result from a low concentration of emissive defect sites that are intrinsic to the alkyl-substituted polymers. On annealing, additional non-radiative defect sites would be introduced as a result of oxidation. The immobilisation of excitons at the intrinsic defects may then explain the preferential quenching of high energy emission. In contrast, the absence of an intrinsic emissive defect from **P6** would result in equal quenching across all wavelengths upon its thermal oxidation.

Charge carrier transport characteristics of the triarylamine-substituted polymers **P6** and **P7** were evaluated using the time-of-flight technique. Photoconductivity transients revealed that transport was dispersive in both materials. In the homopolymer **P6** however, the degree of dispersion was greater for the transit of electrons than it was for the transit of holes. The opposite was true of polymer **P7**, suggesting that the incorporation of the oxadiazole comonomer had indeed altered the transport properties of this material.

The mobility of both materials was dependent upon the applied field. It ranged from  $6.35 \times 10^{-6} \text{ cm}^2/\text{Vs}$  at a field strength of  $0.53 \text{ MV/cm}$  to  $2.86 \times 10^{-5} \text{ cm}^2/\text{Vs}$  at  $0.95 \text{ MV/cm}$  for hole transport in polymer **P6**. This data showed a Poole-Frenkel-type relationship between carrier mobility and applied field. Polymer **P7** exhibited electron mobilities of between  $2.51 \times 10^{-5}$  and  $4.36 \times 10^{-5} \text{ cm}^2/\text{Vs}$  over a similar range of fields. The relationship between mobility and field strength

from this data set was less well-defined. When analysed with regard to a Poole-Frenkel dependence, a negative coefficient was determined. This should only be expected from materials that have a narrow energetic distribution of states. As the photocurrent transients from **P7** suggested a large degree of dispersion this would seem unlikely and may reflect inaccuracies in the determination of the transit times.

Each of the seven polycarbazoles that are discussed in this thesis were incorporated into 'single-component' light-emitting diodes. These devices consisted of a single semiconducting layer deposited between a transparent ITO/PEDOT:PSS anode and Ca/Ag cathode. Some of the devices also incorporated a thin layer of LiF beneath the cathode to enhance electron injection. Although simple, such a structure will only produce efficient electroluminescence if the polymer layer facilitates the balanced injection and transport of both carrier types. Furthermore, the polymer must also function as a site for radiative recombination.

Of the three alkyl-substituted polymers, the carbazole-oxadiazole alternating copolymer (**P3**) produced the most promising device. This LED displayed the lowest 'turn-on' voltage for electroluminescence at 3.5 V and sustained the highest current efficiency, peaking at 0.35 cd/A. Its emission was initially blue in colour with CIE coordinates of  $x = 0.18$  and  $y = 0.15$ . However, as the device was operated, the spectrum evolved with a decrease in intensity at short wavelengths.

In contrast, the alkyl-substituted polymers **P1** and **P2** exhibited very broad and unstable electroluminescence spectra. The devices incorporating these two polymers also suffered high operating voltages and low efficiencies. Comparison of the electrochemical properties of all three polymers indicated that a reduction in the injection barrier to electrons (afforded by the high electron affinity of the oxadiazole moiety) may contribute to the improved EL characteristics observed from **P3**. Significantly, these results suggest that despite the improvement in electrochemical stability that has been observed from the 3,6-protected polycarbazoles,

these materials may still be subject to degradation during electroluminescent operation. Clearly, further work is required to draw a correlation between their electrochemical and electroluminescent stability.

An alternative protection strategy was demonstrated with the aryl-substituted polycarbazole **P5** in which the 3- and 6-positions hosted fluorine substitutions. These function not only to improve the electrochemical stability of the polymer, but also to increase its electron affinity, as was evidenced from cyclic voltammetry measurements. The single-layer device that was fabricated from this material displayed a maximum current efficiency of 0.21 cd/A and a turn-on voltage of 3.6 V. This represented a significant improvement in device performance when compared against the EL characteristics of the unprotected polymer **P4**.

The most promising single-component device characteristics were obtained using the triarylamine-substituted oxadiazole copolymer **P7**. Emission from this device was detected with an applied bias of 2.9 V and a maximum current efficiency of 0.53 cd/A was attained. However, both the PL and EL spectra from this material were significantly red-shifted relative to the other polymers. These characteristics may indicate the presence of a charge-transfer state in which the triarylamine (TAA) moiety functions as a donor species and the oxadiazole-carbazole backbone acts as the acceptor. The colour of emission from this device was blue-green, with CIE coordinates of  $x = 0.29$  and  $y = 0.55$ .

The electrochemical properties of both polymers **P6** and **P7** showed an additional oxidation event, suggesting that the TAA substituent may be electronically decoupled from the backbone. The low ionisation potential of this group (5.0 eV) should facilitate ohmic injection from a PEDOT:PSS anode.

Heterojunction LEDs were fabricated whereby an additional electronically active component was incorporated into the device structure. Bu-PBD (an electron-transporting/hole-blocking molecular material) was used in the fabrication of both distributed and planar heterojunction devices. In the planar structure, this material was dispersed in an inert polystyrene matrix and deposited between the



electroluminescent layer and the cathode. To prevent the dissolution of the underlying polycarbazole film, the PS:Bu-PBD blend was spun from a cyclohexane solution. A third device structure, incorporating the fluorene-based copolymer TFB, was also investigated. This was deposited as a thin hole-injection/transport interlayer on top of the PEDOT:PSS anode.

Distributed heterojunction devices incorporating the poly(aryl carbazole) **P4** and the triarylamine-substituted homopolymer **P6** both displayed enhanced performance over their equivalent single-component structures. This was attributed to an improvement in the balance of charge carriers.

A new low-energy emission band was observed from the **P6**:Bu-PBD distributed heterojunction device. This may result from the formation of intermolecular excitations. The absence of a ground state signature in both the absorption and photoluminescence excitation spectra of the blend indicates the presence of an excited state complex (exciplex). As this emission band was not observed when Bu-PBD was blended with other polycarbazoles, it was concluded that the presence of the triarylamine pendant group is fundamental to exciplex formation. A donor-acceptor interaction between the TAA substitution of **P6** and neighbouring Bu-PBD molecules has been proposed. By separating these two components using a planar heterojunction device structure, the low-energy emission band was largely suppressed. A concurrent increase in the electroluminescence efficiency was also realised.

Devices incorporating a TFB interlayer were fabricated using polymer **P6** and the two oxadiazole-containing copolymers **P3** and **P7**. The **P7** device displayed the most promising characteristics of all the LEDs that were studied during this work, recording the highest luminance at  $2240 \text{ cd/m}^2$  and current efficiency at  $1.12 \text{ cd/A}$ . As this material is predominantly n-type (evidenced by electrochemical and carrier-mobility measurements) the presence of the hole injection/transport interlayer is expected to redress the imbalance of carrier currents. This effect was less apparent in the **P3** device. This LED did however

exhibit a significant improvement in colour saturation and stability which was attributed to occurrence of recombination from within the TFB interlayer.

An improvement in performance was also observed from the TFB/P6 device. This displayed an enhanced stability at high current density over the single-component device structure. A maximum luminance of  $1,032 \text{ cd/m}^2$  was measured with an applied bias of 15 V. In contrast, the luminance of the single-component device was only  $147 \text{ cd/m}^2$  at 15 V. It is thought that the bilayer structure is less susceptible to degradation due to the removal of the anode/emitter interface.

A study of the photoluminescence properties of polymer P6 in solution revealed a strong solvatochromic effect. In the non-polar solvents, xylene and toluene, the emission spectrum of P6 was narrow and featured vibronic structure. Peaking at 418 nm, its fluorescence was deep blue/violet in colour. In polar solvents however, emission from the polymer was significantly different. This was most apparent from the dichloromethane solution which exhibited a very broad and featureless emission band peaking at 498 nm. Residual emission from the 418 nm band was present as a high-energy shoulder.

As this new emission band displayed no concentration dependence and was absent from the thin film spectrum, it is unlikely to originate from the formation of intermolecular species. Similar behaviour observed from other organic molecules has been previously attributed to the presence of a charge-transfer (CT) state. When the molecule is isolated (or in the weakly interacting environment of a non-polar solvent), excitation to the CT state is energetically unfavourable. As a consequence, emission from the locally-excited state is predominant under such conditions. This transition generates the structured blue emission the was observed from P6 when dissolved in xylene and toluene. However, when the surrounding molecules possess a large orientation polarisability, dipole interactions stabilise the CT excited state. This mechanism can induce an inversion of the energy levels such that excitation into the CT state becomes energetically favourable.

The relative intensity and spectral position of the two emission bands is thus controlled by the polarity of the solvent. In addition, conformational relaxation of the triarylamine pendant group may also contribute to the charge-transfer process.

## 8.2 Further Work

This study has provided a broad characterisation of a new class of conjugated polymer, examining several different aspects of their electronic and photophysical properties. Accordingly, there are a number of possible avenues into which future work could be directed.

A major aspect of this project has concerned the stability of the materials. The strategy of 3,6-methyl protection has clearly afforded these carbazole-based polymers an enhanced resistance against electrochemical deterioration.<sup>1</sup> The influence that this has on the electroluminescent stability of the devices is however less apparent. A more detailed investigation into the process of degradation would therefore be beneficial. Specifically, this work should include a comparative study between analogous protected and unprotected polymers.

Fourier transform infrared spectroscopy (FTIR) could be used to identify degradation products in thermally-annealed<sup>2</sup> or UV-irradiated films.<sup>3,4</sup> The data that was collected during this work has shown that thermal degradation will only occur under the presence of oxygen. FTIR measurements may indicate which of the positions within the carbazole monomer are susceptible to oxidation. This in turn could lead to the synthesis of new materials with enhanced oxidative stability.

From the data available, it is unclear whether oxidation is responsible for the instabilities that are observed during device operation. Although all of the devices were encapsulated under an inert nitrogen atmosphere, residual oxygen may be trapped within the active layer as a result of the casting process. Oxygen may

also be liberated from the ITO anode during device operation, although this process is thought to be inhibited by the presence of a PEDOT:PSS layer.<sup>5,6</sup> FTIR measurements carried out on a degraded device may indicate the occurrence (or absence) of oxidation.<sup>4</sup> The inclusion of a getter material may improve the long-term stability of devices by inhibiting the ingress of oxygen through the encapsulant.

MALDI-TOF mass spectrometry could also be used to compliment these measurements. This would however, rely on the synthesis of pure and well defined oligomers. This technique was used to detect the presence of alkyl-ketone defects in a photo-oxidised fluorene trimer.<sup>7</sup> Here, FTIR spectra proved to be insufficient to obtain a clear identification of the degradation product as both fluorenone and the alkyl-ketone species have a characteristic absorption band at the same frequency.

To obtain a full characterisation of carrier transport within these materials, time-of-flight photocurrent measurements should be carried out on the remaining alkyl- and aryl-substituted polycarbazoles. The photocurrent transients that were obtained from polymers **P6** and **P7** were highly dispersive. This can lead to inaccuracies in the determination of a carrier transit time. The fabrication of thicker samples (greater than  $1\ \mu\text{m}$ ) would increase the mean transit time. The degree of dispersion would thus be reduced as the carriers would have more time to energetically relax and reach the mean equilibrium velocity prior to being discharged through the collection electrode. Alternatively, a current-integration time-of-flight circuit could be employed.<sup>8</sup>

The study of single-carrier devices may also provide valuable data. These structures are fabricated such that the injection of one charge carrier is strongly favoured. As a consequence, a unipolar current is induced with the application of a driving bias. Typically, gold or aluminium electrodes are used to make 'hole-only' devices as these will provide a substantial barrier to the injection of electrons in the majority of organic semiconductors owing to their high work

functions. 'Electron-only' devices are more difficult to fabricate due to the reactivity of the low work function metals.<sup>9</sup> The I-V characteristics of these devices can be used to differentiate between injection limited (IL) or space-charge limited currents (SCLC). Furthermore, the predominant injection mechanism can be determined by studying the temperature dependence of these characteristics.<sup>10</sup> The presence of carrier traps is indicated by a modified (trap-limited) SCLC I-V dependence.<sup>11</sup>

In addition, single-carrier devices could be used to provide further information regarding device degradation.<sup>12</sup> The isolation of each carrier type may reveal degradation mechanisms that are specific to an individual excited state. In particular, one may expect to observe enhanced stability from 'hole-only' devices that have been fabricated using the 3,6-protected polymers.

Finally, further work is required to realise a fully optimised device structure for each of the polymers. This should include the investigation into the use of alternative electrode materials. OLEDs incorporating molybdenum oxide as an anode modification have recently been reported. Owing to an enhancement in hole injection, these devices displayed lower operational voltages, higher electroluminescence efficiencies and greater stability.<sup>13</sup>

The study of heterojunction devices has shown that, for many of the polymers, the incorporation of a high-electron affinity dopant is beneficial to device performance. Here, Bu-PBD was incorporated into the devices to improve electron injection and transport. However, there are a number of other materials that could be substituted to carry out this role. With particular regard to polymer P6, device performance was significantly enhanced when the electron transport component was isolated in a separate layer. Although this strategy was successful at suppressing the formation of low-energy and weakly emissive interchain states, it required the use of an electronically inert polymer matrix. An electron transport material that was more stable against crystallisation (and thus negates the use of a polymer matrix) would therefore be preferable. To this end, the use

of high glass-transition temperature starburst molecules incorporating oxadiazole or triazole moieties should be investigated.<sup>14</sup> Alternatively, the enhancement of electron injection may be achieved by modifying the cathode. For instance, the incorporation of a thin layer of cesium fluoride has been shown to reduce the injection barrier to electrons in some devices.<sup>15</sup>

---

## References

- [1] Iraqi, A., Pickup, D. F., and Yi, H. N. *Chem. Mater.* **18**(4), 1007–1015 February (2006).
- [2] Lee, J. I., Klaerner, G., and Miller, R. D. *Chem. Mater.* **11**(4), 1083–1088 April (1999).
- [3] Gong, X. O., Iyer, P. K., Moses, D., Bazan, G. C., Heeger, A. J., and Xiao, S. S. *Adv. Funct. Mater.* **13**(4), 325–330 (2003).
- [4] Bliznyuk, V. N., Carter, S. A., Scott, J. C., Klarner, G., Miller, R. D., and Miller, D. C. *Macromolecules* **32**(2), 361–369 (1999).
- [5] Scott, J. C., Kaufman, J. H., Brock, P. J., DiPietro, R., Salem, J., and Goitia, J. A. *J. Appl. Phys.* **79**(5), 2745–2751 March (1996).
- [6] Scott, J. C., Carter, S. A., Karg, S., and Angelopoulos, M. *Synth. Met.* **85**(1-3), 1197–1200 February (1997).
- [7] Liu, L. L., Tang, S., Liu, M. R., Xie, Z. Q., Zhang, W., Lu, P., Hanif, M., and Ma, Y. G. *J. Phys. Chem. B* **110**(28), 13734–13740 July (2006).
- [8] Campbell, A. J., Bradley, D. D. C., and Antoniadis, H. *Appl. Phys. Lett.* **79**(14), 2133–2135 October (2001).
- [9] Parker, I. D. *J. Appl. Phys.* **75**(3), 1656–1666 (1994).
- [10] Lmimouni, K., Legrand, C., and Chapoton, A. *Synth. Met.* **97**(2), 151–155 (1998).
- [11] Campbell, A. J., Bradley, D. D. C., and Lidzey, D. G. *Opt. Mater.* **9**(1-4), 114–119 January (1998).
- [12] Kondakov, D. Y., Lenhart, W. C., and Nichols, W. F. *J. Appl. Phys.* **101**(2), 024512 January (2007).
- [13] You, H., Dai, Y. F., Zhang, Z. Q., and Ma, D. G. *J. Appl. Phys.* **101**(2), 026105 January (2007).
- [14] Kulkarni, A. P., Tonzola, C. J., Babel, A., and Jenekhe, S. A. *Chem. Mater.* **16**(23), 4556–4573 (2004).
- [15] Chan, M. Y., Lai, S. L., Fung, M. K., Tong, S. W., Lee, C. S., and Lee, S. T. *Appl. Phys. Lett.* **82**(11), 1784–1786 March (2003).